NASA Technical Memorandum 2002–206892, Volume 17

SeaWiFS Postlaunch Technical Report Series

Stanford B. Hooker, Editor
NASA/Goddard Space Flight Center
Greenbelt, Maryland

Elaine R. Firestone, Senior Scientific Technical Editor
Science Applications International Corporation
Beltsville, Maryland

Volume 17, The Seventh SeaWiFS Intercalibration Round-Robin Experiment (SIRREX-7), March 1999

Stanford B. Hooker
NASA/Goddard Space Flight Center
Greenbelt, Maryland

Scott McLean
Jennifer Sherman
Mark Small
Gordana Lazin
Satlantic, Inc.
Halifax, Canada

Giuseppe Zibordi
JRC/SAI/Marine Environment Unit
Ispra, Italy

James W. Brown
RSMAS/University of Miami
Miami, Florida

Preface

The original goals of the Sea-viewing Wide Field-of-view Sensor (SeaWiFS) Project include radiometric absolute and relative (between band) accuracies for water-leaving radiance of 5% and 1%, respectively. These accuracies are required to achieve the desired accuracies in the derived products, such as chlorophyll *a* concentration and the diffuse attenuation coefficient, which are based on bio-optical algorithms that apply the water-leaving radiances. To achieve this level of accuracy, all components of the total radiance measured by the SeaWiFS instrument (Rayleigh, aerosol, surface Fresnel, whitecap, and water-leaving) must be accounted for at higher accuracies. Also, the accuracy of the bio-optical algorithms are dependent on the quality of the *in situ* data used to derive them, and these must span a broad range of bio-optical provinces, i.e., turbid to clear. Finally, the ultimate validation of the satellite-derived water-leaving radiances is primarily based on measurements using commercially available instruments; therefore, the proper calibration of these instruments is critical.

Early in the SeaWiFS Project, the SeaWiFS calibration and validation program initiated a variety of activities designed to reduce the sources of uncertainty which are inherent in field measurements. One activity was a series of calibration round robins. These experiments, all documented in the pre-launch and postlaunch *SeaWiFS Technical Report Series,*† have been hugely successful in reducing instrument (*in situ*, aircraft, and satellite) calibration uncertainties across the ocean color community and in educating the community on metrology fundamentals. At this point in the SeaWiFS mission, the accuracy of the derived radiances are at the level of uncertainty in the *in situ* measurements. Further improvements in the SeaWiFS products, therefore, can only be achieved by improving the *in situ* measurements.

The SIRREX-7 activity was conducted to quantify the accuracy of the calibrations available from one instrument vendor, Satlantic, Inc. (Halifax, Canada). Satlantic instruments provide much of the *in situ* data being collected by the ocean color community, and it was felt that a comprehensive evaluation of the Satlantic facility and methods was appropriate. Satlantic has a sizable investment in their calibration facility and has been an active participant in each of the preceding the SIRREXs. Their enthusiastic collaboration in this and other SeaWiFS calibration and validation program studies is greatly appreciated and exemplifies the level of cooperation and openness which must exist between instrument providers and the research community if the science objectives are to be achieved.

Greenbelt, Maryland
December 2001

— C. R. McClain

† The original (pre-launch) documentation of the SeaWiFS Project was titled the *SeaWiFS Technical Report Series,* which ended after 43 volumes were published. A follow-on series was started after the successful launch and orbit raising of the SeaWiFS instrument, titled the *SeaWiFS Postlaunch Technical Report Series.*

Table of Contents

Table of Contents (*cont.*)

Table of Contents (*cont.*)

Abstract

This report documents the scientific activities during the seventh SeaWiFS Intercalibration Round-Robin Experiment (SIRREX-7) held at Satlantic, Inc. (Halifax, Canada). The overall objective of SIRREX-7 was to determine the uncertainties of radiometric calibrations and measurements at a single calibration facility. Specifically, this involved the estimation of the uncertainties in a) lamp standards, b) plaque standards (including the uncertainties associated with plaque illumination non-uniformity), c) radiance calibrations, and d) irradiance calibrations. The investigation of the uncertainties in lamp standards included a comparison between a calibration of a new FEL by the National Institute of Standards and Technology (NIST) and Optronic Laboratories, Inc. In addition, the rotation and polarization sensitivity of radiometers were determined, and a procedure for transferring an absolute calibration to portable light sources was defined and executed.

Prologue

The Sea-viewing Wide Field-of-view Sensor (SeaWiFS) Project at the National Aeronautics and Space Administration (NASA) Goddard Space Flight Center (GSFC) has two important goals with respect to the spaceborne radiance measurements (Hooker and Esaias 1993): a) normalized water-leaving radiance with an uncertainty to within 5%, and b) chlorophyll *a* concentration with an uncertainty to within 35%. These goals are very ambitious, and can only be achieved by augmenting the SeaWiFS measurements with a program of ongoing validation measurements to a) verify the radiometric uncertainty and long-term stability of the SeaWiFS instrument's radiance responsivities, and b) validate the atmospheric correction models and algorithms used to convert SeaWiFS radiances to water-leaving radiances, $L_W(\lambda)$. One of the principal approaches to this critical aspect of the SeaWiFS mission are frequent direct comparisons between spaceborne and *in situ* measurements of $L_W(\lambda)$. Because there are many sources of uncertainty contributing to the final uncertainty objective (5%), each source must be minimized and kept at the lowest level possible. The goal for the calibration of the field instruments has always been to have reproducible calibrations from 400–850 nm as close to 1% as possible (with 2% as a hoped for upper limit).

The calibration goal for SeaWiFS field instruments is not only driven by a simple argument of sums. Given the myriad objectives associated with SeaWiFS validation, the only economically feasible approach for acquiring a large and globally distributed database of *in situ* radiometric measurements, is to solicit contributions of data from the oceanographic community at large. Such an approach demands an assurance that the aggregate data set will be of uniform quality, and one of the first points of quality control is maintaining a high standard for instrument calibration (Hooker and McClain 2000).

The entire process is more complicated than a careful scrutiny of calibration facilities, and the SeaWiFS Project is addressing this problem through the SeaWiFS Calibration and Validation Program (McClain et al. 1992). At the outset, the Project sponsored a workshop to draft protocols for ocean optics measurements to support SeaWiFS validation (Mueller and Austin 1992), which included instrument performance specifications, and requirements for instrument characterization and calibration. The importance of the protocols to the community was established by the considerable expansion of the original document to accommodate a broader range of measurements, techniques, and sampling considerations (Mueller and Austin 1995).

The strategy adopted for the validation of the SeaWiFS remote sensing data is to calibrate all of the field instruments within a network consisting of the instrument manufacturers plus a few additional laboratories that have recurringly provided instrument calibrations. In recognition of the need to maintain internal consistency between calibrations of *in situ* instruments and that of the SeaWiFS instrument itself, the SeaWiFS Project, under the Calibration and Validation Program, implemented an ongoing series of SeaWiFS Intercalibration Round-Robin Experiments (SIRREXs). The objectives of the SIRREX activity, at each separate event and over time, are to accomplish the following:

1. Intercalibrate FEL lamp working standards of spectral irradiance and to reference each to the National Institute of Standards and Technology (NIST) scale of spectral irradiance via a secondary or tertiary standard;
2. Intercalibrate the integrating sphere sources of spectral radiance;
3. Intercompare the plaques used to transfer the scale of spectral irradiance from an FEL lamp to a scale of spectral radiance, as well as the support electronics involved (most critically shunts and voltmeters);
4. Evaluate the suitability of the equipment and laboratory methods being employed for radiometric calibrations at each institution; and
5. Intercompare radiometers in the field while evaluating the measurement protocols being used.

In the progression from the first to the third SIRREX, which were all held at the Center for Hydro-Optics and Remote Sensing (CHORS), uncertainties in the traceability to NIST of intercomparisons between the spectral irradiance of lamps improved from 8% to 2% to 1% (Mueller 1993; Mueller et al. 1994; and Mueller et al. 1996; respectively). Intercomparisons of sphere radiance showed little improvement between SIRREX-1 and SIRREX-2, with uncertainties as large as 7% in both activities. In SIRREX-3, however, a more rigorous characterization of both spheres and transfer radiometers reduced the uncertainties to approximately 1.5% in absolute spectral radiance and 0.3% in radiance stability for most spheres (inadequate lamp current regulation was the primary source of larger uncertainties). Shunts and voltmeters were intercompared during the first three SIRREXs, and in general, the equipment used by all participants met the specified levels of uncertainty (although some deficiencies were discovered and corrected).

Plaque reflectance measurements in SIRREX-3 represented a qualitative improvement over results obtained during earlier SIRREXs, primarily due to improved performance with the SeaWiFS Transfer Radiometer (SXR). The need for significant improvements were discovered in this technique, however, if several poorly quantified uncertainties are to be resolved, including the development of proper methods for stray light baffling, goniometric corrections for FEL off-axis irradiances, and quantitative characterization of the bidirectional reflectance distribution function (BRDF) of Spectralon™† plaques.

In addition to further investigating the use of plaques, SIRREX-3 demonstrated the need for rigorous laboratory practices. The shift in spectral irradiance of a lamp emphasized the need to closely adhere to several important protocols for lamp usage and record keeping in general, and with NIST secondary standards in particular (i.e., lamp operating hours should always be recorded). The voltage across the lamp terminals, as well as the lamp operating current, should be measured and recorded each time a lamp is used. As a matter of routine practice, the irradiance of a NIST secondary standard of spectral irradiance should be transferred locally to several additional working standard FEL lamps, and the transfer periodically verified for each of the local working standards at intervals in keeping with the use of the lamp.

Given the repeated failures in laboratory technique during the first three SIRREX activities, the primary recommendation from SIRREX-3 was ... *an emphasis on training and work to foster and encourage uniform use of accepted protocols for laboratory calibration of radiometric instruments.* This was the starting point for SIRREX-4 (Johnson et al. 1996) which was held at NIST during 3–10 May 1995. The idea was to host the activity in a setting where proper technique could be discussed and demonstrated. Each day was split between morning lectures and afternoon laboratory sessions or *practicals.* The former gave the attendees a chance to present what was important to them and discuss it with acknowledged experts in radiometry, while the latter presented a unique opportunity for training and evaluation in the presence of these same experts. There were five laboratory sessions, which were concerned with a) determining the responsivity of a spectroradiometer and the spectral radiance of an unknown integrating sphere source, b) demonstrating spectral field calibration procedures for an integrating sphere using three different instruments, c) measuring spectral radiance using the lamp and plaque method, d) setting up and aligning lamp calibration transfer standards using NIST specifications for irradiance measurements, and e) characterizing radiometric instruments.

SIRREX-5 was also held at NIST on 23–30 July 1996 and was the first time above- and in-water instrument intercomparisons were performed at field sites, in this case at small lakes close, to or on, the NIST campus (Johnson et al. 1999). The goals were to continue the emphasis on training and the implementation of uniform measurement practices, investigate the calibration methods in use by the scientific community, provide discussion opportunities between the attendees and NIST experts, demonstrate new technology, and intercompare selected field instruments. Daily lectures in the morning and practicals in the afternoon dealt with 1) measuring in-water and in-air radiant flux, 2) using the lamp and plaque method for measuring spectral radiance responsivity, 3) testing portable sources as calibration devices or stability monitors, and 4) participating in various ancillary exercises designed to illustrate radiometric concepts.

After the launch of the SeaWiFS instrument (1 August 1997), the immediate requirements and budget priorities of the SeaWiFS Project did not permit the continued sponsorship of the SIRREX activity, so SIRREX-6 was supported and executed by the Sensor Intercomparison and Merger for Biological and Interdisciplinary Ocean Studies (SIMBIOS) Project. This activity was very different from the previous SIRREXs: four Satlantic, Inc. (Halifax, Canada) in-water radiometers, two 7-channel ocean color radiance series 200 (OCR-200) sensors and two 7-channel ocean color irradiance series 200 (OCI-200) sensors, were calibrated at nine different calibration laboratories (Riley and Bailey 1998). The reference lamps, calibration methods, and data reduction procedures appropriate to each laboratory were used to derive the calibration coefficients for the four radiometers. A comparison of the data from all the sensors showed an overall agreement at better than the ±2% level.

† "Spectralon" is a registered trademark of Labsphere, Inc. (North Sutton, New Hampshire). Identification of commercial equipment to adequately specify the experimental problem, does not imply recommendation or endorsement, nor does it imply that the equipment identified is necessarily the best available for the purpose.

An overview of the SIRREX-7 activity is presented in Chapter 1, and the instrumentation used is presented in Chapter 2. The experiments are organized into generalized groups based on the type of radiometry or instrumentation involved and are presented in Chapters 3–8. A synthesis of the results is presented in Chapter 9 along with a discussion of the principal conclusions derived from the experimental data with respect to the objectives of the individual trials and the activity as a whole. The primary product of the activity is an estimation of the individual sources of uncertainty along with a combined uncertainty budget for the Satlantic calibration facility. The science team members are presented in Appendix A. A summary of the material presented in each chapter is given below.

1. SIRREX-7 Overview

The primary objective of SIRREX-7 was a thorough inquiry into the absolute capability of a single calibration facility. A small team of investigators was assembled to address this question at Satlantic, Inc. The experimental group was kept small, because the entire activity had to take place in a single room with a small number of experimental stations. Because this required a substantial commitment in time and resources, there was a strong desire to learn as much as possible about the equipment and methods normally used in the calibration process. Consequently, a wide diversity of each equipment type was assembled: 10 FEL lamps, 7 reflectance plaques, 10 fixed wavelength radiometers, 1 hyperspectral radiometer, the SXR, 1 single-channel mapping (narrow field-of-view) radiometer, plus the original SeaWiFS Quality Monitor (SQM) and 4 second-generation SQMs (SQM-IIs). The instrumentation came from three different organizations with differing calibration and measurement objectives, so the assembled equipment had a diverse range of calibration histories, ages, sizes, intended uses, sensitivities, flux levels, etc. Although SIRREX-7 was conducted at only one facility, the diversity in equipment ensures that a significant subset of the results achieved will have a wider applicability to the larger community.

2. SIRREX-7 Instrumentation

The highest priority for the instrumentation used for SIRREX-7 was to bring together as wide a diversity of equipment used in the laboratory calibration and field measurement process as possible, so the agreed upon minimum number of replicates for a particular equipment type was three. Each participating group contributed more than one example of a particular equipment type, which ensured equipment with a wide range of ages, calibration histories, sensitivities, flux levels, etc. Equipment that was used as part of the digitization or control process, like voltmeters and shunts, were calibrated as close to the SIRREX-7 activity as possible; all other types of equipment were reviewed to ensure their calibration histories were within the guidelines prescribed by the manufacturer or the protocols governing their use (like lamps and plaques). In some cases, equipment that did not meet the recency of calibration requirements were used, so the effect of ignoring this practice (regardless of the reason) could be quantified. In addition, some equipment with known problems were included to see if the outer range of variance in the results was defined by substandard equipment or if other factors (like operator error) were more important.

3. Uncertainties in Lamp Standards

The uncertainties associated with the use of lamp standards was estimated by using several lamps with different calibration histories to illuminate a NIST reflectance standard (T005), and then comparing the calibrated radiance from the plaque (calculated from the calibrated reflectance of the plaque and the calibrated irradiance from the lamp), with that measured by the SXR. The average uncertainty of the most *trusted* lamps, those with no known problems and established good performance capabilities, was approximately 1.2%. All of the lamps had a calibration repeatability less than 0.5%, and all of the lamps except one had a repeatability less than 0.2%. A comparison of an Optronic calibration of an FEL lamp with a NIST calibration of the same lamp showed an overall average agreement to within approximately 1.3%. A similar comparison exercise executed as a part of SIRREX-5 showed the Optronic calibration of FEL F-409 differed from the NIST calibration by an average of approximately 2.6%, whereas a second calibration by Optronic differed from the NIST calibration by about 0.8%.

4. Uncertainties in Plaque Standards

The experiments conducted to estimate the uncertainties associated with the use of plaque standards involved calculating the reflectances of seven plaques using SXR measurements and the calibrated irradiance provided with the lamp standard, which were then compared to the reflectances provided with each plaque. The average uncertainties between the calculated and calibrated reflectances showed a range of 1.0–3.2%. With the exception of the gray plaque (T007), maximum uncertainties occurred in the blue part of the spectrum, and minimum uncertainties in the red. The importance of bidirectional effects was determined by comparing the SXR plaque measurements made from two different sides of a plaque, but with the same viewing geometry. The smallest uncertainties were associated with T005 (the NIST plaque), and the largest with T007 (the gray plaque), 0.3 and 2.1%, respectively. All of the other plaques had relative percent difference (RPD) values which fell into a narrow range with the same spectral dependence and an overall average RPD of approximately 1.0%. Plaque uniformity improved with all increases in the lamp-to-plaque distance. Regardless of the lamp-to-plaque distance, there was a constant offset of aproximately 20 mm in the vertical (z) direction between

the maximum signal and the center of the plaque for all the lamps; some of the lamps also showed offsets in the horizontal (x) direction.

5. *Uncertainties in Radiance Calibrations*

Three types of experiments were conducted to estimate the uncertainties in radiance calibrations using a plaque and FEL lamp: a) The average repeatability uncertainty (based on one plaque and one FEL used with 11 trials for three different radiometers) was less than 0.1% (0.06% in the blue–green part of the spectrum and 0.09% in the red); b) the uncertainty that can be removed from radiance calibrations if ambient rather than dark measurements are used was 0.13% (0.11% in the blue–green and 0.17% in the red); and c) the overall uncertainty from secondary reflections, (for example, originating from an alignment laser) was 0.11% (0.06% in the blue–green wavelength domain and 0.19% in the red).

6. *Uncertainties in Irradiance Calibrations*

Three types of experiments were conducted to estimate the uncertainties associated with irradiance calibrations using an FEL standard lamp: a) the repeatability uncertainty (based on one FEL standard lamp used during 11 trials with three different irradiance sensors) was less than 0.5% (0.2% on average, with usually larger uncertainties in the blue part of the spectrum and smaller uncertainties in the red); b) the additional uncertainty that can be removed from radiance calibrations if ambient rather than dark measurements are used was 0.05% (0.05% in the blue, 0.04% in the green, and 0.06% in the red); and c) the overall uncertainty from secondary reflections, originating from ancillary equipment used during the calibration process (in this case, an alignment laser) was 0.06% (0.03% in the blue–green wavelength domain and 0.12% in the red).

7. *Rotation and Polarization Uncertainties*

Separate experiments were conducted during SIRREX-7 to estimate the rotation and polarization uncertainties of radiometers during the calibration process. Rotational uncertainties for radiance sensors were usually less than 1%, with single and multiple aperture systems having average rotational uncertainties of 0.2–0.3% and 0.4–0.9%, respectively. Rotational uncertainties for a multiple aperture irradiance sensor was 0.7% on average, which was in close agreement with multiple aperture radiance sensors. The only significant spectral dependence was with an OCR-2000 (hyperspectral) sensor which had maximal effects in the bluest and reddest wavelengths and minimal effects in the green domain. The average polarization parameter, in percent, varied between 0.6–4.6%. The Satlantic instruments had an average polarization below 2.0%, but the OCR-200 sensors showed maximum polarization sensitivity in the blue part of the spectrum (1.4–2.4%), while the OCR-2000 instrument had maximum sensitivity in the red wavelength domain (2.1–2.6%).

8. *Absolute Calibration of the SQM and SQM-II*

To better understand the capability of portable sources, a series of experiments were conducted to transfer an absolute calibration to the original SQM and four SQM-IIs, and to map the homogeneity of an SQM-II exit aperture. Approximately 25% of the central portion of the exit aperture was within 2% of the maximum signal, and about 40% was to within 5%. The decay in SQM flux over a 500 day time period, which included one shipping event, was estimated to be approximately 0.9% every 100 days. The decay for an SQM-II over the same time period, but encompassing four shipping events, was approximately 2.2% every 100 days. The average and standard deviations in the coefficient of variation was used as a stability parameter for the SQM and SQM-II. Both sources showed a spectral dependence with the greatest stability in the red part of the spectrum, and the least stability in the blue. The standard deviation in the coefficient of variation was independent of wavelength for the SQM, but the SQM-II had a noticeable spectral dependence—the reddest wavelength (775 nm) had a standard deviation approximately half that of the blue wavelengths. Using the overall averages as generalized metrics for stability, the SQM was more stable than the SQM-II: the overall average was a factor of three smaller, and the overall standard deviation was an order of magnitude smaller.

9. *SIRREX-7 Synthesis, Discussion, and Conclusions*

A combined uncertainty budget for radiometric calibrations can be constructed from the SIRREX-7 data set. Although it is comprehensive, it does not address every source of uncertainty at the same level of detail and some must be considered as approximate. Nonetheless, the care taken in each experiment ensures the uncertainty estimates are representative of what can be expected if careful metrology and practices are used. Perhaps just as importantly, the consequences of discrepancies are also well estimated. To provide a range of possible outcomes in the calibration process, minimum, typical, and maximum uncertainties are computed from the various entries, which range from 1.1–3.4% and 1.5–6.7% for irradiance and radiance calibrations, respectively. The Satlantic facility falls somewhere between the minimum and typical values. If an additional (average) 1.0% is included to account for an unknown bias detected with the lamp and plaque uncertainty experiments (described in Sects. 3.2 and 4.2, and discussed in Sects. 9.2 and 9.5), the uncertainty for Satlantic irradiance calibrations is 1.8%, and the uncertainty for radiance calibrations is 2.3%.

Chapter 1

SIRREX-7 Overview

Stanford B. Hooker
NASA/Goddard Space Flight Center
Greenbelt, Maryland

Scott McLean
Satlantic, Inc.
Halifax, Canada

Abstract

The primary objective of SIRREX-7 was a thorough inquiry into the absolute capability of a single calibration facility. A small team of investigators was assembled to address this question at Satlantic, Inc. The experimental group was kept small, because the entire activity had to take place in a single room with a small number of experimental stations. Because this required a substantial commitment in time and resources, there was a strong desire to learn as much as possible about the equipment and methods normally used in the calibration process. Consequently, a wide diversity of each equipment type was assembled: 10 FEL lamps, 7 reflectance plaques, 10 fixed wavelength radiometers, 1 hyperspectral radiometer, the SXR, 1 single-channel mapping (narrow field-of-view) radiometer, plus the original SQM and 4 SQM-IIs. The instrumentation came from three different organizations with differing calibration and measurement objectives, so the assembled equipment had a diverse range of calibration histories, ages, sizes, intended uses, sensitivities, flux levels, etc. Although SIRREX-7 was conducted at only one facility, the diversity in equipment ensures that a significant subset of the results achieved will have a wider applicability to the larger community.

1.1 INTRODUCTION

The determination of the absolute radiometric response of an irradiance or radiance sensor requires a properly staffed and equipped calibration facility. For SeaWiFS calibration and validation activities, the latter must include stable sources and sensors with defined spectral radiometric characteristics traceable to NIST. The calibration facility must also have a variety of specialized radiometric and electronic equipment, including reflectance plaques, spectral filters, integrating spheres, and highly regulated power supplies for the operation of the lamps. Precision electronic measurement capabilities are also required, both for setting and monitoring lamp current and voltage, and for measuring the output of the radiometer.

Although there have been six previous SIRREXs and significant progress was made at each one, in terms of understanding the sources of uncertainties in radiometric calibrations, a thorough inquiry into the absolute capability of a calibration facility regularly used by the ocean color community was not investigated. This was an important task, because, as already mentioned, the goal of a calibration facility used for SeaWiFS validation is to provide reproducible calibrations from 400–850 nm to within ±1%. SIRREX-7 was convened with a small team of investigators to estimate calibration uncertainties at Satlantic, Inc. The experimental group was kept small, because the entire activity had to take place in a single room. Satlantic agreed to be the hosting organization, because:

1. Many SeaWiFS and SIMBIOS investigators rely on Satlantic equipment and calibrations;
2. They have a state-of-the-art facility (all calibrations are done in a clean room with exceptional baffling and optical alignment equipment);
3. They commercialized the original SQM (so several units were available for an absolute intercomparison experiment); and
4. They have the interest and commitment (having participated in all of the previous SIRREXs) to underwrite the significant financial requirements for the hosting organization.

A final uncertainty budget for any instrument requires a thorough understanding of laboratory and field performance. The SeaWiFS Project participated to provide expertise and unique equipment (the original SQM and SXR), a variety of sources and targets (plaques, FEL lamps, etc.),

Table 1. A summary of the primary calibration equipment used during SIRREX-7 categorized according to the type of source or target, the contributing group, the model and type, the serial number (S/N), and the temporary (identification) number (T/N) issued only for SIRREX-7 to facilitate file naming and record keeping. For the latter, all lamps start with the letter "L", all plaques with the letter "T", and all field sources with the letter "S". The rationale behind the radiometer letter codes is based on the measurement type and is presented in Table 7 (Sect. 2.4).

Equipment	*Group*	*Make*	*Model and Type*	*S/N*	*T/N*
Laboratory	Satlantic	NIST	1,000 W FEL Lamp	F-409	L007
Source	Satlantic	Optronic	1,000 W FEL Lamp	F-539	L003
	Satlantic	Optronic	1,000 W FEL Lamp	F-536	L006
	Satlantic	Optronic	1,000 W FEL Lamp	F-547	L008
	Satlantic	Optronic	1,000 W FEL Lamp	F-548	L009
	Satlantic	Optronic	1,000 W FEL Lamp	F-516	L000
	JRC	Hoffman	1,000 W FEL Lamp	H97505	L004
	JRC	Hoffman	1,000 W FEL Lamp	H96551	L005
	NASA	NIST	1,000 W FEL Lamp	F-137	L001
	NASA	NIST	1,000 W FEL Lamp	F-182	L002
Plaque	Satlantic	Labsphere	18 in White Spectralon	05816	T001
	Satlantic	Labsphere	18 in White Spectralon	13172	T002
	Satlantic	Labsphere	18 in White Spectralon	01873	T003
	JRC	Labsphere	18 in White Spectralon	22463	T004
	NASA	NIST	2.25 in White PTFE†	K299	T005
	NASA	Labsphere	10 in White Spectralon	25322	T006
	NASA	Labsphere	10 in Gray Spectralon	24328	T007
Radiometer	Satlantic	Satlantic	OCR-2000 Radiance	002	P002
	Satlantic	Satlantic	OCR-1000 Radiance	033	Q033
	Satlantic	Satlantic	OCR-200 Radiance	064	R064
	Satlantic	Satlantic	OCI-200 Irradiance	121	I121
	Satlantic	Satlantic	OCR-250 Radiance‡	001	Y001
	JRC	Satlantic	OCR-200 Radiance	067	R067
	JRC	Satlantic	OCI-200 Irradiance	097	I097
	JRC	Satlantic	OCI-200 Irradiance	098	I098
	NASA	Satlantic	OCR-200 Radiance	035	R035
	NASA	Satlantic	OCR-200 Radiance	036	R036
	NASA	Satlantic	OCR-200 Radiance	037	R037
	NASA	Satlantic	OCI-200 Irradiance	040	I040
	NASA	Satlantic	OCI-200 Irradiance	050	I050
	NASA	NIST	SXR Radiance	001	X001
Field Source	Satlantic	Satlantic	SQM-II	001	S001
	Satlantic	Satlantic	SQM-II	002	S002
	JRC	Satlantic	SQM-II	003	S003
	NASA	Satlantic	SQM-II	004	S004
	NASA	Reyer	SQM	001	S000

† Polytetrafluoroethylene.
‡ The xz-mapping radiometer.

plus a set of radiometers whose long-term performance in the field has been well quantified and documented (Hooker and Maritorena 2000). The Joint Research Centre (JRC) participated to provide expertise, a connection to the international community (JRC is involved in several European calibration and validation activities), and to satisfy the minimum diversity in equipment, i.e., three different sets of plaques, radiometers, FEL lamps, etc.

A summary of the primary calibration equipment used during SIRREX-7 and the contributing organization for each is given in Table 1. The equipment is divided into four general groups: laboratory sources, reflectance plaques, radiometers, and field sources. The lamps are distinguished by whether they were calibrated by NIST or not. Of the

plaques used, only one was calibrated by NIST, and the remaining were either large (18 in) or small (10 in). Note that one of the small plaques was gray, whereas, all the others were white. Six different kinds of radiometers were used: the OCI-200, OCR-200, OCR-250, OCR-1000, and SXR are filter radiometers, whereas, the OCR-2000 is a hyperspectral instrument. The OCR-250 radiometer (Y001) is a specially designed unit for mapping apertures, plaques, and other two-dimensional apertures or plaques. The field sources were composed of the original SQM and the commercialized SQM-II units.

In the planning for SIRREX-7, equipment diversity was considered an important parameter, because although the plan was to conduct the activity at only one facility, the results were presumed to have wider applicability as long as the equipment diversity and the methods involved with the use of the equipment encompassed the larger community. Consequently, every effort was made to use equipment with different ages, calibration histories, sensitivities, flux levels, etc. The idea was to simulate different aspects of the generalized problem in one experiment.

1.2 OBJECTIVES

The primary objective of SIRREX-7 was a thorough inquiry into the absolute capability of a calibration facility. Although previous SIRREX activities had dealt with many aspects of calibration uncertainties, a definitive quantification of the uncertainties in calibration at a single facility had never been attempted. Selection of the facility was primarily dictated by the calibration choices already being made by the ocean color community, that is, the obvious choice was to select Satlantic, because it is a widely-used facility by SeaWiFS and SIMBIOS investigators.

Because SIRREX-7 required a substantial commitment in time and resources at the hosting facility, there was a strong desire to extract as much information as possible about the equipment and methods normally used in the calibration process. The starting point for considering what specific inquiries should be made was the *Ocean Optics Protocols for SeaWiFS Validation, Revision 1* (Mueller and Austin 1995) which recommends the following methods for calibrations using a 1,000 W FEL standard of spectral irradiance with calibration traceable to NIST and lamp operation in accordance with Walker et al. (1987):

- An irradiance sensor calibration requires the sensor is placed normal to, and at the prescribed distance from, a standard lamp of spectral irradiance. The lamp should provide an irradiance at the sensor that will be at least 30%, and preferably above 50%, of the full-scale response for the channel being calibrated, although this is not always achievable in practice. The calibration environment must be appropriately baffled and draped so that occulting the direct path between the lamp and the sensor produces a response that is less than 0.1% of the response to the lamp flux.
- A radiance sensor calibration requires a standard lamp of spectral irradiance is placed a prescribed distance from a plaque of known lambertian reflectance. The plaque is normal to, and centered on, the lamp calibration axis. The radiance sensor is positioned to view the plaque at an angle of 45° from the plaque normal (any other angle at which the diffuse reflectance of the plaque is known is also acceptable). It must be established that the plaque fills the sensor's field of view (FOV) and that the presence of the sensor case has not perturbed the irradiance on the plaque. The instrument response and dark signal is recorded. It must be verified that the plaque fills the FOV with uniform radiance for each channel of a multichannel radiance sensor. Separate calibration setups may be required for different channels and the lamps may have to be moved as much as 3 m away from the plaque to assure uniform illumination. This procedure is difficult to apply to sensors with a large FOV.
- If a portable irradiance and radiance reference standard will be used to trace instrument stability during field deployments, it should be used immediately following the calibration to establish the instrument response to this reference unit.

The detailed objectives associated with the various aspects of calibration were to:

1. Estimate the uncertainties in lamp standards, including a comparison of the calibration of a new lamp standard by NIST and Optronic Laboratories;
2. Estimate the uncertainties in plaque standards, including the uncertainties associated with plaque illumination non-uniformity;
3. Estimate the uncertainties in radiance calibrations, including the sensitivity to sensor rotation;
4. Estimate the uncertainties in irradiance calibrations, including the sensitivity to sensor rotation;
5. Estimate the uncertainties of SXR measurements;
6. Estimate the rotation and polarization uncertainties of radiometers (including the SXR); and
7. Transfer an absolute calibration to the original SQM and four new SQM-IIs.

Note that the last objective requires a long-term analysis which cannot be satisfied in a single experiment, so the results for it are incomplete.

1.3 AGENDA

During the planning sessions for SIRREX-7, it was clear some of the experiments would be very time consuming, but fortunately they could be automated and would require minimum participation of any operators, e.g., mapping the homogeneity of a plaque takes a lot time and can be executed automatically once it is initiated. Rather than

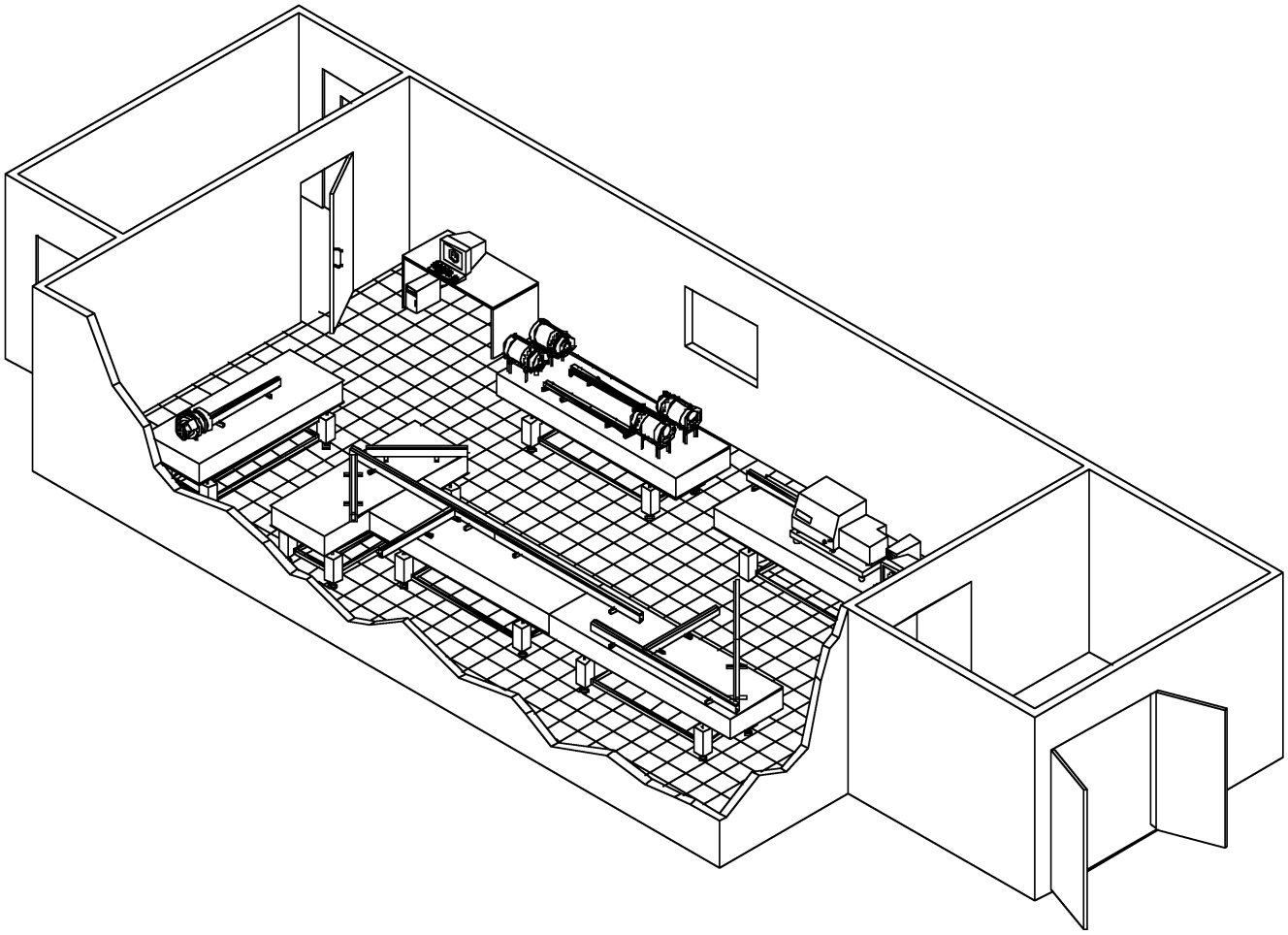

Fig. 1. The Satlantic calibration facility showing the different optical benches (tables) and a simplified configuration of the apparatus used (i.e., most of the ancillary equipment and baffling are not shown).

execute this work when the entire team was assembled, the decision was made to conduct these experiments before or after the main set of experiments. A preliminary number of automated experiments took place between 17–26 February, with the main set of activities requiring participants taking place between 4–12 March; the final activities were completed during 15 March through 7 April.

Some experiments were discussed at previous SIRREXs, but were never actually executed (e.g., a complete inquiry into lamp and plaque calibration uncertainties, as well as the rotation and polarization sensitivity experiments), so there was a high probability that some of these new experiments would have to be refined and repeated once the data were collected and analyzed. Other experiments, like the absolute calibration of the SQMs, required a deployment to the field with a subsequent return to the laboratory before the experiment could be concluded. Consequently, there were several reasons for experiments to extend beyond the main activity. The majority of the experiments were completed during the middle February to early April time period, although, some activities were not completed until as late as August and beyond (Table 2).

1.4 FACILITY

The Satlantic calibration laboratory is a state-of-the-art facility that is contained within a separate $20 \times 38 \times 9$ ft ($6.1 \times 11.6 \times 2.7$ m) room. Entry is via one of two airlocks, and positive pressure is maintained in the room and airlocks to assure a constant outflow of air with the internal doors opened. The air inside the laboratory is exhanged at a rate of approximately 40 times per hour, and the room has thermal control to 20.5 ± 1 C and humidity control to $30 \pm 5\%$.

Within the laboratory, six optical benches or *calibration tables* are arranged alone or in tandem to produce five experimental areas (Fig. 1). For SIRREX-7, four of these were used for the primary experiments, one was used as the master logging station where the start and stop times of the various activities were recorded, and another was used for staging equipment. Accessories and tools for mounting and aligning the optical equipment were stored in shelf and cabinet units near the logging station.

One of the unique features of the calibration laboratory is it is configured within a clean room designed for class

Table 2. A summary of the experimental schedule for SIRREX-7. The activities for each sequential day of the year (SDY) are shown for the morning (0800), afternoon (1300), and evening (1700$^+$). The preliminary work took place between 17–26 February, with the main set of activities taking place between 4–12 March; the final activities were completed during 15 March through 7 April.

Day	*Date*	*SDY*	0800	1300	1700$^+$	*Experiment*
Wednesday	17 February	48		×	×	Plaque Mapping (Broadband)
Thursday	18 February	49		×	×	Plaque Mapping (Broadband)
Friday	19 February	50		×	×	Plaque Mapping (Broadband)
Saturday	20 February	51	×			Plaque Mapping (Broadband)
	20 February	51		×	×	Plaque Mapping (412 nm)
Sunday	21 February	51	×			Plaque Mapping (555 nm)
Wednesday	24 February	55	×	×	×	Plaque Mapping (555 nm)
Thursday	25 February	56	×	×		Laboratory Setup
Friday	26 February	57		×	×	Plaque Mapping (412 nm)
Saturday	27 February	58	×	×	×	Plaque Mapping (412 nm)
Monday	1 March	60			×	Plaque Mapping (412 nm)
Tuesday	2 March	61	×	×	×	Plaque Mapping (Broadband)
Wednesday	3 March	62	×			Plaque Mapping (Broadband)
	3 March	62	×	×		Laboratory Setup
Thursday	3 March	62		×		Laboratory Setup Uncertainties
	4 March	63	×			Preliminary Meeting
	4 March	63	×			Radiometer Polarization Test
	4 March	63		×		GSFC Data Acquisition System Checks
	4 March	63			×	SQM-II Characterization
Friday	5 March	64	×			SQM-II Characterization
	5 March	64		×	×	Plaque Uncertainty
Saturday	6 March	65	×	×	×	Lamp Uncertainty (w/NIST plaque)
Sunday	7 March	66	×	×		Lamp Uncertainty (w/Spectralon plaque)
	7 March	66			×	SQM Aperture Uniformity (1 A Lamps)
Monday	8 March	67	×	×		Lamp Uncertainty (w/Spectralon plaque)
	8 March	67			×	SQM Uncertainty Setup
	8 March	67			×	Irradiance Calibration Uncertainty
	8 March	67			×	SQM Aperture Uniformity (2 A Lamps)
Tuesday	9 March	68	×	×	×	SQM Calibration Uncertainty
	9 March	68	×	×	×	Irradiance Calibration Uncertainty
Wednesday	10 March	69	×	×	×	SQM Calibration Uncertainty
	10 March	69	×	×	×	Radiance Calibration Uncertainty
Thursday	11 March	70	×	×		SQM Calibration Uncertainty
	11 March	70	×	×		Radiance Calibration Uncertainty
	11 March	70		×		SQM High Bank Comparison
Friday	12 March	71	×	×		SQM Calibration Uncertainty
	12 March	71	×			Irradiance Calibration Uncertainty
	12 March	71		×		Radiance Calibration Uncertainty
	12 March	71		×		SXR Polarization Uncertainty Test
	12 March	71			×	End of Experiment Meeting
Tuesday	23 March	85	×			Radiometer Rotation Uncertainty
	23 March	85	×	×		Radiometer Polarization Uncertainty
Thursday	1 April	91	×			Radiometer Rotation Uncertainty
Monday	5 April	95	×	×		SXR Polarization Uncertainty
Wednesday	7 April	97	×			Radiometer Rotation Uncertainty

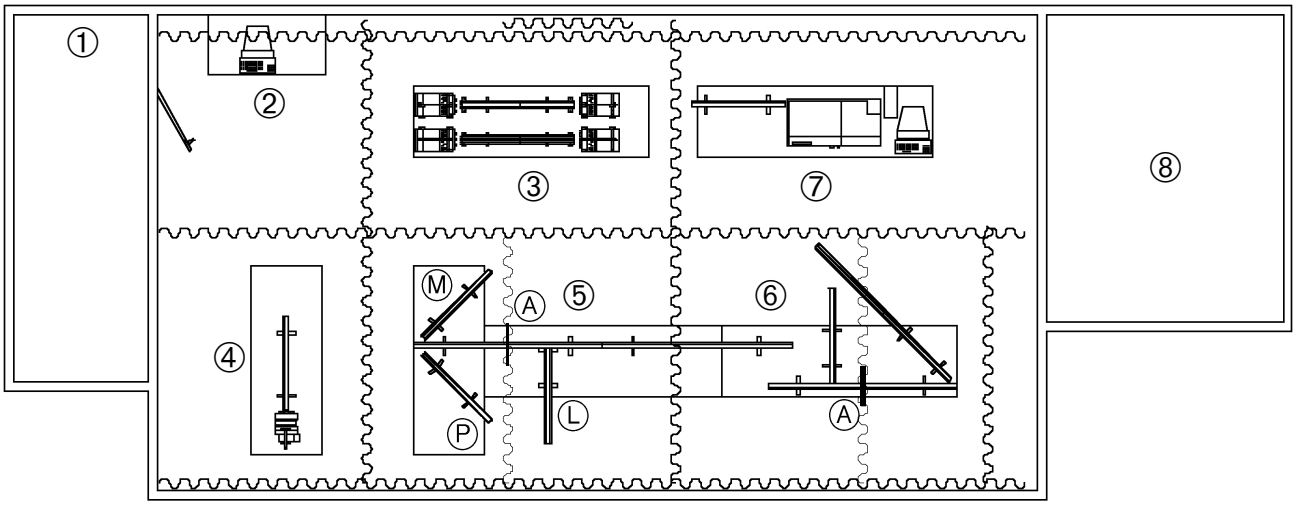

Fig. 2. The baffling in the Satlantic calibration facility showing the partitioning of the space into smaller work areas: 1) personnel and small equipment airlock; 2) master logging station; 3) SQM-II table; 4) SQM table; 5) calibration table 1; 6) calibration table 2; 7) staging area; and 8) large equipment airlock. The $-45°$, $+45°$, and lamp monitoring rails for calibration table 1 are indicated by the M, P, and L bullets respectively. The A bullets indicate adjustable apertures surrounded by black curtains which are used to ensure the plaques used during irradiance calibrations are illuminated primarily by direct light from the standard lamps. Note that calibration table 2 has one 45° rail and a lamp monitoring rail, but because there is only one angled rail, no identification code is required. All of the tables are 3×10 ft (0.9×3 m), except the SQM table and the table holding the two angled rails for calibration table 1.

10,000† operation, but is not certified, and tends to run around the 5,000 level despite the dress code (laboratory coats, outer protective or slip-on shoes, and sticky floor mats in front of the laboratory doors in the airlocks). The room is divided into eight filtration zones each with its own High Efficiency Particle Arrestor (HEPA) filter and return duct, so each area can be closed off (with black curtains) and still maintain the particle count specification.

The walls, doors, and ceilings of the laboratory are painted black with Red Spot™ (Evansville, Indiana) NEXTEL Suede Coating Series 3101 (two-part urethane) paint, and the floors are black vinyl tiles. The NEXTEL coating combines the advantages of an ultra-low gloss texture with outstanding resistance to marking, scuffing, and abrasion. It uniformly scatters incident light, regardless of the incidence angle, and has a uniform (suede-like) appearance. It has a soft *cushioned* feel which is not suseptible to burnishing and helps reduce vibrational sound intensity.

The interior of the room is partitioned into six smaller work areas (Fig. 2) through the use of black curtains (a black curtain also covers the small window shown in Fig. 1). The curtains are a darkroom fabric manufactured by AMCAM, Inc. (Northbrook, Illinois) and are mounted to the ceiling on slides, so they can be moved back and forth for easy access to the work areas. Different room configurations can be produced by opening or closing the partitions (the curtains are held together with black binding clips to prevent light leakage within a partition). *Valences*, made of the same material as the curtains, are used to shield the more reflective surfaces of the room lights which are mounted along the edges of the walls. This is an important point, because several experiments were always going on at the same time, so it was important that any illumination from one experiment had a negligible impact on another.

1.5 PROCEDURES

Several types of data collection activities or procedures were a central part of many of the SIRREX-7 experiments. Rather than present them repeatedly in the following chapters and sections, they are summarized here. The generalized procedures involved a light source (usually a lamp), a light target (a reflectance plaque), and a device under test (DUT) which was usually the sensor to be calibrated. The objectives of each procedure were largely defined by the characteristics of the DUT, which was most frequently a field radiometer, but in some cases, this was a laboratory radiometer that was being used to monitor a target or source as part of the quantification of uncertainties associated with the target or source.

Many of the experiments required the use of more than one recording system at once, so all of the computers used during SIRREX-7 were connected to the Satlantic internal

† The class refers to the number of particles per cubic foot greater than $0.5\,\mu$m which is constantly monitored with a laser particle counter. The metric equivalent of class 10,000 is M5.5.

Table 3. Example entries from the SIRREX-7 Master Log. The temperature of the room is given in degrees Celsius.

Date (SDY)	*GMT*	*Temp.*	*Experiment*	*Event*	*Comments and Notes*
5 March (64)	1913	21.4	1.3 (Table 1)	F-539 Power On	T05816 at 130.0 cm (at 152.08 cm)
	1933	21.4	1.3 (Table 1)	F-539 Ready	8.2003 A and 114.03 V
	1934				Update F-539 log sheet
	1940	21.4	1.3 (Table 1)	Align T05816	Position 30.00 cm (lamp at 130.0 cm)
	1959	21.4	1.3 (Table 1)	SXR Dark	File=S7E13T1LDM01, gain=1, −45° rail
	2009	21.4	1.3 (Table 1)	SXR Ambient	File=S7E13T1LAM01
	2018	21.4	1.3 (Table 1)	SXR Signal	File=S7E13T1L3M01
	2030	21.3	1.3 (Table 1)	R035 Signal	File=S13T1L3A, T05816, +45° rail
	2031				SXR check
	2040	21.3	1.3 (Table 1)	Baffling Change	Improvements to baffling
6 March (65)	2217	20.2	1.2 (Table 1)	H96551 Power On	Set to 8.20 A, total hours=01:00
	2222	20.2	1.2 (Table 1)	SXR Background	File=S7E12T5LBP12
	2240	20.3	1.2 (Table 1)	SXR Signal	File=S7E12T5L5P01, TK299, +45° rail
	2241	20.3	1.2 (Table 1)		8.1968 A, 109.60 V
	2247	20.3	1.2 (Table 1)	H96551 Power Off	8.1969 A, 109.602 V
7 March (66)	1948	21.1	1.7 (Table 1)	F-548 Power Off	8.1960 A, 117.391 V
	1953	21.2	1.7 (Table 1)	F-547 In Box	F-548 to cool down
	1955	21.1	1.7 (Table 1)	F-516 Power On	Set to 8.200 A, total hours=204:50
	1957	21.1	1.7 (Table 1)	SXR Background	File=S7E17T1LBP10
	2017	21.1	1.7 (Table 1)	SXR Signal	File=S7E17T1L0P01, T05816, +45° rail
	2018			F-516	8.1962 A, 113.95 V
	2024	21.1	1.7 (Table 1)	F-516 Power Off	8.1963 A, 113.93 V
	2029	21.1	1.7 (Table 1)	F-548 In Box	F-516 to cool down
	2031	21.1	1.7 (Table 1)	F-137 Power On	Set to 8.000 A, total hours=00:59
	2033	21.1	1.7 (Table 1)	SXR Background	File=S7E17T1LBP11
9 March (68)	1733	20.8	1.7 (Table 1)	SXR Signal	File=S7E11T1L3MP41, T05816
	1738	20.8	1.5 (Table 2)	I097 Dark	File=S7EI097D002
	1741	20.8	1.5 (Table 2)	I097 Signal	File=S7EI097F002
	1742	20.8	1.1 (Table 2)	F-539 Off	8.1968 A, 114.123 V
	1747	20.8	1.5 (Table 2)	I040 Dark	File=S7EI040D003
10 March (69)	1932	22.7	1.1 (Map Table)	S001 Ramp Up	Low bank
	1934	22.7	1.1 (Map Table)	S003 and Q033	File=S7AQ033L305
	1934	22.7	1.4 (Table 2)	R036 Signal	File=S7DR036F009
	1939	22.7	1.1 (Map Table)	S003 and SXR	File=S7E11S3LBXX51, SXR ambient
	1940	22.7	1.1 (Map Table)	S003 and R037	File=S7AR037D305, black fiducial 5
	1940	22.7	1.4 (Table 2)	R067 Dark	File=S7DR067D009
	1942	22.8	1.4 (Table 2)	R067 Signal	File=S7DR067F009
	1948	22.8	1.1 (Map Table)	S003 and R037	File=S7AR037L305
	1952	22.8	1.1 (Map Table)	S003 and SXR	File=S7E11S3LLXX51 and S7AX001L305
	1956	22.9	1.4 (Table 2)	R036 Dark	File=S7DR036D010

(Ethernet) network. One computer was selected as a time server, and all the other computer clocks were synchronized with the server which was set to Greenwich Mean Time (GMT). A separate computer system was used at the master logging station to maintain an electronic record of when experiments started and ended, the file names of the data being recorded, and any other pertinent information. The master log is in excess of 100 pages, so it is not presented here, but a subsample of the type of record keeping used is shown in Table 3. The samples show the type of ancillary variables that were recorded (e.g., lamp current and voltage), and the basic types of data acquisition events (e.g., dark data, lamp power on or off, ambient data, etc.). The room temperature was also recorded to verify that the environment was changing slowly and was basically the same from day to day.

Table 4. Detailed positioning information concerning the seven plaque standards used during SIRREX-7 for the standard lamp-to-plaque distance of 1.3 m. The calibration file name suffixes end with letter codes (`A`, `B`, etc.) which indicate the number of times the plaque was calibrated.

Plaque		*Model*	*Calibration*	*Carrier 1 on Table 1*		*Carrier 2 on Table 2*	
T/N	*S/N*	*No.*	*File Name*	α_1 [cm]	β_1 [cm]	α_2 [cm]	β_2 [cm]
T001	05816	SRT–99–180	`T05816A.FIT`	18.300	30.000	19.373	30.673
T002	13172	SRT–99–180	`T13172H.FIT`	18.427	30.127	19.500	30.800
T003	01873	SRT–99–180	`T01873GU.FIT`	18.415	30.115	19.488	30.788
T004	22463	SRT–99–180	`T22463A.FIT`	18.322	30.022	19.395	30.695
T005	K299	NIST	`TK299A.FIT`	21.176	32.876	22.249	33.549
T006	25322	SRT–99–100	`T25322B.FIT`	19.029	30.729	20.102	31.402
T007	24328	SRT–10–100	`T24328A.FIT`	18.928	30.628	20.001	31.301
			Lamp at 130 cm	152.08 cm		150.75 cm	

At Satlantic, the alignment of a DUT and plaque involves procedures which are a consequence of FOV effects for off-axis viewing, particularly for a multi-aperture sensor (the most common Satlantic sensor). Although sometimes overlooked, these effects can be significant. Considering first a single aperture, approximately 50% of the signal received by a detector comes from angles beyond the angle that defines the FOV. For a properly baffled gershun tube, this light can be restricted to angles less than 23° in air (as defined by the FOV which captures 99% of the light incident on the detector). When this cone is projected onto the plaque at an incidence angle of 45°, the projection covers most of the horizontal extent of the plaque. A radiometer with its optical axis pointed at the center of the plaque can have some of its projected FOV beyond the plaque edges, which results in too low a flux reaching the detector and an overestimate of the calibration coefficient.

For a multi-aperture sensor, such as the Satlantic 13-channel OCR-1000 sensor, the projection of the FOVs of the individual apertures on a plaque rotated 45° is a set of overlapping conic sections, with the longest axis aligned in the horizontal plane (or x-axis) of the plaque. The overlapping conic sections approximately define an oval, the center of which is displaced with respect to the center of the plaque. At Satlantic, the plaque is translated along the illumination axis until these two centers nearly coincide (the difference between α_1 and β_1 or α_2 and β_2 in Table 4 gives the offset values for the plaques used during SIRREX-7 (nominally about 11 cm).

The parameter α is the rail measurement at the face of the plaque optical carrier to obtain the proper plaque-to-lamp distance reference during radiance sensor alignment when the plaque is rotated 22.5° relative to the lamp optical axis. Each plaque-carrier-table combination has slightly different offsets. Note that during alignment (when the laser reflects off a front-surface mirror placed on the face of the plaque), the optical axis of the sensor is aligned perpendicular to the optical axis of the lamp while the sensor is pointed at the center of the plaque.

The parameter β is the rail measurement at the face of the plaque optical carrier to obtain the proper plaque-to-lamp distance reference during radiance sensor calibration when the plaque is perpendicular to the lamp optical axis. The purpose of moving the plaque carrier to the β position is to offset the optical axis of the radiance sensor from the center of the plaque to a position 112 mm from the center such that the 99% FOV of a 13-channel radiometer is entirely on the plaque. A 10° (half angle) FOV (defined as a response of half that at normal incidence) radiometer has a 13° FOV in air.

1.5.1 Data Collection

Four types of data collection were used during the various SIRREX-7 experiments:

Dark Sensor caps were placed on the DUT, so only noise or *dark* voltage levels on the DUT detectors were recorded.

Background The adjustable aperture was closed to prevent any direct illumination of the target by the source, so the DUT measured the indirect light reaching the target, or some other reflective surface within the FOV of the DUT, and then the DUT aperture.

Ambient Direct illumination of the target by the source, but an intervening occulter or *on-axis baffle* blocked the DUT aperture, so only indirect light (from the source and any other light emissions from equipment in the room) reached the DUT aperture.

Signal Direct target illumination by the source with no on-axis baffle, so direct and indirect light reached the DUT aperture.

For many experiments, the SXR was the primary data acquisition unit. Whenever the SXR took data, 11 data records were taken for each channel, and each data record

was composed of the mean of 11 samples, so in total, 121 samples were taken for each of the six channels. This took approximately 7 min. For all of the other radiometers that acquired data during SIRREX-7, they either took data over the same time period used for the SXR, or the acquisition session lasted 3 min. The latter is a standard time interval established with SQM sessions: because most Satlantic instruments sample at 6 Hz, a 3 min acquisition sequence results in 1,080 samples, which is enough data for fast Fourier transform (FFT) analysis.

1.5.2 Alignment of a DUT and a Plaque

The procedures for aligning a DUT with respect to a plaque were as follows:

1. An acid-free, paper cover was placed over the plaque surface, and then a plastic cover with a centering cross was placed over the paper cover. This ensured the plaque surface could not be touched.
2. The lamp was moved out of the optical path using the translator.
3. The positioning screw for the plaque was loosened, so it could be rotated.
4. The front of the plaque carrier was set to the proper alignment value for the calibration table it was on (α_1 for calibration table 1, or α_2 for calibration table 2) as given in Table 4.
5. The alignment laser was powered on, and a front surface mirror was placed over the plaque centering cross.
6. The plaque was rotated 22.5° or until the laser beam struck the center of the radiometer aperture or as close to center as possible.
7. The DUT was placed in its carrier (either a V-block or a ring mount) with the S/N facing up.
8. The height of the DUT was adjusted until the laser beam struck the center of the DUT aperture and the center of the laser. If the ring mount was used, the adjustments involved using the front and back rings by adjusting them in a series of tilting, rotating, raising, and lowering iterations until the laser beam reflected back on itself. If a V-block was used, the adjustments involved raising and lowering iterations until the laser beam reflected back on itself.
9. Occasionally, it was necessary to adjust the angle of the reflectance plaque slightly.
10. The DUT was considered correctly aligned when the laser beam reflected back along its own path and was seen as a red spot on the front of the laser.
11. If the DUT was the SXR, the boresight optic was focused, and then the lens was focused (usually at approximately 90 cm).
12. After the DUT was aligned (and focused if need be), the plaque was rotated back to the center optical rail (around 90°). Once again, the mirror was used to reflect the laser beam back on itself, and the plaque was rotated until the laser beam was directly on the center of the laser.
13. The front of the plaque carrier was set to the proper measurement value for the calibration table it was on (β_1 for calibration table 1, or β_2 for calibration table 2) as given in Table 4.
14. The positioning screw for the plaque was tightened to secure the plaque in place, and the alignment laser was powered off and covered with a black cloth.
15. The lamp was centered by moving the translator to the center mark on the translator.
16. After all alignments were completed, the paper and plastic covers were removed from the plaque.

1.5.3 Powering On a Lamp

The power supplies used at Satlantic for powering on a lamp are capable of many built-in functions that are accessed through a front keypad. This required some programming steps prior to the start of SIRREX-7 which is not recounted here. The powering on of a lamp is concerned with increasing the current to the lamp over a selected time interval to ensure the lamp is not degraded by a sudden application of current. For the Satlantic power supplies, the application of the ramp up in power is a built-in function. The steps involved consisted of the following:

1. The lamp to be used was removed from its storage container.
2. The lamp was placed in the lamp mount and the mounting screws were tightened, thereby properly aligning the lamp.
3. A check was made to ensure the front of the lamp carrier was placed at 152.08 cm (the lamp offset was 4.37 cm) for calibration table 1, and 150.75 cm (the lamp offset was 6.35 cm) for calibration table 2 (Table 4).
4. The lamp was identified within the memory of the current supply by pressing the `Mem` key and turning the dial either left or right until the appropriate lamp number was displayed.
5. The enter (←) key was pressed to select the lamp.
6. The lamp was turned on by pressing the `Lamp` key, and the time of day was recorded on the lamp log sheet.
7. The lamp was warmed up for at least 20 min before any data were recorded.
8. After the warm-up period, the (shunt) resistance standard and lamp current were measured using the voltmeter, and the values were recorded on the lamp log sheet (the voltmeter was nulled before the readings were taken).

9. The lamp was centered by moving the translator to 12.50 mm.

1.5.4 Stray Light Minimization

To ensure minimal contamination from stray light, either from unwanted reflections or extraneous light sources, the following procedures were followed before any data were collected:

1. All equipment that might reflect light was covered with black cloth.
2. All sources of extraneous illumination (i.e., computer screens, voltmeter displays, etc.) were placed outside the area of observation, below the level of the calibration table involved, or otherwise placed to minimize any negative effects.
3. All (baffling) curtains were drawn shut.
4. All unnecessary lights in the calibration facility were turned off.

1.5.5 Powering Off a Lamp

The powering down of a lamp consisted of the following steps:

1. The (shunt) resistance standard and lamp current were measured using the voltmeter, and the values were recorded on the lamp log sheet (the voltmeter was nulled before the readings were taken).
2. The lamp was turned off by pressing the `Lamp` key on the current supply, and the time was recorded in the lamp log.
3. The lamp was allowed to cool for about 15 min.
4. The mounting screws were loosened and the lamp was carefully removed.
5. The lamp was placed in its storage container.

1.5.6 Aligning a Monitor with a Lamp

Aligning a monitoring sensor with a lamp required a previous alignment of the lamp holder with the alignment laser, so all that was needed was the lamp alignment grid and the laser:

1. The front of the lamp carrier was placed at a position of 152.08 cm (the lamp offset was 4.37 cm) for calibration table 1, and 150.75 cm (the lamp offset was 6.35 cm) for calibration table 2 (Table 4).
2. The lamp alignment grid was placed in the lamp holder.
3. The monitoring sensor was mounted on the horizontal rail facing the side view of the lamp with the S/N facing up.
4. The front of the ring carrier was set at 30.50 cm, which was 42.40 cm away from the center of the lamp.
5. The alignment laser was powered on, and the laser beam was reflected off of the lamp alignment grid by rotating the grid (approximately 45°).
6. An aperture cap was placed over the faceplate of the monitoring sensor, and a front surface mirror was held over the center of the cap.
7. The height of the monitoring sensor was adjusted until the laser beam struck the center of the reference faceplate and the center of the laser. If the ring mount was used, the adjustments involved using the front and back rings by adjusting them in a series of tilting, rotating, raising, and lowering iterations until the laser beam reflected back on itself.
8. A check was made to see if the laser beam remained in the center of the faceplate of the monitoring sensor after the aperture cap was removed. If it did, the sensor was deemed to be correctly aligned; if it did not, then the height adjustment of the monitoring sensor was repeated until it was correctly aligned.
9. The alignment laser was powered off and covered with a black cloth.

1.5.7 Aligning a DUT with a Lamp

Aligning a DUT with a lamp required a previous alignment of the lamp holder with the alignment laser, so all that was needed was the lamp alignment grid and the laser:

1. The front of the lamp carrier was placed at a position of 152.08 cm (the lamp offset was 4.37 cm) for calibration table 1, and 150.75 cm (the lamp offset was 6.35 cm) for calibration table 2 (Table 4).
2. A set of rings with a carrier mount or a V-block mount were placed on the center rail, and the front of the carrier was set to the prescribed distance.
3. The DUT was placed in the rings or the V-block, such that the D-shaped collar was firmly up against the inside of the rings or the outside of the V-block.
4. A known spot on the DUT was noted (the S/N facing up or the flat on the D-shaped collar facing down), so the DUT could be repeatedly placed in the rings or V-block in the same orientation.
5. The lamp alignment grid was placed in the lamp holder.
6. The alignment laser was powered on, and the laser beam was transmitted through the alignment grid.
7. An aperture cap was placed over the faceplate of the DUT, and a front surface mirror was held over the center of the cap.
8. The height of the DUT was adjusted until the laser beam struck the center of the DUT faceplate and the center of the laser. If the ring mount was used, the adjustments involved using the front and back rings by adjusting them in a series of tilting, rotating, raising, and lowering iterations until the laser

beam reflected back on itself; if a V-block jig was used, the adjustments involved raising and lowering iterations until the laser beam reflected back on itself.

9. A check was made to see if the laser beam remained in the center of the faceplate of the DUT after the aperture cap was removed. If it did, the DUT was deemed to be correctly aligned; if it did not, then the height adjustment of the DUT was repeated until it was correctly aligned.
10. The alignment laser was powered off and covered with a black cloth.

1.6 SOFTWARE

Three types of software were used to control instrumentation and data acquisition during SIRREX-7: SatView (v1.0d), the SeaWiFS Advanced Radiometer Control System (SeaARCS), and the SeaWiFS Lamp Monitoring and Performance (SeaLaMP). The former was hosted for personal computers (PCs) and is provided by Satlantic for controlling all of their instruments; the latter two were hosted on a Macintosh computer and are custom applications developed by the University of Miami Rosenstiel School for Marine and Atmospheric Science (RSMAS) and the SeaWiFS Project for controlling the SXR and the SQM, respectively. Although previous versions of the two recording environments were very different, recent changes in SatView allow for data file formats that are very similar to the SeaARCS and SeaLaMP protocols. In particular, SatView options now permit time stamps for each data record, timed recording sessions (3 min being the most frequently used during calibration and SQM activities), and the data can be stored as American Standard Code for Information Interchange (ASCII), tab-delimited (spreadsheet) files.

Chapter 2

SIRREX-7 Instrumentation

Stanford B. Hooker
NASA/Goddard Space Flight Center
Greenbelt, Maryland

Scott McLean
Satlantic, Inc.
Halifax, Canada

Abstract

The highest priority for the instrumentation used for SIRREX-7 was to bring together as wide a diversity of equipment used in the laboratory calibration and field measurement process as possible, so the agreed upon minimum number of replicates for a particular equipment type was three. Each participating group contributed more than one example of a particular equipment type, which ensured equipment with a wide range of ages, calibration histories, sensitivities, flux levels, etc. Equipment that was used as part of the digitization or control process, like voltmeters and shunts, were calibrated as close to the SIRREX-7 activity as possible; all other types of equipment were reviewed to ensure their calibration histories were within the guidelines prescribed by the manufacturer or the protocols governing their use (like lamps and plaques). In some cases, equipment that did not meet the recency of calibration requirements were used, so the effect of ignoring this practice (regardless of the reason) could be quantified. In addition, some equipment with known problems were included to see if the outer range of variance in the results was defined by substandard equipment or if other factors (like operator error) were more important.

2.1 INTRODUCTION

The equipment used during SIRREX-7 was representative of the instrumentation used on a regular basis by the ocean color community either for laboratory calibration or field measurements. Although several manufacturers were not represented in the suite of instruments used, the functionality of the missing devices was represented, so individual groups using nonrepresentative equipment can still derive lessons and conclusions from SIRREX-7. With a small number of participants, it was not feasible to accept the added complexity of differing instruments; by using predominantly one manufacturer, it was possible to maximize the number of experiments or the number of replicate samplings within an experiment over the relatively short time period of the activity.

2.2 LAMPS

Many laboratories base their absolute calibrations of irradiance and radiance responsivities on the NIST scale of spectral irradiance, which is available to the wider community through calibrated tungsten–halogen FEL lamps (Walker et al. 1987). Some laboratories acquire a calibrated FEL lamp standard of spectral irradiance directly from NIST, but more typically, a laboratory bases its irradiance scale on a lamp which was calibrated and certified as traceable to the NIST scale by a commercial standardizing laboratory. The former are usually referred to as *secondary* standards, and the latter as *tertiary* standards. In some cases, a laboratory will purchase additional seasoned, but uncalibrated lamps, and transfer the spectral irradiance scale from their primary calibrated lamp using a transfer radiometer (the JRC was experimenting with this approach using L005). The use of less expensive standards for calibration experiments is a common practice in most cases, because it avoids a shortening in the useful lifetime of the primary reference lamp. One of the questions addressed here is what extra uncertainty is associated with this cost-effective practice.

Another type of lamp is the so-called *working lamp*. This lamp is used for illumination requirements in keeping with FEL light levels wherein it would not be prudent or cost effective to reduce the lifetime of a standard lamp. Detailed information about the standard and working lamps used during SIRREX-7 is presented in Table 5. The former are indicated by the "L" codes and the latter by the "W" codes.

Table 5. Detailed information about the 10 secondary and tertiary lamp standards and the 8 working lamps used during SIRREX-7. The secondary lamps are shown with the T/N codes in bold (L001 is not considered a secondary standard, even though it is a NIST lamp, because it was damaged at a previous point in its history). The calibration file name is provided for completeness. The operating current is given in amps and the lamp usage time is given in hours and minutes (*hh*:*mm*). Note that lamp F-550 (L010) was calibrated twice: once by Optronic and then by NIST (Sect. 3.3).

T/N	*Manufacturer*	*Owner*	*S/N*	*Calibration Date and Group*	*File Name*	*Current*	*Time*
L000	Sylvania	Satlantic	F-516	30 June 1998 Optronic	F516.FIT	8.200	68:55
L001	GE	NASA	F-137	1 December 1982 NIST	F137N.FIT	8.000	0:55
L002	GE	NASA	F-182	18 October 1984 NIST		7.900	
			F-182	28 August 1994 NIST	F182N.FIT	7.900	4:10
L003	GE	Satlantic	F-539	24 January 1999 Optronic	F539.FIT	8.200	6:16
L004	Sylvania	JRC	H97505	23 May 1997 Hoffman	H97505B.FIT	7.308	16:00
L005	Sylvania	JRC	H96551	18 July 1997 JRC†	H95661.FIT	8.200	1:00
L006	GE	Satlantic	F-536	20 December 1998 Optronic	F536.FIT	8.200	55:52
L007	Sylvania	Satlantic	F-409	21 July 1996 NIST	F409N.FIT	8.000	9:57
L008	GE	Satlantic	F-547	26 February 1999 Optronic	F547.FIT	8.200	0:00
L009	GE	Satlantic	F-548	26 February 1999 Optronic	F548.FIT	8.200	0:00
L010	GE	NASA	F-550	24 March 1999 Optronic		8.200	
			F-550	15 April 1999 NIST	F550N.FIT	8.200	0:00
W001	Sylvania	Satlantic	F-360	20 September 1995 Optronic	F360.FIT	8.000	90:05
W002	Sylvania	Satlantic	F-407	6 August 1997 Optronic	F407.FIT	8.000	80:38
W003	Sylvania	Satlantic	F-444	14 February 1997 Optronic	F444.FIT	8.000	71:34
W004	Sylvania	Satlantic	F-497	13 January 1997 Optronic	F497.FIT	8.000	83:02
W005	Sylvania	Satlantic	F-505	20 March 1998 Optronic	F505.FIT	8.200	110:02
W006	Sylvania	Satlantic	F-511	14 March 1998 Optronic	F511.FIT	8.200	107:29
W007	GE	Satlantic	F-524	29 September 1998 Optronic	F524.FIT	8.200	102:09
W008	GE	Satlantic	F-528	29 September 1998 Optronic	F528.FIT	8.200	92:33

† An unseasoned lamp intercalibrated by JRC using NIST lamp F-466 (not used in the SIRREX-7 activity) as a reference and a Spectrum Engineering spectrometer SE-590.

A subset of the primary and secondary standards was created from the most *trusted* lamps: L002 (F-182), L003 (F-539), L007 (F-409), L008 (F-547), and L009 (F-548). This level of trustworthiness was based on the calibration source (NIST lamps are considered the most trustworthy), and the experience of the user with the lamp. The remaining lamps were not considered as trustworthy, because of known or potential problems:

- L000 F-516 had been used too long a time period (more than 60 h);
- L001 F-137 was mistreated at a previous point in its history (plastic melted on the glass);
- L004 H97505 was calibrated by Hoffman Engineering, Inc., and is NIST traceable, but it is operated at a low current level (about 7.3 A) with respect to the other FEL lamps (approximately 8.0 A);
- L005 H96551 is not NIST traceable and was unseasoned (i.e., it was not *burned* for 50 h prior to calibration)—it was calibrated with respect to a NIST lamp by the JRC to evaluate the accuracy of a simple irradiance calibration transfer through a Spectrum Engineering spectrometer SE-590;
- L006 F-536 had been used too long (almost 60 h); and
- L010 F-550 was reserved for an evaluation of Optronic calibrations.

2.3 PLAQUES

Many laboratories use reflectance plaques to convert known spectral irradiance from a lamp to calculated spectral radiance when the plaque is viewed by a radiometer at fixed angles of illumination and reflection. In some cases, the FEL lamp and plaque source of spectral radiance are used directly to calibrate a field radiometer. In other cases, it is used to calibrate a stable transfer radiometer, which may then be used to transfer the radiance scale to an integrating sphere, which can provide a larger and more uniform source of diffuse radiance.

Small 2.25 in (5.715 cm) pressed polytetrafluoroethylene (PTFE) plaques are available from NIST as primary standards of known reflectance. At most laboratories, however, plaques are used in routine laboratory and field measurements and are usually fabricated from Spectralon, a sintered version of halon. For comparison at SIRREX-7,

Table 6. Detailed information about the seven reflectance standards (plaques) used during SIRREX-7. The size of each plaque is given in inches and is the diameter of the reflectance material (all of the plaques are square except S/N K299 which is circular). The 18 in plaques are constructed from two pieces of Spectralon, so there is a seam down the center of the plaque. With the exception of plaque T003, all of the 18 in white plaques were being used for calibration activities. T003 was not being used for calibrations—it was included to quantify the effects of using an old plaque. Note that all of the plaques are white with the exception of S/N 24328, which is gray.

T/N	*Manufacturer*	*Owner*	*S/N*	*Calibration Date and Group*	*Color*	*Size*	*Material*
T001	Labsphere	Satlantic	05816	25 November 1998 Labsphere	White	18.00	Spectralon
T002	Labsphere	Satlantic	13172	10 October 1998 Labsphere	White	18.00	Spectralon
T003	Labsphere	Satlantic	01873	27 March 1998 Labsphere	White	18.00	Spectralon
T004	Labsphere	JRC	22463	23 April 1998 Labsphere	White	18.00	Spectralon
T005	NIST	NASA	K299	27 February 1999 NIST	White	2.25	PTFE
T006	Labsphere	NASA	25322	22 February 1999 Labsphere	White	10.00	Spectralon
T007	Labsphere	NASA	24328	22 February 1999 Labsphere	Gray	10.00	Spectralon

18 in (45.72 cm) Spectralon plaques were contributed by Satlantic and JRC; NASA contributed the PTFE plaque and two 10 in (25.4 cm) Spectralon plaques. All of the plaques were white except for one of the 10 in plaques which was gray. Table 6 presents detailed information about the plaques used during SIRREX-7. Note that T003 was not being used for calibrations—it was included to quantify the effects of using an old plaque.

Radiance calibration activities require a uniform source of known radiance that completely fills the angular FOV of the radiance sensor. The two most common procedures for accomplishing this requirement involve either i) a lamp standard of spectral irradiance placed at a prescribed distance from a plaque of known lambertian reflectance, or ii) an integrating sphere with an exit port of sufficient size to completely fill the FOV of the radiance sensor. Because no integrating spheres are used by the SIRREX-7 participants, the emphasis was necessarily on plaques illuminated by FEL lamps.

The gray plaque was included because gray plaques are used in the field as part of above-water protocols for measuring *in situ* radiance. The nominal 10% reflectance of gray plaques permits radiometers with typical above-water saturation values to make *in situ* measurements without saturating (approximately $6\,\mu\mathrm{W\,cm^{-2}\,nm^{-1}\,sr^{-1}}$). Unlike the 99% reflectance of pure (white) Spectralon plaques used for laboratory calibrations, gray plaques are much less lambertian, because of the added impurities of the black doping material.

Any time a plaque is used for calibrations, the homogeneity of the plaque should be checked at a minimum of four spots on the plaque surface, and variations greater than 2% between the spots should eliminate the use of the plaque for any calibration work. A directional/directional (i.e., 0°/45°) plaque calibration, instead of the standard directional/hemispherical calibration was used for this activity, because this is the actual viewing geometry used during the calibration process.

Although Spectralon is very hydrophobic, it readily absorbs grease and oil which are very difficult to remove and can cause significant variance in calibrations. Special precautions must be taken to avoid touching the diffusive material thereby transfering contaminants to the plaque surface. During SIRREX-7, all plaques were kept in a mount with an acid-free paper cover.

2.4 COMMERCIAL RADIOMETERS

Three classes of commercial radiometers (Table 1) were used during SIRREX-7: the OCI-200 and OCR-200 are 7-channel radiometers that use 16-bit analog-to-digital (A/D) converters and are capable of detecting light over a four decade range; the OCR-1000 is a 13-channel radiometer that uses 24-bit A/D converters, and is capable of detecting light over a seven decade range; and the OCR-2000 is a hyperspectral instrument with 132 channels (each with a 10 nm bandwidth) and 18-bit A/D converters. A summary of the channel numbers and center wavelengths (in nanometers) for the radiometers used during SIRREX-7 is presented in Table 7.

Most of the radiometers were designed for in-water measurements of downwelling irradiance (E_d), upwelling irradiance (E_u), or upwelling radiance (L_u): I040, I050, and I097 measure $E_d(\lambda)$; I098 measures $E_u(\lambda)$; and R035, R036, R037, R067, and Q033 measure $L_u(\lambda)$. E_u sensors are more sensitive (have higher gains) than comparable E_d sensors which influences the calibration distances they can be used with; it also influences their suitability to alternative light sources, like the SQM, particularly in the blue part of the spectrum.

2.5 SXR

One of the original concepts to be tested in the SIREX activity was to verify the sources and calibration setup procedures at individual calibration facilities for both

Table 7. Channel numbers and center wavelengths (in nanometers) for the radiometers used during SIRREX-7. The sensors are presented according to their measurement types which includes their full-angle FOV (FAFOV) measured at full width, half maximum (FWHM). In-water irradiance sensors are identified by the letter "I", in-water OCR-200 sensors (20° FAFOV) start with the letter "R" and in-water OCR-1000 sensors (20° FAFOV) with the letter "Q", above-water radiance sensors (6° FAFOV) start with the letter "T", and the SXR (2.4° FAFOV) is identified by the letter "X". The band sets are a direct reflection of the primary purpose of the sensors, which is to support SeaWiFS calibration and validation activities. All of the channels have 10 nm bandwidths.

Chan-	*OCI-200*					*OCR-200*					*SXR*	*OCR-1000*
nel	I040	I050	I097	I098	I121	R035	R036	R037	R064	R067	X001	Q033
1	411.5	411.3	412.3	412.4	411.1	411.1	411.6	411.0	412.7	412.5	411.2	406.5
2	442.5	442.5	442.1	443.5	442.9	442.9	442.7	442.8	443.5	442.2	441.5	412.2
3	489.3	489.3	490.5	490.8	489.9	489.9	489.9	489.8	490.0	490.9	486.9	435.3
4	509.6	509.1	510.3	509.9	509.7	509.7	510.3	509.7	781.9	510.3	547.9	443.4
5	555.4	554.8	554.5	554.7	555.0	554.8	554.2	555.0	510.9	554.5	661.7	455.9
6	665.7	666.0	665.7	664.9	665.5	665.0	665.3	664.8	554.6	665.4	774.8	489.9
7	683.2	682.9	683.8	683.2	683.7	683.1	683.8	682.7	666.4	684.0		510.4
8												531.6
9												554.6
10												590.3
11												665.1
12												670.0
13												700.6

spacecraft and *in situ* instruments. To do so required an accurate, stable, and portable radiometer, a so-called transfer radiometer, designed specifically for SeaWiFS calibration applications. The SXR was designed and built by the Optical Technology Division at NIST in collaboration with the SeaWiFS Project. It is a six-channel radiometer with four gain settings calibrated for spectral radiance over the (approximate) wavelength range of 400–800 nm (Johnson et al. 1998a). Each channel consists of a temperature-stabilized silicon detector, a narrow bandpass interference filter, and a precision current-to-voltage amplifier. The 2.4° full angle field-of-view (FAFOV) aperture is imaged onto the six detectors, and can be boresight focused from approximately 0.85 m to infinity.

The SXR was used at SIRREX-2 through SIRREX-4, the Marine Optical Buoy (MOBY) support facility in Honolulu (Hawaii), and at NEC in Yokohama (Japan) during an Ocean Color and Temperature Sensor (OCTS) integrating sphere comparison (Johnson et al. 1997). It has proved to be a reliable transfer radiometer, with an uncertainty in radiance repeatability of less than 0.1% and an estimated uncertainty of approximately 1.5% in radiance responsivity at all wavelengths.

2.6 SQM

Another instrumentation need that was identified early in the activities of the SeaWiFS Project was for a portable source that would allow routine stability checks between radiometer calibrations in the field. Instrumental drift from filter deterioration and transportation stresses, which can cause shifts in the radiometric response of a device, must be tracked. Because no commercial device was available, the SeaWiFS Project teamed with the NIST Optical Technology Division to produce one. The engineering design and characteristics of the SQM are described by Johnson et al. (1998b), so only a brief description is given here. A separate rack of electronic equipment, composed principally of two computer-controlled power supplies and a multiplexed, digital voltmeter (DVM), are an essential part of producing the stable light field. The SQM does not have, nor does it require, an absolute calibration, but it has design objectives of better than 2% stability during field deployments.

The SQM has two sets of halogen lamps with eight lamps in each set; both lamp sets are arranged symmetrically on a ring and operate in series, so if one lamp fails, the entire set goes off. The lamps in one set are rated for 1.06 A (4.2 V) and are operated at 1.01 A, and the lamps in the other set are rated for 2.00 A (5.0 V) and are operated at 1.95 A; the lamp sets are hereafter referred to as the 1 A and 2 A lamps, respectively. The lamps are operated at approximately 95% of their full amperage rating to maximize their lifetimes.

A low, medium, and high intensity flux level is provided when the 1 A, 2 A, and both lamp sets are used, respectively. Each lamp set was *aged* for approximately 50 h before deploying the SQM to the field. The interior light chamber has bead-blasted aluminum walls, so the diffuse

component of the reflectance is significant. The lamps illuminate a circular, blue plastic diffuser protected by safety glass and sealed from the environment by o-rings. The safety glass is composed of two pieces of glasses with a thin white diffuser in the middle. The diffuser is resilient to ultraviolet yellowing, but can age nonetheless. The exit aperture is 20 cm in diameter and has a spatial uniformity of 98% or more over the interior 15 cm circle.

A faceplate or *shadow collar* provides a mounting assembly, so the DUT, usually a radiance or irradiance sensor, can be positioned in the shadow collar. The DUT has a D-shaped collar (Fig. 3) fitted to it at a set distance, 3.81 cm (1.5 in), from the faceplate (front) of the DUT. This distance was chosen based on the most restrictive clearance requirement of the radiometers used in the different field campaigns.

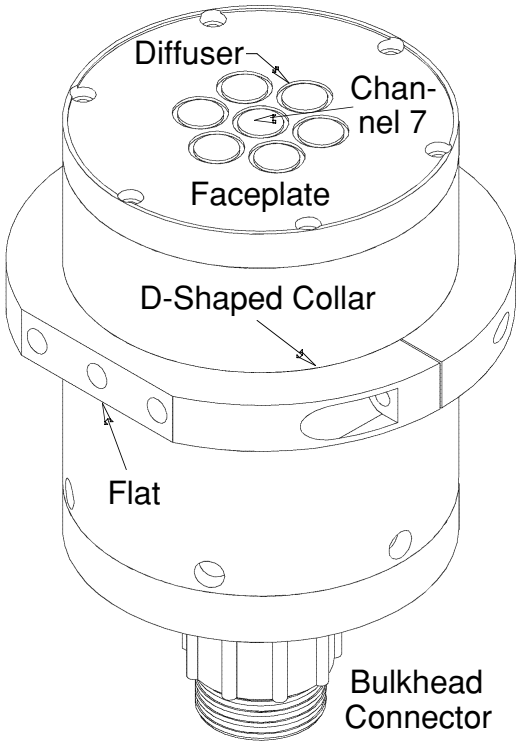

Fig. 3. An OCI-200 (irradiance) sensor fitted with a D-shaped collar. The flat side on the collar has three $1/4\,\text{in} \times 20$ taps which can be used, in addition to the collar itself, for fixing the orientation of the sensor in jigs or mounting brackets. Note that channel 7 is the centermost diffuser. The OCI-1000 sensors have six additional channels arranged symmetrically around the outermost ring of diffusers.

The D-shaped collar ensures the DUT can be mounted to the SQM at a reproducible location and orientation with respect to the exit aperture each time the DUT is used. The former minimizes uncertainties (principally with irradiance sensors) due to distance differences between measurement sessions, while the latter minimizes uncertainties (principally with radiance sensors) due to inhomogeneities in the exit aperture light field. In either case, the D-shaped collar keeps these sources of uncertainties below the 1% level.

The SQM faceplate can be changed to accept a variety of instruments from different manufacturers (although, this was not necessary during SIRREX-7). Radiometers above a certain size, approximately 15 cm, would be difficult to accomodate, but the entire mounting assembly can be changed to allow for reasonable viewing by seemingly difficult to handle radiometers. To date, three radiometer designs from different manufacturers have been used with the SQM, and there were no problems in producing the needed faceplates, D-shaped collars, or support hardware to accomodate these units.

The SQM light field can change because of a variety of effects; for example, the presence of the DUT, the aging of the lamps (which usually reduces the flux output, but can occasionally result in temporary increases in flux levels), a deterioration in the plastic diffuser, a change in the transmittance of the glass cover (and plastic diffuser, if used), a drift in the control electronics, a repositioning of a mechanical alignment, etc. To account for these changes, three photodiodes, whose temperatures are kept constant with a precision thermoelectric cooler ($\pm 0.01\,\text{K}$), measure the exit aperture light level: the first has a responsivity in the blue part of the spectrum, the second in the red part of the spectrum, and the third has a broadband or *white* response. All three internal monitors view the center portion of the exit aperture. The back of the SQM is cooled by a three-position fan to prevent a build up in temperature beyond what the thermoelectric cooler can accomodate. The SQM has an internal heater to help maintain temperature stability in colder climates and to shorten the time needed for warming up the SQM.

Another SQM quality control procedure is provided by three special DUTs called *fiducials*: a white one, a black one, and a black one with a glass face (the glass is the same as that used with the Satlantic field radiometers). A fiducial has the same size and shape of a radiometer, but is nonoperational. The reflective surface of a fiducial is carefully maintained, both during its use and when it is not being used (so it is always kept in a foam-lined carrying case). Consequently, the reflective surface degrades very slowly, so over the time period of a field expedition, it remains basically constant. A field radiometer, by comparison, has a reflective surface that changes episodically from the wear and tear of daily use. This change in reflectivity alters the loading of the radiometer on the SQM light chamber and is a source of variance for the monitors inside the SQM which are viewing the exit aperture, or the radiometer itself when it is viewing the exit aperture. The time series of a fiducial, as measured by the internal monitors, gives an independent measure of the temporal stability of the light field.

Table 8. Detailed information about the SQM and SQM-IIs used during SIRREX-7. The 1.05 A (4.2 V) lamps are model 187 from Gilway Technical Lamp (Woburn, Massachusetts). The 1.06 A (4.25 V) and 2.00 A (5.0 V) lamps are model 01218 and 01123, respectively, from Welch Allyn (Skaneateles Falls, New York). The amount of time on each lamp set does not include the seasoning time: 50 h for the SQM 1.05 A lamps, and 100 h for all the others.

T/N	Model	*S/N*	*Manufacturer and Date*			*Lamps*	*Time* [*hh*:*mm*]
S000	SQM	001	Reyer Corp.	March	1996	1.05 A , 2.00 A	430:34 , 0:34
S001	SQM-II	001	Satlantic, Inc.	December	1997	1.06 A , 2.00 A	0:00 , 0:00
S002	SQM-II	002	Satlantic, Inc.	September	1998	1.06 A , 2.00 A	0:00 , 0:00
S003	SQM-II	003	Satlantic, Inc.	December	1998	1.06 A , 2.00 A	0:00 , 0:00
S004	SQM-II	004	Satlantic, Inc.	February	1999	1.06 A , 2.00 A	0:00 , 0:00

2.7 SQM-II

The SIMBIOS Project provided some initial funding to offset the costs associated with designing a commercial prototype of the original SQM produced by NASA and NIST. This commercialization effort resulted in two new instruments: the SQM-II manufactured by Satlantic, Inc. (Halifax, Canada), and the OCS-5002 manufactured by Yankee Environmental Systems, Inc. (Turners Falls, Massachusetts).

The main difference between the original SQM and the SQM-II is the high degree of integration in the latter. The SQM is a modular design composed of several separate subsystems, whereas the SQM-II consists of two components: the SQM-II and a deck box that provides direct current (DC) power. The latter contains the lamp rings (which use the same lamps as the original SQM), heating and cooling subsystems, control circuitry, the system computer, plus display and data storage. The SQM-II system is designed to be self contained and does not require a PC to operate. Only two cables are required to complete system assembly: an alternating current (AC) power cord for the deck box and a DC power cord to link the deck box to the SQM-II. Although this integration reduces system complexity, it comes with reduced flexibility; a failure in any one of the subsystems can render the entire system inoperable with no opportunity for simply swapping in a new (external) subassembly (like a power supply or DVM), and if a different combination of bulb wattages in excess of the design limits are wanted, higher wattage power supplies cannot be quickly substituted. As was done with the original SQM, Satlantic recommends running the SQM-II on an uninterruptable power supply (UPS), and this was done during SIRREX-7.

User input to start and monitor the SQM-II is via a simple 4-button keypad and a 4×20 fluorescent display at the rear of the device. Commands can be entered using the menus on the display or remotely from a PC (through a serial interface). A PC can also be connected to the system to log data during a calibration evaluation and radiometric testing (CERT) session, or the data can be stored internally in a flash card and downloaded later. The differences between the two SQM units are not restricted to their control architecture. The SQM-II has many improvements that use of the original SQM showed were desirable under different circumstances:

1. The bulbs are mounted at the front, facing away from the exit aperture, which increases the average path length of the light emitted by each bulb, and it makes it easier to service the lamps (individually and as a subassembly);
2. The inside of the light chamber is lined with white (99% reflectance) Spectralon, so the emitted flux is higher, and the aperture uniformity is greater; and
3. At 490 nm and with identical 1 A lamps, the SQM-II is approximately seven times more intense than the SQM (the apparent blackbody temperature of the SQM-II is 3,100 K, whereas, for the SQM it is about 2,400 K);

Although the greater flux of the SQM-II is a desirable attribute for the blue part of the spectrum, the high output in the red saturates many in-water field radiometers. This was subsequently corrected by adding a blue filter to the exit aperture.

A detailed comparison of the attributes of the SQM and SQM-II units used during SIRREX-7 is presented in Table 8.

2.8 XZ-Mapper

The filters used with the xz-mapping radiometer were as follows (the number in brackets is the bandwidth of the filter in nanometers):

- 600 nm short pass filter (Oriel model 57377),
- 412[9] nm (lot 8GEB; FID 30),
- 555[9] nm (lot 7FDY; FID 94),
- 412[20] nm (lot 7DAW; FID 50), and
- 555[20] nm (lot 7DAX; FID 3).

There are separate filter holders for the broadband and narrowband filters. Both filter holders slide onto the front

Table 9. Detailed information about the ancillary equipment used during SIRREX-7. OL83A S/N 99115110 blew a fuse on 12 March (1440). This has been a recurring problem with the Optronic power supplies (which is why S/N 96115058 was rewired to operate on 240 V).

Type	*T/N*	*Model*	*S/N*	*Manufacturer*	*Calibration Date and Company*
Current Source	C001	OL83A	99115110†	Optronic	26 February 1999 Optronic
	C002	OL83A	96115058	Optronic	1 March 1999 Optronic
	C003	OL83DS	93200490	Optronic	10 February 1999 Optronic
Volt-meter	V001	HP34401A	US36037038	Hewlett Packard	18 November 1998 Pylon
	V002	HP34401A	3146A09840	Hewlett Packard	17 February 1999 Pylon
	V003	HP34401A	3146A28915‡	Hewlett Packard	22 January 1999 Hewlett Packard
Shunt	Z001	LN4222	1551570	Leeds & Northrup	9 October 1996 Tucker
	Z002	RUG-ZR100-0.1	008308-C36814	Isotex	1 October 1998 Pylon

† Operates on 240 V; the other current sources operate on 120 V.
‡ Part of the SXR data acquisition system.

of the mapping detector. The narrowband filters simply slide into the holder and sit against the edge of the mapping detector. Care must be used when removing the filter holder from the mapping detector, because the narrowband filter tends to stick to the mapping detector. The broadband filter holder contains a retaining ring on the front that unscrews easily.

2.9 ANCILLARY EQUIPMENT

A variety of ancillary equipment was used during the SIRREX-7 experiments to provide stable lamp power, voltage measurements, etc. A detailed comparison of the attributes of the most important ancillary equipment used is presented in Table 9.

Chapter 3

Uncertainties in Lamp Standards

Stanford B. Hooker
NASA/Goddard Space Flight Center
Greenbelt, Maryland

Giuseppe Zibordi
JRC/SAI/Marine Environment Unit
Ispra, Italy

Scott McLean
Jennifer Sherman
Satlantic, Inc.
Halifax, Canada

Abstract

The uncertainties associated with the use of lamp standards was estimated by using several lamps with different calibration histories to illuminate a NIST reflectance standard (T005), and then comparing the calibrated radiance from the plaque (calculated from the calibrated reflectance of the plaque and the calibrated irradiance from the lamp), with that measured by the SXR. The average uncertainty of the most *trusted* lamps, those with no known problems and established good performance capabilities, was approximately 1.2%. All of the lamps had a calibration repeatability less than 0.5%, and all of the lamps except one had a repeatability less than 0.2%. A comparison of an Optronic calibration of an FEL lamp with a NIST calibration of the same lamp showed an overall average agreement to within approximately 1.3%. A similar comparison exercise executed as a part of SIRREX-5 showed the Optronic calibration of FEL F-409 differed from the NIST calibration by an average of approximately 2.6%, whereas a second calibration by Optronic differed from the NIST calibration by about 0.8%.

3.1 INTRODUCTION

Three experiments were conducted to examine the uncertainties associated with using lamps during calibrations. The first involved using a NIST reflectance standard and the SXR to estimate the uncertainties in using Labsphere (Spectralon) plaques, the second quantified how much of the variability in calibrations is due to changes in the lamp from one calibration session to the next, and the third compared the NIST and Optronic calibrations for a newly purchased lamp.

3.2 LAMP UNCERTAINTIES

The uncertainties associated with the use of lamp standards was estimated by using several lamps with different calibration histories to illuminate a NIST reflectance standard (T005), and then comparing the calibrated radiance from the plaque (calculated from the calibrated reflectance of the plaque and the calibrated irradiance from the lamp), with that measured by the SXR. A monitoring sensor (R035) was mounted on the rail opposite the SXR to provide an independent measure of the illumination stability of the plaque.

3.2.1 Equipment

The equipment used for determining the uncertainties in lamp standards involved the following:

- Satlantic NIST lamp F-409 (L007), and SeaWiFS NIST lamps F-182 (L002) and F-137 (L001);
- JRC Hoffman Lamps H97505 (L004) and H96551 (L005);
- Satlantic Optronic lamps F-539, F-536, and F-516 (L003, L006, and L000, respectively), plus two new Satlantic Optronic lamps F-547 (L008) and F-548 (L009);
- NIST plaque K299 (T005);
- The SXR (X001) with custom mount and digital voltmeter (V003);

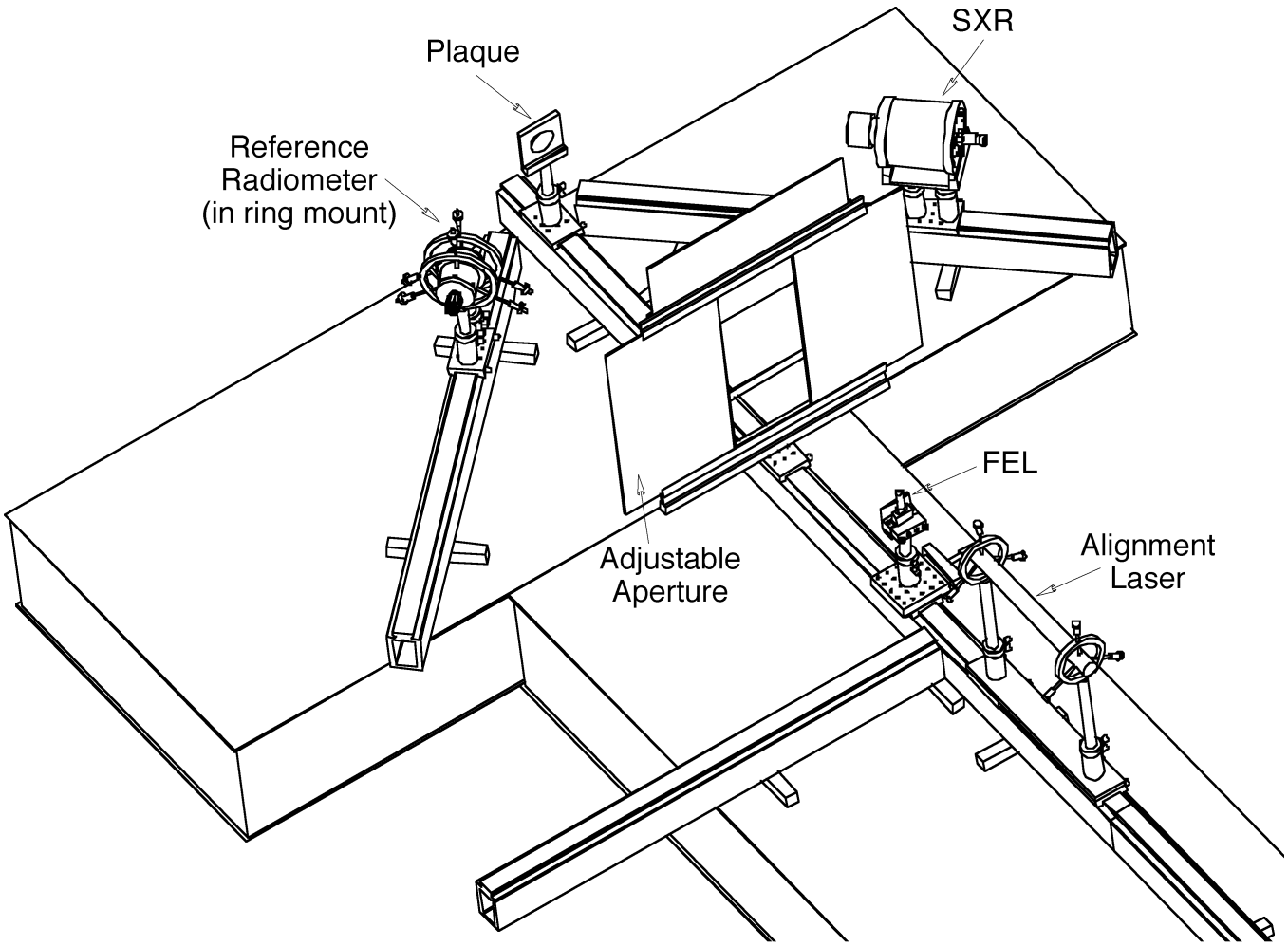

Fig. 4. The experimental setup for determining the uncertainties in lamp standards. The rightmost 45° rail was designated the positive rail, while the leftmost 45° rail was designated the negative rail.

- OCR-200 R035 with DATA-100 (S/N 043);
- Current sources OL83A 96113058 (C002) and 83DS 93200490 (C003);
- Shunt resistor 1551570 (Z001);
- Voltmeter 3146A09840 (V002); and
- Lamp mount, ring mount, plaque mount, four carriers, and alignment laser LHRR-055 (S/N 3598–1592–65).

The FEL lamps were divided into two groups based on whether or not there were any known or potential problems with the lamp. Lamps with no known or expected defects were considered *trustworthy*. The problematic lamps were L000 (F-516), which had been used for more than 60 h; L001 (F-137), which was slightly damaged at a previous point in its history; L004 (H97505), which is operated at a low current level; L005 (H96551), which was unseasoned and intercalibrated by the JRC in an experiment to see if the spectrometer they had available was capabable of trustworthy calibrations; and L006 (F-536), which had been used for almost 60 h. The trustworthy lamps for this experiment were, therefore, L002 (F-182), L003 (F-539), L007 (F-409), L008 (F-547), and L009 (F-548). Lamp L010 (F-550) was reserved for intercomparing the calibration supplied by Optronic with respect to NIST and was used for no other purpose.

3.2.2 Procedures

The SXR (X001) was placed on the −45° rail on calibration table 1 and secured in its custom carrier mount. The front of the carrier was placed at 75 cm on the rail and the aperture was set to $f1.4$. The NIST plaque (T005) was placed on the center rail in the proper carrier mount. The SXR was aligned and focused with respect to the plaque following the procedures given in Sect. 1.5.2.

As shown in Fig. 4, the experimental setup included a monitoring sensor (R035), which was mounted on the +45° rail using the ring carrier. The front of the ring carrier was placed at 30.0 cm on the rail. The reference radiometer was aligned with respect to the plaque following the procedures

given in Sect. 1.5.2. The lamp being used was aligned and powered on following the procedures given in Sect. 1.5.3. The aperture was adjusted so there were no shadows or diffraction edges on the plaque, and any stray light was minimized by following the practices given in Sect. 1.5.4.

The first step in collecting calibration data was placing aperture caps on the reference radiometer and the SXR, after which, dark readings were taken. The reference radiometer and SXR data were recorded using SatView and SeaARCS software, respectively. After the darks were completed, background data were recorded with the sensor caps removed, but the lamp aperture was closed, so there was no direct illumination of the plaque. The lamp aperture was then opened and signal data were recorded. The lamp was turned off following the practices given in Sect. 1.5.5.

The next lamp was selected, and the entire process was repeated until all of the lamps were measured three times (using the same plaque for each lamp). Note that all of lamps were powered on and off independently, but the plaque was not independently repositioned for each trial.

3.2.3 Results

The estimation of lamp uncertainties requires the reflectance of the NIST plaque (T007), $R_{T7}(\lambda)$, and the SXR radiance measurements of the plaque, $L^{X1}_{T_{\rm ID}}(\lambda)$. The irradiance of the lamp for trial t_i, $E^{50}_{L_{\rm ID}}(\lambda, t_i)$, is calculated as

$$E^{50}_{L_{\rm ID}}(\lambda, t_i) \;=\; \frac{\pi\, L^{X1}_{T_{\rm ID}}(\lambda, t_i)}{R_{T7}(\lambda)} \left[\frac{d}{50\ {\rm cm}}\right]^2 , \qquad (1)$$

where $L_{\rm ID}$ is the lamp identification code, and d is the distance from the lamp to the plaque measured in centimeters.

The RPD, δ, in irradiance is calculated as

$$\delta^{X1}_{L_{\rm ID}}(\lambda, t_i) \;=\; 100\, \frac{E^{50}_{L_{\rm ID}}(\lambda, t_i) \;-\; E^{\rm cal}_{L_{\rm ID}}(\lambda)}{E^{\rm cal}_{L_{\rm ID}}(\lambda)} \;, \qquad (2)$$

where $E^{\rm cal}_{L_{\rm ID}}(\lambda)$ is the calibrated spectral irradiance supplied with the lamp or the calibration facility. The average RPD, $\bar{\delta}$, is defined as

$$\bar{\delta}^{X1}_{L_{\rm ID}}(\lambda) \;=\; \frac{1}{N} \sum_{i=1}^{N} \delta^{X1}_{L_{\rm ID}}(\lambda, t_i) \;, \qquad (3)$$

where N is the total number of replicates executed for the lamp ($N = 3$ for this experiment).

The average RPDs for the lamp uncertainty trials are presented in Fig. 5, for which three trials were executed for each lamp. The average RPD of the *trusted* lamps varies from a maximum of 2.1% at 412 nm to approximately −0.1% at 775 nm, with an overall absolute average of about 1.2%. The superior performance in the red part of the spectrum, and the poorer performance in the blue domain, is well correlated with the high flux and stability of FEL lamps in the red and their low flux and stability in the blue domain.

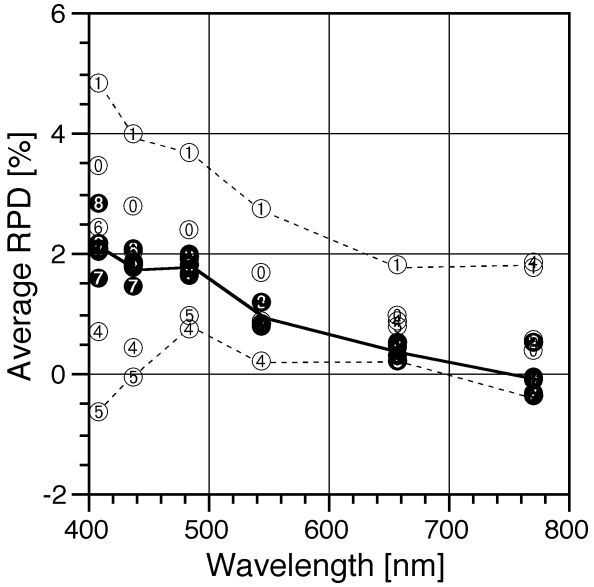

Fig. 5. The average RPDs between the SXR plus plaque determinations of lamp irradiance versus the calibrated lamp irradiance provided with the lamp. The bullet symbols correspond to the lamp codes given in Table 5, i.e., 0 for L000, 1 for L001, etc. The darkened bullets correspond to the so-called *trusted* lamps. The solid lines indicate the average RPD of the trusted lamps, and the dashed lines the overall performance limits of all the lamps.

The majority of the RPD values in Fig. 5 are positive which suggests a deterministic aspect in one of the components or the experimental setup. If the results were at the level of the uncertainties in the different components, the average RPD values of the trusted lamps (the solid lines) should be well distributed around zero, but they are not—there is almost a linear relationship in the differences, with a maximum at 412 nm (about 2%) and a minimum at 683 nm (almost 0%).

The performance of the other lamps in Fig. 5 illustrates the consequences of several of the known or potential problems with the lamps:

1. L001 (F-137), the damaged primary standard, establishes the upper edge of the performance range and has the largest RPD values (although, note the anomalous L004 value at 775 nm).
2. L004 (H97505) and L005 (H96551) establish most of the lower edge of the performance range with RPDs within ±1%, except for the anomalous L004 value at 775 nm). The difference between these lamps and the trusted lamps is largest in the blue part of the spectrum. In the case of L004, the large differences

in the blue might be due to the low operating current of the lamp, and thus a low flux in the blue part of the spectrum (or a problem with the calibration supplied by Hoffman). For L005, the spectrometer used to intercalibrate this lamp had a known low sensitivity at shorter wavelengths.

3. L000 (F-516), a tertiary standard with excessive usage time, has a performance range that is only slightly above the trusted lamps in the blue which converges with the trusted lamps in the red.
4. L006 (F-536), has a performance indistinguishable from the trusted lamps even though the number of hours on this lamp is close to the allowed maximum.

3.3 CALIBRATION COMPARISON

Lamp standards of spectral radiance and irradiance are provided by NIST and various commercial standardizing laboratories and manufacturers who furnish tertiary standards traceable to NIST. The question addressed here is how well do the calibrations from tertiary standards agree with the secondary standards available from NIST.

3.3.1 Equipment

The equipment used for the calibration comparison in lamp standards involved the following:

- Satlantic NIST lamp F-409 (L007); and
- SeaWiFS NIST lamp F-550 (L010).

3.3.2 Procedures

As a side activity to SIRREX-5, Satlantic had NIST calibrate a newly purchased Optronic lamp (F-409). The differences between the NIST and Optronic calibrations were sufficiently large that Satlantic had Optronic recalibrate the lamp. Optronic reviewed their procedures before the second calibration, and made changes to improve their calibrations. This process was repeated during SIRREX-7, except the SeaWiFS Project purchased the lamp for calibration comparisons.

3.3.3 Results

The RPD between the Optronic and NIST calibrations was calculated as

$$\delta_{L_{\rm ID}}(\lambda, t_i) \;=\; 100\,\frac{E^O_{L_{\rm ID}}(\lambda, t_i) \;-\; E^N_{L_{\rm ID}}(\lambda)}{E^N_{L_{\rm ID}}(\lambda)}\;, \qquad (4)$$

where $E^O_{L_{\rm ID}}(\lambda)$ is the calibrated lamp irradiance provided by Optronic and $E^N_{L_{\rm ID}}(\lambda)$ is the calibrated lamp irradiance provided by NIST.

The RPDs for the calibration comparisons are shown in Fig. 6. The first Optronic calibration of F-409 differed from the NIST calibration by an average of approximately 2.6%, whereas the second calibration differed by about 0.8%. The spectral distribution of the differences is mostly flat, except in the near-ultraviolet part of the spectrum. The RPDs for the F-550 calibration are spectrally flat, but the overall average is approximately 1.3%, which is half a percent more than was achieved with the second recalibration of F-409.

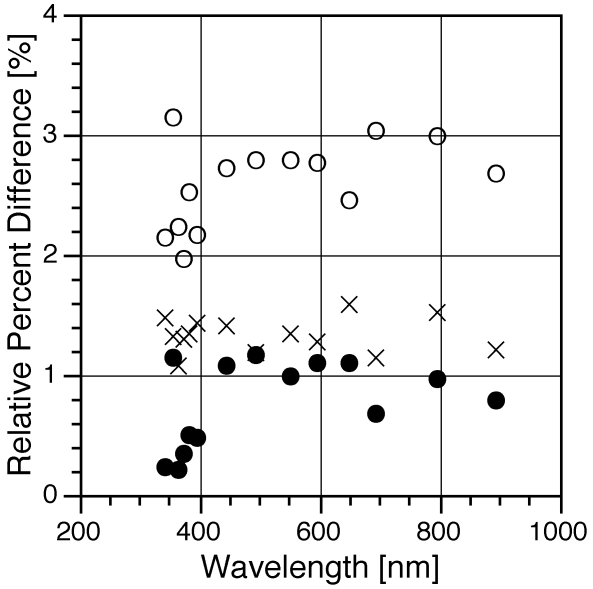

Fig. 6. The RPDs between the Optronic and NIST calibrations for the first calibration of F-409 (open circles), the second calibration of F-409 (solid circles), and the calibration of F-550 (crosses).

A more detailed presentation of the spectral differences between the NIST and Optronic calibrations of F-550 is shown in Fig. 7.

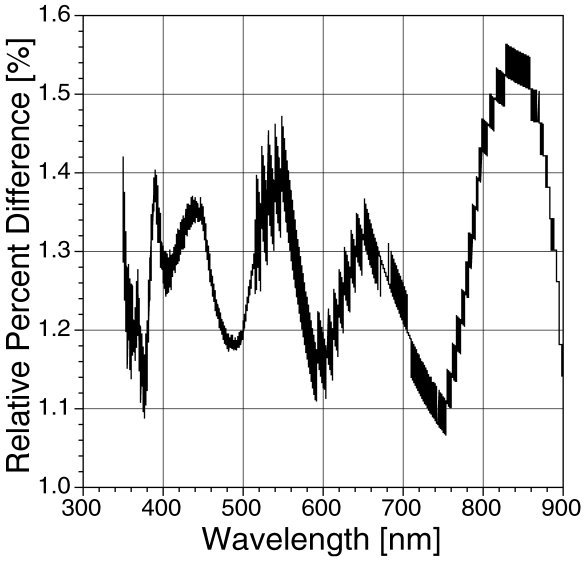

Fig. 7. The RPD values between the NIST calibration of F-550 and the Optronic calibration supplied with the lamp.

The Fig. 7 data show the spectral differences between the NIST and Optronic calibrations of F-550 are composed of a fairly flat average with larger sinusoidal excursions. The latter have a peak-to-peak deflection of approximately 0.3%, with the largest deflection in the red part of the spectrum (about 0.4%).

3.4 LAMP REPEATABILITY

This experiment was designed to quantify the variability between independent uses of each lamp, i.e., to determine how much of the variability in calibrations is due to changes in the lamp from one calibration session to the next.

3.4.1 Equipment

The various types of equipment used for the lamp repeatability experiment were as follows:

- Satlantic NIST lamp F-409 (L007), and SeaWiFS NIST lamps F-182 (L002) and F-137 (L003);
- JRC Hoffman Lamps H97505 (L004) and H96551 (L005), and two new Satlantic Optronic lamps F-547 (L008) and F-548 (L009);
- Satlantic Optronic working lamps F-539 (L003), F-536 (L006), and F-516 (L000);
- Satlantic plaque 05816 (T001);
- The SXR (X001) with custom mount and digital voltmeter (V003);
- OCR-200 R035 with DATA-100 (S/N 043);
- Current sources OL83A 96113058 (C002) and 83DS 93200490 (C003);
- Shunt resistor 1551570 (Z001);
- Voltmeter 3146A09840 (V002); and
- Lamp mount, ring mount, plaque mount, four carriers, and alignment laser LHRR-055 (S/N 3598–1592–65).

3.4.2 Procedures

In this experiment, each lamp illuminated the same plaque, 05816 (T001), and the radiance from the plaque was measured with the SXR at least three times. All trials were executed with the SXR mounted on the positive (+45°) rail.

3.4.3 Results

Because only the SXR was used as the viewing radiometer, a simple measure of lamp repeatability is to quantify changes in the corrected SXR voltage over the three sessions for each lamp. The parameter used here is the normalized standard deviation (NSD) for each lamp, $\zeta^{X1}_{L_{\rm ID}}(\lambda)$, which is also known as the coefficient of variation. The NSD is calculated as the ratio of the standard deviation in corrected SXR voltages, $\sigma^{X1}_{L_{\rm ID}}(\lambda)$, to the average corrected SXR voltage, $\bar{\mu}^{X1}_{L_{\rm ID}}(\lambda)$. The final statistical parameter for analysis is the average NSD computed over the number of replicates, N:

$$\bar{\zeta}^{X1}_{L_{\rm ID}}(\lambda) \;=\; \frac{1}{N}\sum_{i=1}^{N}\zeta^{X1}_{L_{\rm ID}}(\lambda, t_i). \qquad (5)$$

where t_i sets the individual trial number.

A plot of the average NSD values for the lamp repeatability experiment is given in Fig. 8. Almost all of the lamps have a repeatability to within 0.2% except for L005 in the blue part of the spectrum. Lamp L005 was not seasoned before it was intercalibrated (Sect. 3.2.1), and unseasoned lamps frequently exhibit flux variations at shorter wavelengths. The results shown in Fig. 8 are in keeping with this problem.

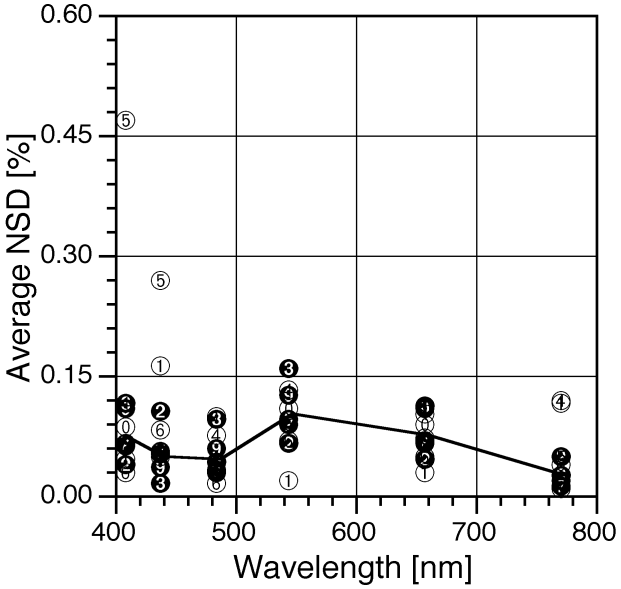

Fig. 8. The average NSDs for the lamp repeatability experiment. The bullet symbols correspond to the lamp codes given in Table 5, i.e., 0 for L000, 1 for L001, etc. The darkened bullets correspond to the so-called *trusted* lamps. The solid lines give the average NSD of the trusted lamps.

There is another aspect of the Fig. 8 results that is worth noting. Lamp L001 is outside the range of deviations at 442, 548, and 775 nm; and lamp L004 is above the range of deviations at 775 nm. Lamp L001 is the damaged NIST lamp, so a poor repeatability with this lamp is in keeping with its history. Lamp L004, however, has no history of misuse, so the behavior at 775 nm is difficult to explain (although, it is the only lamp with a Hoffman calibration). Taking all the data into consideration, including all the elevated deviations, the lamps have a repeatability that is less than 0.5%.

Chapter 4

Uncertainties in Plaque Standards

Stanford B. Hooker
NASA/Goddard Space Flight Center
Greenbelt, Maryland

Giuseppe Zibordi
JRC/SAI/Marine Environment Unit
Ispra, Italy

Scott McLean
Jennifer Sherman
Gordana Lazin
Satlantic, Inc.
Halifax, Canada

Abstract

The experiments conducted to estimate the uncertainties associated with the use of plaque standards involved calculating the reflectances of seven plaques using SXR measurements and the calibrated irradiance provided with the lamp standard, which were then compared to the reflectances provided with each plaque. The average uncertainties between the calculated and calibrated reflectances showed a range of 1.0–3.2%. With the exception of the gray plaque (T007), maximum uncertainties occurred in the blue part of the spectrum, and minimum uncertainties in the red. The importance of bidirectional effects was determined by comparing the SXR plaque measurements made from two different sides of a plaque, but with the same viewing geometry. The smallest uncertainties were associated with T005 (the NIST PTFE plaque), and the largest with T007 (the gray plaque), 0.3 and 2.1%, respectively. All of the other plaques had RPD vlaues which fell into a narrow range with the same spectral dependence and an overall average RPD of approximately 1.0%. Plaque uniformity improved with all increases in the lamp-to-plaque distance. Regardless of the lamp-to-plaque distance, there was a constant offset of aproximately 20 mm in the vertical (z) direction between the maximum signal and the center of the plaque for all the lamps; some of the lamps also showed offsets in the horizontal (x) direction.

4.1 INTRODUCTION

Three experiments were conducted to examine the uncertainties associated with using plaques during calibrations. The first involved using a NIST reflectance standard and the SXR to estimate the uncertainties in using Labsphere (Spectralon) plaques, the second estimated the importance of bidirectional effects by comparing calibrations from two different sides of a plaque, but with the same viewing geometry, and the third used a mapping radiometer to estimate the uniformity of Labsphere plaques illuminated with the same FEL lamp.

4.2 PLAQUE UNCERTAINTIES

This experiment was designed to estimate the uncertainties in plaque standards by comparing the calculated reflectance of a number of different plaques illuminated with a single NIST standard lamp. The reflectance of each plaque was calculated using the SXR measurements and the calibrated irradiance provided with the lamp. The calculated reflectances were then compared to the reflectances provided with each plaque.

4.2.1 Equipment

The equipment used for determining the uncertainties in plaque standards involved the following:

- Satlantic Optronic Lamp F-539 (L003);
- NIST plaque K299 (T005);
- The SeaWiFS gray (10 in) plaque 24328 (T007), the JRC white (18 in) plaque 22463 (T004), the new Satlantic white (18 in) plaque 05816 (T001), and the two old Satlantic white (18 in) plaques 13172 (T002) and 01873 (T003);

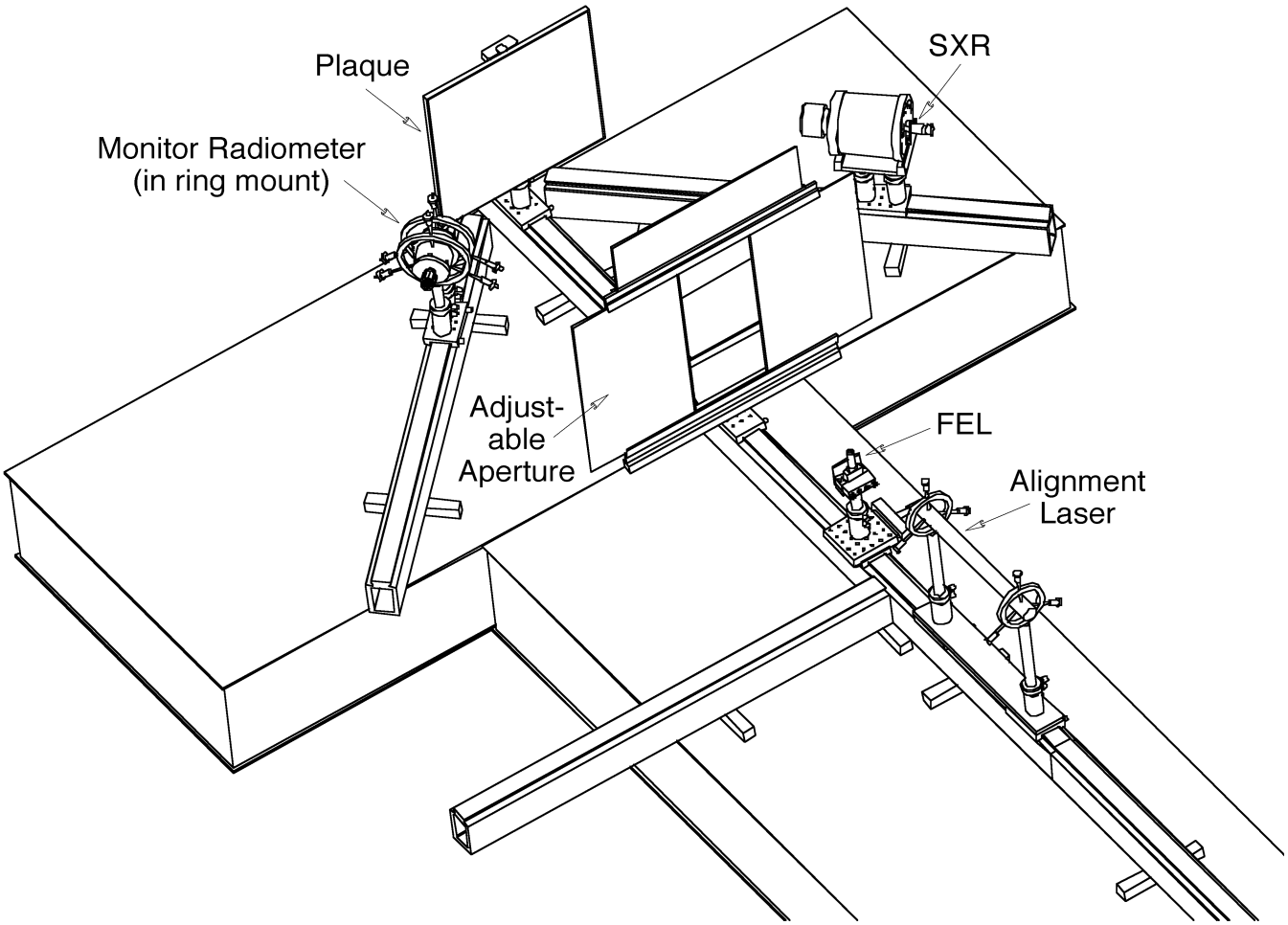

Fig. 9. The experimental setup for determining the uncertainties in plaque standards. The SXR is shown mounted on the −45° rail and the reference radiometer on the +45° rail. The opening of the adjustable aperture was manipulated to ensure the plaque was completely illuminated, while making sure there were no shadows or diffraction edges on the plaque. Note that the reference radiometer views the plaque and not the FEL lamp.

- The SXR (X001) with custom mount and digital voltmeter (V003);
- OCR-200 R035 with DATA-100 (S/N 043);
- Current source OL83A 99115110 (C001);
- Shunt resistor 1551570 (Z001);
- Voltmeter 3146A09840 (V002); and
- Lamp mount, ring mount, plaque mount, four carriers, and alignment laser LHRR-055 (S/N 3598–1592–65).

4.2.2 Procedures

The SXR (X001) was placed on the −45° rail on calibration table 1 and secured in its custom carrier mount. The front of the carrier was placed at 75 cm on the rail and the aperture was set to $f1.4$. The first plaque was placed on the center rail in the proper carrier mount. A paper cover was placed over the active area of the plaque to protect it during all adjustments and to provide for proper focusing of the SXR. The SXR was aligned and focused with respect to the plaque using the alignment laser and the procedures given in Sect. 1.5.2 (T005, the small NIST plaque, was not translated, so the SXR could view the middle of the plaque).

Radiometer R035 was used as a reference sensor and was mounted on the +45° rail using the ring carrier. The front of the ring carrier was placed at 30.0 cm on the rail. The reference radiometer was aligned with respect to the plaque using the alignment laser and the procedures given in Sect. 1.5.2. After all alignments were completed, the laser was turned off, and the paper cover was removed from the plaque. Figure 9 shows the experimental setup used.

Lamp F-539 (L003) was aligned and powered on following the procedures given in Sect. 1.5.3. If present, the

adjustable aperture was opened and closed until there were no shadows or diffraction edges on the plaque (the adjustable aperture was not used if the lamp-to-plaque distance was 0.5 m). Any stray light was minimized by following the practices given in Sect. 1.5.4.

The first step in collecting calibration data was placing aperture caps on the reference radiometer and the SXR, after which, dark readings were acquired. The reference radiometer and SXR data were recorded using SatView and SeaARCS software, respectively. After the darks were completed, background data were recorded with the sensor caps removed, but with the lamp aperture covered, so there was no direct illumination of the plaque. The lamp aperture was then uncovered, and signal data were recorded for both instruments.

The SXR, with its custom carrier mount, was moved to the +45° rail, and radiometer R035 with its ring mount was moved to the −45° rail. The two instruments were positioned and aligned following the procedures described above. Following the same practices used for the measurements on the opposite rail, dark and background data were collected for both sensors, and then signal data were recorded.

The signal data were acquired three times, and then the plaque being used was removed and the next plaque to be used was placed on the center rail in the proper carrier mount (as usual, a paper cover was placed over the active area of the plaque to protect it during all adjustments and to provide for proper focusing of the SXR). The same sequence of events used with the previous plaque were used with the new plaque except new alignment and measurement distances, α_1 and β_1, respectively, given in Table 4 were used for each plaque.

The sequential cycling of the seven plaques continued until each one was measured four times (one time on the −45° rail and three times on the +45° rail), after which, the lamp was powered off following the procedures given in Sect. 1.5.5. Note that this experiment did not involve the independent power cycling of the lamp for each of the four plaque measurements. The cost of a calibrated FEL is too high to permit the additional time for independent power cycles, because each cycle would have to include a minimum 20 min warm-up time.

4.2.3 Results

In this experiment, a NIST calibrated lamp (L003) and the three SXR measurements from the +45° rail were used to determine the reflectance of several plaques. The reflectance of the (plaque) target was calculated from the SXR radiance measurement of the plaque, $L^{X1}_{T_{\rm ID}}(\lambda, t_i)$:

$$R^{X1}_{T_{\rm ID}}(\lambda, t_i) \;=\; \frac{\pi\, L^{X1}_{T_{\rm ID}}(\lambda, t_i)}{E^{\rm cal}_{L3}(\lambda)} \left[\frac{d}{50\ {\rm cm}}\right]^2, \qquad (6)$$

where $E^{\rm cal}_{L3}(\lambda)$ is the calibrated lamp irradiance supplied with lamp L003.

The RPD between the reflectances calculated from the SXR measurement and the reflectance supplied with the plaque (Table 6), $R^{\rm cal}_{T_{\rm ID}}(\lambda)$, was computed as

$$\delta^{X1}_{T_{\rm ID}}(\lambda, t_i) \;=\; 100\, \frac{R^{X1}_{T_{\rm ID}}(\lambda, t_i) \;-\; R^{\rm cal}_{T_{\rm ID}}(\lambda)}{R^{\rm cal}_{T_{\rm ID}}(\lambda)}. \qquad (7)$$

The average RPD is defined as

$$\bar{\delta}^{X1}_{T_{\rm ID}}(\lambda) \;=\; \frac{1}{N} \sum_{i=1}^{N} \delta^{X1}_{T_{\rm ID}}(\lambda, t_i), \qquad (8)$$

where, again, N is the number of +45° rail measurements executed for the plaque (in this case $N = 3$). A plot of the average RPDs between the reflectance provided with the plaque and the reflectance determined with the SXR measurements and the calibrated irradiance of lamp L003 is presented in Fig. 10.

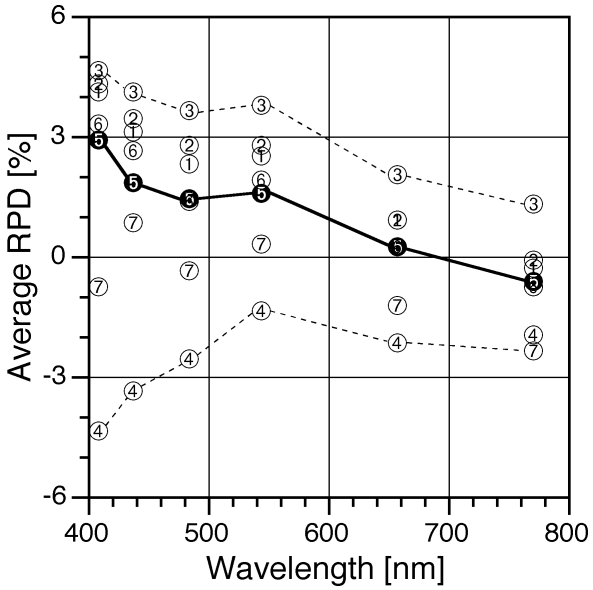

Fig. 10. The average RPD values between the reflectances determined experimentally and those provided with the plaques. The bullet symbols correspond to the target codes given in Table 6, i.e., 1 for T001, 2 for T002, etc. The darkened bullets correspond to the NIST plaque, T005. The solid lines give the average RPD values of the NIST plaque, and the dashed lines the overall performance limits of all the plaques.

The largest range of variance in the Fig. 10 RPD values is with plaques T003 and T004, which have overall average RPDs of 3.2 and 2.7%, respectively. The smallest range of variance is with plaques T005 and T007 which have overall average absolute RPDs of 1.4 and 1.0%, respectively. With the exception of T007, maximum RPDs occur in the blue part of the spectrum, and minimum RPDs in the red.

These RPD values separate the plaques into three groups: T004 with large negative values, T007 with near-zero values, and the remainder. For the latter, T005 forms the bottom edge of minimum RPD values, T003 the top edge of maximum RPD values, and the other plaques all fall within a narrow range with the same spectral dependence.

The plaque groupings have some unique aspects which are worth noting:

1. T003 was the oldest Satlantic plaque and had been resurfaced in the past;
2. T004 was subsequently determined to have a damaged surface which must have occurred during shipment in preparation for SIRREX-7, because even with extensive use, no irregularities were seen prior to shipment (when it was returned to Lapshere after SIRREX-7, it required resurfacing before it could be recalibrated);
3. T007 was the only gray plaque; and
4. T005 was the only NIST (and PTFE) plaque.

The remaining plaques were all white Spectralon plaques (although, T006 was a 10 in plaque).

Interestingly, the small (10 in) white Spectralon plaque (T006) has RPD values very similar to T005. This is somewhat unexpected, because large plaques are usually selected instead of small plaques for calibration work, so the differing FOVs of above- and in-water radiometers can be accommodated with one apparatus (an obvious cost-saving measure). The only difference between the small and large Spectralon plaques used during SIRREX-7 was the latter were made of two pieces of Spectralon, so there was a seam through the middle of the plaque (always oriented vertically), whereas the former were manufactured from one piece.

4.3 PLAQUE UNIFORMITY

This experiment was designed to estimate the uniformity of plaque standards by mapping a plaque with a variety of FEL lamps and lamp-to-plaque distances using the xz-mapping radiometer (which can be automatically positioned with a computer control program). Another objective of the experiment was to understand how ancillary parameters, like lamp type, influence the uniformity of plaques.

4.3.1 Equipment

The equipment used for determining the uniformity of plaque standards involved the following:

- Satlantic lamps F-548 (L009), F-511 (W006), and F-528 (W008);
- Satlantic white (18 in) plaque 05816 (T001);
- The xz-mapping radiometer (Y001) with its table, 1.0° FAFOV detector, custom filter holder, and Oriel (model 57378) broadband filter (with a 600 nm short pass);
- Current source OL83A 99115110 (C001);
- Shunt resistor 1551570 (Z001);
- Voltmeter 3146A09840 (V002); and
- Lamp mount, plaque mount, three carriers, and alignment laser LHRR-055 (S/N 3598–1592–65).

4.3.2 Procedures

The xz-mapping table was mounted at 45° with respect to the main optical rail using the table mount. It was placed such that when the mapping radiometer was at the central position, it would view the center of the plaque. The plaque was placed on the center rail in the proper carrier mount, and a paper cover was placed over the active area of the plaque to protect it during all adjustments. The broadband filter (with 600 nm short pass) was installed in the front of the 1.0° FAFOV mapping detector. The distance between the lamp and plaque was set to 0.5 m, which required the removal of the adjustable aperture. The mapping radiometer was aligned with respect to the plaque using the alignment laser and the procedures given in Sect. 1.5.2.

Lamp F-516 (L000) was aligned and powered on following the procedures given in Sect. 1.5.3. The aperture was adjusted, so there were no shadows or diffraction edges on the plaque, and any stray light was minimized by following the practices given in Sect. 1.5.4. Figure 11 shows the experimental setup used.

After dark data were collected, the xz-mapping software was used to scan the target over the full range of motion of the xz-mapping table, 290 mm, in 20.7 mm increments. This yields a map of 15×15 points covering a large portion of the 500×500 mm^2 surface area of the plaque: to 410 mm in the horizontal (x) direction by 290 mm in the vertical (z) direction (the difference in coverage between the two dimensions, of course, is due to the angle of the mapping table with respect to the plaque).

One plaque mapping took approximately 45 min to complete. At the conclusion of the mapping, the lamp was powered off following the procedures given in Sect. 1.5.5. After the first mapping, two more mappings were executed for lamp-to-plaque distances of 1.3 and 2.1 m. For these larger distances, the aperture was placed in between the plaque and the lamp.

Additional high-resolution maps were produced using a 5 mm mapping increment. The high-resolution maps were very similar to the low-resolution maps using a 20.7 mm increment. The high-resolution maps took approximately 11.6 h to execute, and did not provide any significant additional information.

Two types of FEL lamps were used in the plaque uniformity experiments: the older design by Osram Sylvannia, and the present design by General Electric. Both lamps are shown in Fig. 12. Although there are differences in the design and size of the glass envelope, the principle difference between the two lamp types is the filament for the

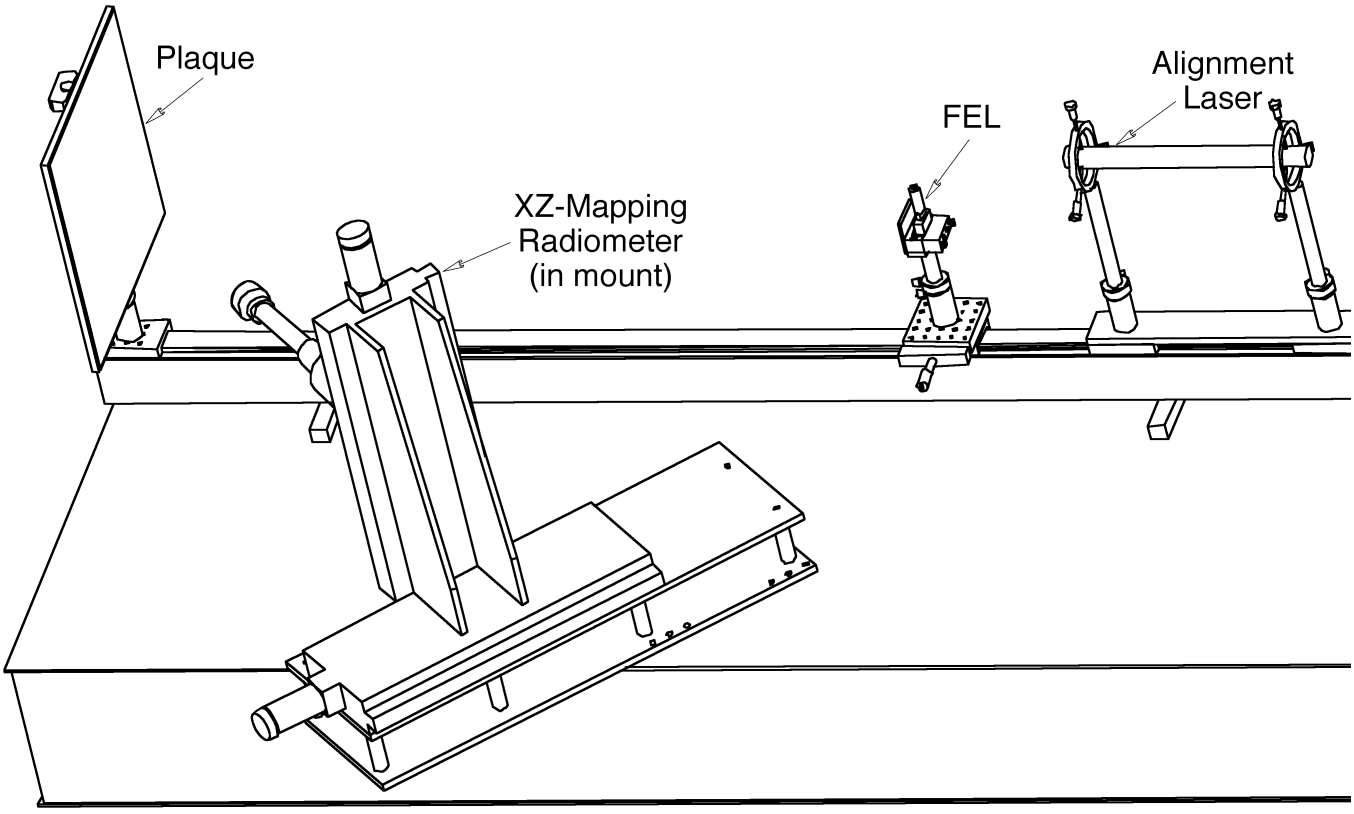

Fig. 11. The experimental setup for measuring the uniformity of plaques. The xz-mapping radiometer table mount is mounted 45° with respect to the plaque. Note the absence of the usually present adjustable aperture and the 45° rail.

former is supported at the top, side, and bottom, whereas the filament for the latter is supported only at the top and bottom.

Fig. 12. The two different types of FEL lamps used during SIRREX-7: Osram Sylvannia (left) and General Electric (right).

4.3.3 Results

All plaque uniformity analyses were based on using the maximum detected signal to normalize all remaining signal levels by the maximum value (which was then expressed as a percentage). In order to examine the difference in the maps caused by different lamps, two of each design were used for plaque uniformity maps using a plaque-to-lamp distance of 0.5 m. All of the 1.3 and 2.1 m maps were made using (General Electric) lamp L009 (F-548), because this design is currently used for all Satlantic calibrations. Although the different lamps produced slightly different patterns on the plaque, the differences were within the range of differences seen between lamps from the same manufacturer.

Three plaque uniformity maps, for three different lamp-to-plaque distances, are shown in Fig. 13. Also shown in the panels are two dashed lines to demark the center of the plaque, and the approximate limits of the 50% and 99% viewing areas of a seven-channel OCR-200 in-water sensor placed 45° with respect to the plaque at the standard calibration distance, the inner and outer ovals, respectively (as labeled in panel a). It's important to note only the area actually mapped is shown; the edges of the plaque extend to ±225 mm on both axes.

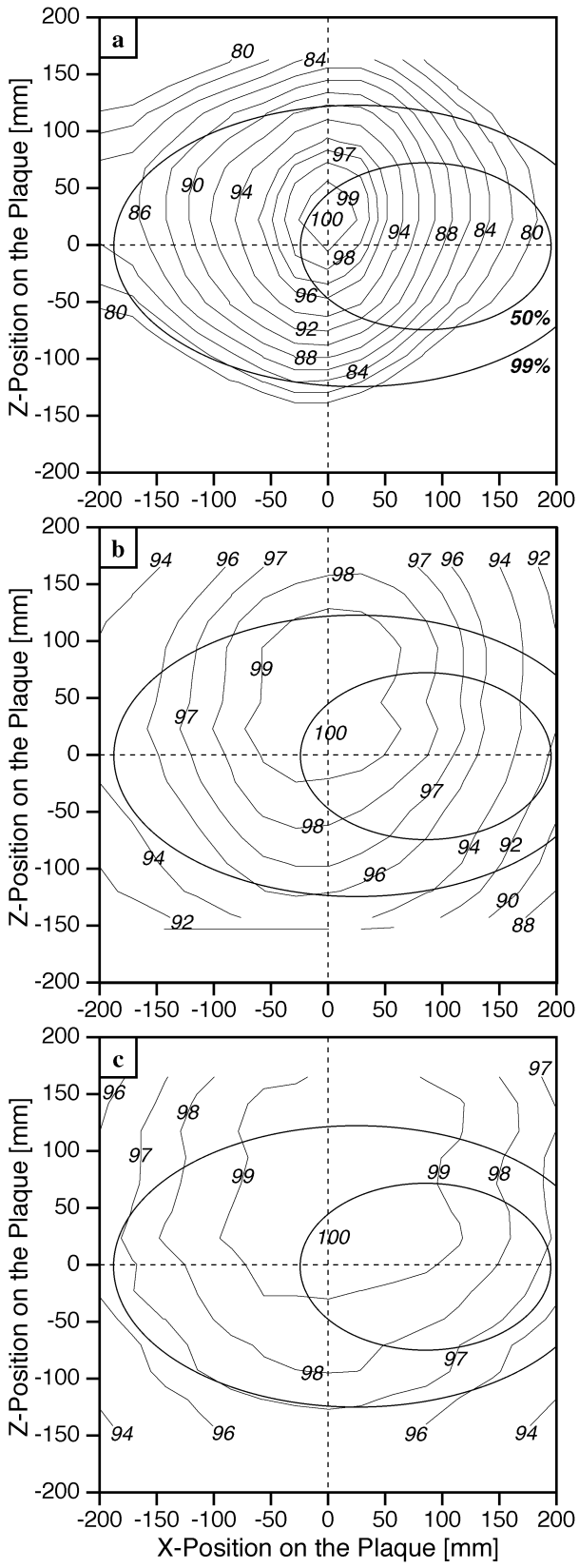

Fig. 13. The illumination uniformity of plaque T001 using lamp L009 and a lamp-to-plaque distance of **a)** 0.5 m, **b)** 1.3 m, and **c)** 2.1 m.

The individual 50% viewing areas (not shown in Fig. 13) represent the (half-angle) FOV specified at FWHM. The approximate or ensemble outer envelope of all seven channels is the 50% viewing area (and similarly for the 99% viewing area). The sensor is shown viewing the plaque with an offset in the x-axis of 113.1 mm, which ensures that when the plaque is translated by the offset along the (y) illumination axis, the 99% viewing area will be very nearly centered on the plaque.

Using the extent of the 150 mm coordinates in Fig. 13 as a bounding box, the horizontal changes in illumination uniformity across the bounding box change from approximately 16.0% ($y = 0.5$ m), to 5.0% ($y = 1.3$ m), and then to 2.5% ($y = 2.1$ m). Although plaque uniformity improves with all increases in the lamp-to-plaque distance, the largest improvement in uniformity occurs when the lamp-to-plaque distance increases from 0.5 to 1.0 m.

Regardless of the lamp-to-plaque distance, there is a constant offset of approximately 20 mm in the vertical (z) direction between the maximum signal and the center of the plaque for all the lamps. Each lamp was carefully aligned using a laser and a lamp alignment jig, so the offsets are not the result of positioning uncertainties. Some of the lamps also showed offsets in the horizontal (x) direction which suggests the offsets are a function of each particular lamp. To check the repeatability of the results, the lamps were taken out of their mounts, reseated, and the scans repeated—the results were completely repeatable.

4.4 BIDIRECTIONAL EFFECTS

This experiment was designed to investigate the importance of bidirectional effects in plaque calibrations by determining the uncertainty between calibrations using the positive and negative rails and the same viewing geometry (45° with respect to the center of the plaque).

4.4.1 Equipment

The equipment used for determining the importance of bidirectional effects with plaque standards was the same used for estimating plaque uncertainties (Sect. 4.2.1). Note again, that T005 (the small NIST plaque) was not translated, so the SXR could view the middle of the plaque.

4.4.2 Procedures

The procedures used for determining the bidirectional effects of plaque standards was the same used for estimating plaque uncertainties (Sect. 4.2.2).

4.4.3 Results

The SXR radiance measurements of the plaque on the −45° rail, $L_{T_{\rm ID}}^{-X1}(\lambda)$, are differenced with respect to the average of the three SXR radiance measurements of the plaque on the +45° rail, $\bar{L}_{T_{\rm ID}}^{+X1}(\lambda)$. The RPD is formed by

ratioing the difference with respect to the measurement on the positive rail:

$$\delta^{\pm X1}_{T_{\rm ID}}(\lambda, t_i) \;=\; 100\,\frac{L^{-X1}_{T_{\rm ID}}(\lambda) \;-\; \bar{L}^{+X1}_{T_{\rm ID}}(\lambda)}{\bar{L}^{+X1}_{T_{\rm ID}}(\lambda)} \qquad (9)$$

The average RPD is calculated using the forumlation given in (8).

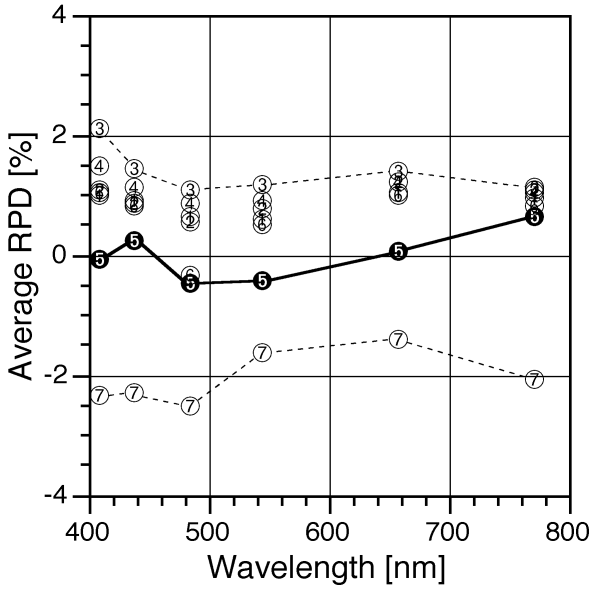

Fig. 14. The average RPDs between the SXR plaque measurements on the positive and negative rails. The bullet symbols correspond to the target codes given in Table 6. The dark bullets and solid lines correspond to T005, and the dashed lines set the overall performance limits of all the plaques.

The average RPDs between the SXR plaque measurements on the $+45°$ and $-45°$ rails are shown in Fig. 14. The smallest uncertainties are associated with T005 (the NIST PTFE plaque), and the largest with T007 (the gray plaque); the average absolute RPDs are 0.3 and 2.1%, respectively. The other plaques have similar RPD values (which fall within a narrow range), the same spectral dependence, and an overall average RPD of approximately 1.0%. The plaques fall into slightly different groups than was established with the plaque uncertainty results (Sect. 4.2). In this case, the grouping is determined by the composition of the plaque: T007 is made from gray Spectralon, T005 is made from white PTFE, and the remainder are all made from white Spectralon.

The outer edge of the variance for the white Spectralon plaques is set by plaque T003, which was the oldest plaque (and had been resurfaced), and, T004, the damaged plaque is pretty similar. If these two plaques are grouped together, the average RPD values for them is 1.2%; the remaining plaques have an average RPD of 0.8%. In either grouping, the range in RPD values is maximal in the blue part of the spectrum, minimal in the green domain, and then maximal again in the red.

Chapter 5

Uncertainties in Radiance Calibrations

Stanford B. Hooker
NASA/Goddard Space Flight Center
Greenbelt, Maryland

Scott McLean
Jennifer Sherman
Satlantic, Inc.
Halifax, Canada

Abstract

Three types of experiments were conducted to estimate the uncertainties in radiance calibrations using a plaque and FEL lamp: a) The average repeatability uncertainty (based on one plaque and one FEL used with 11 trials for three different radiometers) was less than 0.1% (0.06% in the blue–green part of the spectrum and 0.09% in the red); b) the uncertainty that can be removed from radiance calibrations if ambient rather than dark measurements are used was 0.13% (0.11% in the blue–green and 0.17% in the red); and c) the overall uncertainty from secondary reflections, (for example, originating from an alignment laser) was 0.11% (0.06% in the blue–green wavelength domain and 0.19% in the red).

5.1 INTRODUCTION

The calibration coefficient for a radiance sensor (identified by $S_{\rm ID}$) is computed using a plaque (identified by $T_{\rm ID}$) with a calibrated reflectance, $R^{\rm cal}_{T_{\rm ID}}$, plus a standard lamp (identified by $L_{\rm ID}$) with a calibrated irradiance, $E^{\rm cal}_{L_{\rm ID}}$. The general procedures require the lamp to be positioned a distance d on axis and normal to the center of the plaque (specific details for each step are given in Sect. 1.5). The radiance sensor is capped, and dark voltage levels for the sensor are recorded. An average dark level for each channel, $\bar{D}_{S_{\rm ID}}(\lambda)$, is calculated from the dark samples.

The radiance sensor is positioned to view the plaque at 45° with respect to the lamp illumination axis†. The lamp is powered on, and the voltage levels of the individual sensor channels are recorded, from which an average calibration voltage for each channel, $\bar{V}_{S_{\rm ID}}(\lambda)$, is obtained. The calibration coefficient is calculated as:

$$C^{\rm Rad}_{S_{\rm ID}}(\lambda) \;=\; \frac{\frac{1}{\pi}\,R^{\rm cal}_{T_{\rm ID}}(\lambda)\,E^{\rm cal}_{L_{\rm ID}}(\lambda,50)}{\bar{V}_{S_{\rm ID}}(\lambda)-\bar{D}_{S_{\rm ID}}(\lambda)}\left[\frac{50\ {\rm cm}}{d}\right]^2, \qquad (10)$$

where d is given in centimeters.

† An alternative angle for which the reflectance of the plaque is known is also acceptable, but for all of the SIRREX-7 experiments, 45° was the calibrated reflectance angle of the plaque and the corresponding sensor viewing angle.

Three types of experiments were conducted to explore the uncertainties associated with radiance calibrations: a) one plaque and one FEL were used with three OCR-200 radiometers to estimate the repeatability uncertainty in radiance calibrations (based on 11 trials for each sensor); b) three OCR-200 sensors and the SXR were used to explore the uncertainties in ambient versus dark measurements; and c) the uncertainty from secondary reflections used in the calibration process (in this case, an alignment laser) was measured with the SXR and three OCR-200 sensors.

5.2 RADIANCE REPEATABILITY

The uncertainties in radiance calibrations were estimated by independently calibrating three OCR-200 sensors (R035, R036, and R067) 11 times each (following the usual procedures). The trials were all with the same plaque and FEL, but the lamp was not powered on and off each time; it was left on to minimize lamp usage time (standard FEL lamps are too expensive to include the warm-up time for each trial in the experiment).

5.2.1 Equipment

The equipment used for the radiance repeatability trials was as follows:

- Satlantic Optronic lamp F-547 (L008);
- Satlantic white (18 in) plaque 05816 (T001);

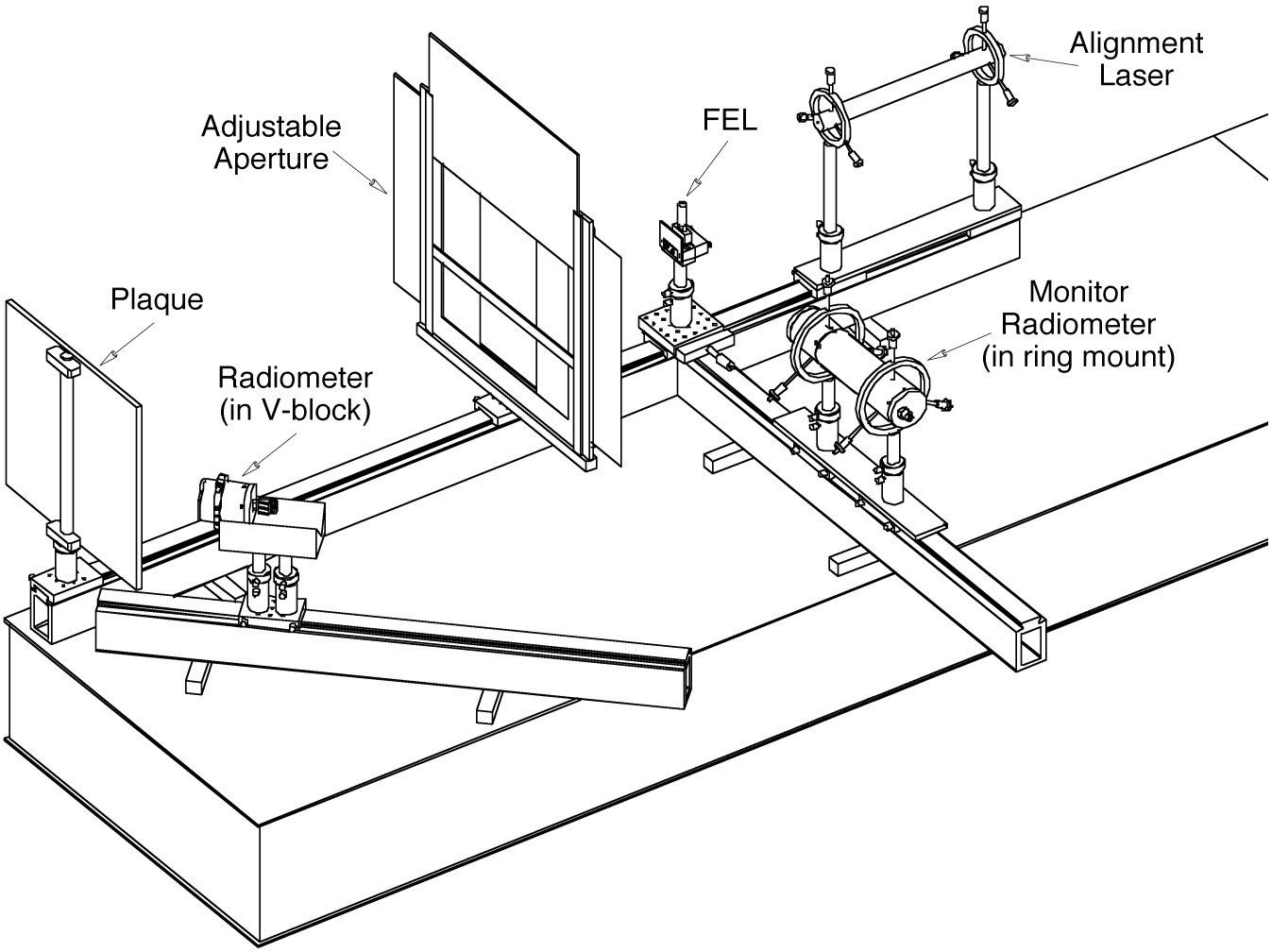

Fig. 15. The experimental setup for determining the repeatability in radiance calibrations. The radiometer being calibrated is shown in a V-block (Satlantic calibrations usually used a ring mount).

- OCR-200 R035, R036, and R067 with DATA-100 (S/N 043);
- OCI-200 I121 with DATA-100 (S/N 047);
- Current source OL83A 99115110 (C001);
- Shunt resistor 1551570 (Z001);
- Voltmeter US36037038 (V001); and
- Lamp mount, plaque mount, ring mount, V-block and mount, four carriers, alignment grid, and alignment laser (S/N 6391CK).

5.2.2 Procedures

Radiometer I121 was used as a monitoring sensor, and the experiment took place on calibration table 2. The I121 sensor was mounted on the horizontal rail facing the side view of the lamp using the ring mount and carrier. The monitoring sensor was aligned following the procedures given in Sect. 1.5.6. A V-block was placed on the 45° rail and the front of the carrier was set to 35.6 cm. The first DUT was placed in the V-block such that the D-shaped collar was firmly up against the outside of the V-block. A known spot on the DUT was noted, so the sensor could be placed in the V-block again in the same alignment. The front of the DUT was set at 30 cm on the 45° rail.

The plaque was placed on the center rail in the proper mount with carrier and aligned with respect to the DUT as described in Sect. 1.5.2. The DUT alignment was done only once—the V-block remained stable over time and was used for all subsequent trials. Lamp F-547 (L008) was aligned and powered on following the procedures given in Sect. 1.5.3. The aperture was adjusted, so there were no shadows or diffraction edges on the plaque, and any stray light was minimized by following the practices given in Sect. 1.5.4. The experimental setup is shown in Fig. 15.

The first step in collecting calibration data was placing aperture caps on the monitoring sensor and the DUT, so dark data could be taken. Once the darks were completed, the aperture caps were removed and light (signal) data

were recorded for the DUT and the monitoring sensor. After the signal data for a DUT were recorded, the next DUT was placed in the V-block. It was not necessary to realign the subsequent DUTs, since the V-block remained locked in place and stable (a big advantage of the V-block and D-shaped collar approach over the ring carrier). The DUT was placed with a known spot upright, and the D-shaped collar firmly up against the V-block. The data collection sequence was then repeated (dark data followed by signal data). This procedure was repeated until each DUT was measured 11 times, after which, the lamp was powered off following the procedures in Sect. 1.5.5 The cyclic order for the DUTs was R035, R036, and then R067.

5.2.3 Results

The calibration coefficients for each sensor (at each wavelength) during each trial were calculated using (10). The average and the standard deviation across all 11 trials were computed for each wavelength, and were used to calculate the NSD:

$$\zeta_{S_{\mathrm{ID}}}(\lambda) \;=\; 100\,\frac{\bar{C}^{\mathrm{cal}}_{S_{\mathrm{ID}}}(\lambda)}{\hat{C}^{\mathrm{cal}}_{S_{\mathrm{ID}}}(\lambda)}, \tag{11}$$

where $\bar{C}^{\mathrm{cal}}_{S_{\mathrm{ID}}}(\lambda)$ is the average calibration coefficient, and $\hat{C}^{\mathrm{cal}}_{S_{\mathrm{ID}}}(\lambda)$ is the standard deviation in the calibration coefficients.

A plot of the NSD values in the radiance calibration coefficients is given in Fig. 16. Although there is an increase in the NSD for all sensors at certain wavelengths and the largest deviations occur in the red part of the spectrum, the NSD values are always less than 0.2%. Across all sensors, the average NSD in the blue–green part of spectrum is 0.06%, whereas it is 0.09% in the red, and the average across all wavelengths is 0.07%.

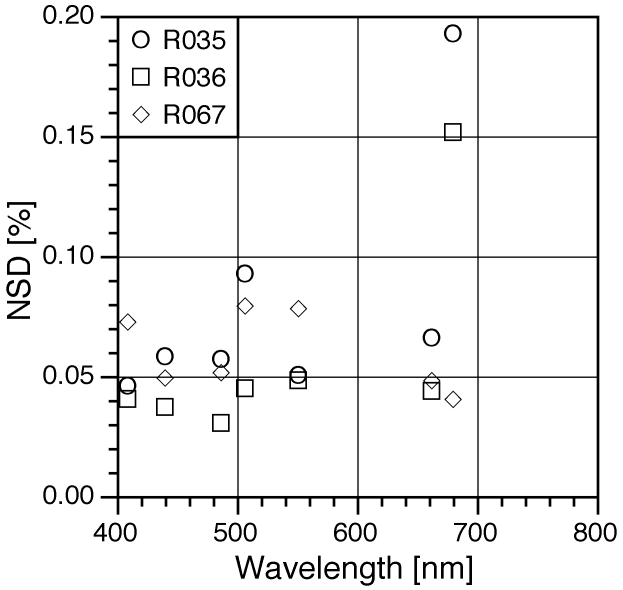

Fig. 16. The NSDs in the determination of the calibration coefficients for radiance sensors.

5.3 AMBIENT MEASUREMENTS

Ambient and dark measurements were compared for the estimation of bias voltages using three OCR-200 sensors and the SXR. The latter were also used to measure the importance of secondary reflections from the calibration apparatus, in this case, an alignment laser.

5.3.1 OCR Ambient Measurements

This experiment was designed to estimate the uncertainty between using so-called *ambient* versus dark measurements in OCR-200 radiance calibrations (Sect. 1.5.1). The latter involves placing sensor caps on the DUT, so only noise or *dark* levels on the DUT detectors are recorded; whereas, for the former, an intervening occulter or *on-axis baffle* is used to block the direct illumination of the target by the source DUT aperture, so only indirect light (from the source and any other light emissions from equipment in the room) reach the DUT aperture.

5.3.1.1 Equipment

The equipment used for the radiance ambient measurements were as follows:

- Satlantic Optronic lamp F-547 (L008);
- Satlantic white (18 in) plaque 05816 (T001);
- OCR-200 R035, R036, and R067 with DATA-100 (S/N 043);
- OCI-200 I121 with DATA-100 (S/N 047);
- The SXR (X001) with custom mount and digital voltmeter (V003);
- Current source OL83A 99115110 (C001);
- Shunt resistor 1551570 (Z001);
- Voltmeter US36037038 (V001); and
- Lamp mount, ring mount, plaque mount, V-block with mount, six carriers, alignment grid, black occulter ($9.0\times9.1\,\mathrm{cm}^2$) and mount, and alignment laser (S/N 6391CK).

5.3.1.2 Procedures

Radiometer I121 was used as a monitoring sensor, and the experiment took place on calibration table 2. I121 was mounted on the horizontal rail facing the side view of the lamp using the ring mount and carrier. The monitoring sensor was aligned following the procedures given in Sect. 1.5.6. The V-block was placed on the 45° rail, and the front of the carrier was set to 35.6 cm. The first DUT was placed in the V-block such that the D-shaped collar was firmly up against the outside of the V-block. A known spot on the DUT was noted, so the sensor could be replaced in the V-block with the same alignment. The front of the DUT was set at 30 cm on the 45° rail.

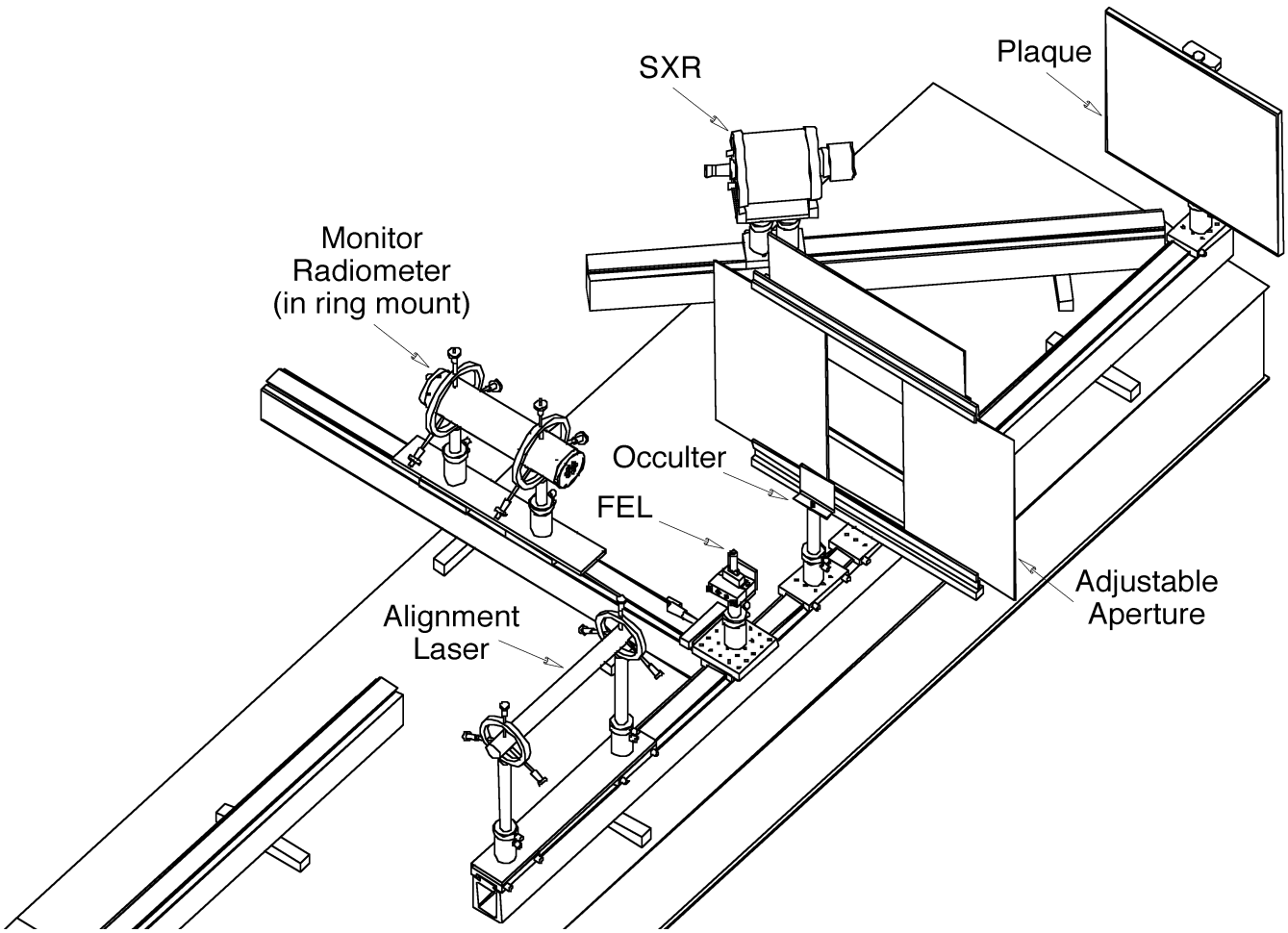

Fig. 17. The experimental setup for determining the uncertainty between ambient and dark measurements in SXR calibrations.

The plaque was placed on the center rail with the proper mount and carrier, and then it was aligned with respect to the DUT as described in Sect. 1.5.2. The DUT alignment was done only once—the V-block remained stable over time and was used for all subsequent DUTs. Lamp F-547 (L008) was aligned and powered on following the procedures given in Sect. 1.5.3. The aperture was adjusted so there were no shadows or diffraction edges on the plaque, and any stray light was minimized by following the practices given in Sect. 1.5.4. Figure 17 shows the experimental setup.

The first step in collecting calibration data was placing aperture caps on the monitoring sensor and the DUT, so dark data could be taken. After the dark data were recorded, the aperture caps were removed and the occulter was placed in front of the lamp. The front of the carrier of the occulter was set to 136.50 cm, after which, ambient data were recorded. The occulter was then removed and signal data were recorded. When this was completed, the cloth cover was removed from the alignment laser and another signal session was recorded. This second set of signal data were recorded to look at the contamination effects of an uncovered, reflective apparatus.

When the measurements with the first DUT were completed, the next DUT was placed in the V-block. It was not necessary to realign the subsequent DUTs, because the V-block remained locked in place and stable. The DUT was placed with a known spot upright, and the D-shaped collar was positioned firmly up against the V-block. The data collection sequence was then repeated: dark data followed by two sets of signal data. This procedure was repeated until each DUT was measured three times. The cyclic order for the DUTs was R035, R036, and then R067.

Once the DUTs were measured three times, the V-block was removed from the 45° rail and replaced with the SXR in its custom mount and carrier. The front of the carrier was set at 76 cm on the rail, then the SXR aperture was set to $f1.4$ and focused at 85 cm. The SXR was aligned with respect to the plaque following the procedures given in Sect. 1.5.2. The acquisition system for the SXR was kept outside the cloth baffling for calibration table 2.

Aperture caps were placed on the monitoring sensor

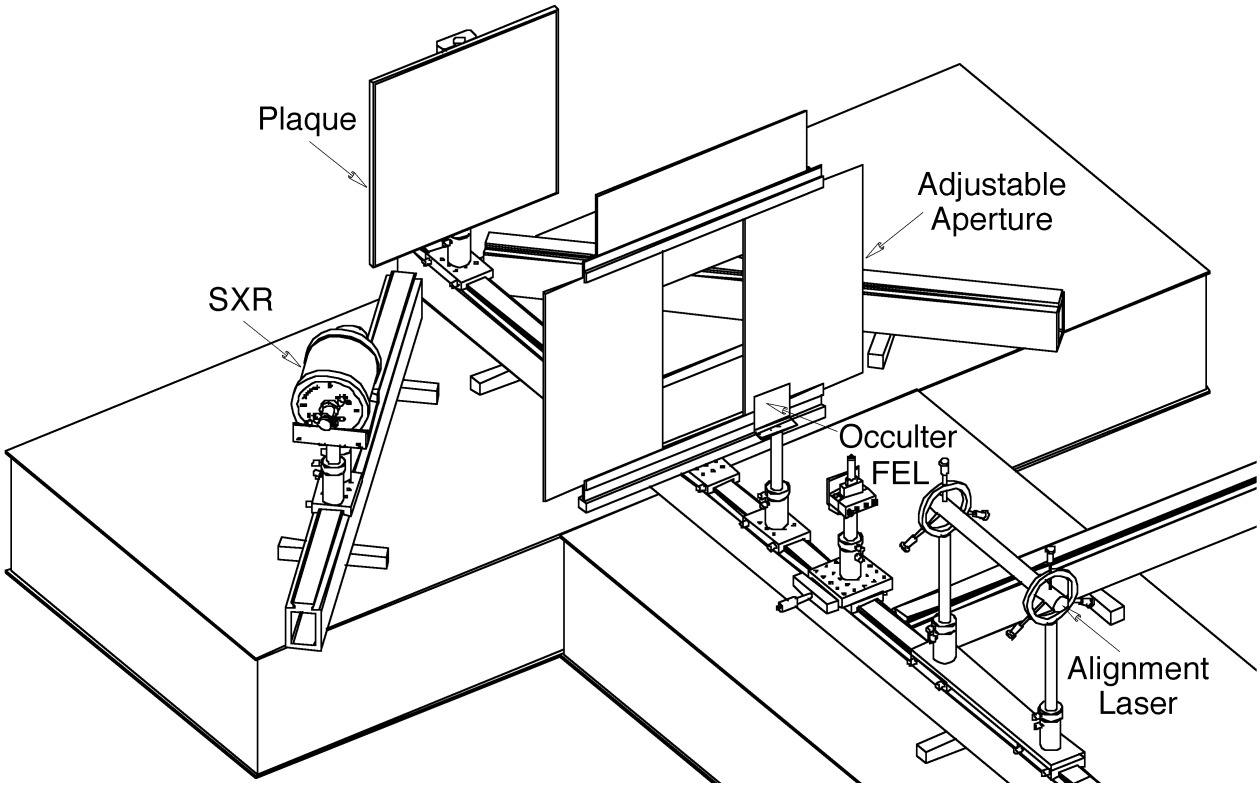

Fig. 18. The experimental setup for determining the uncertainty between ambient and dark radiance calibrations with the SXR.

and the SXR lens. SXR dark data were recorded with 11 samples taken 11 times, and coincident dark data were also recorded for the monitoring radiometer. The occulter was then placed in the same location as with the other DUTs, and the aperture covers removed, so ambient data could be recorded. Once completed, the alignment laser was uncovered, and another ambient reading was recorded. The occulter was then removed and signal data were recorded with the laser covered and then uncovered. The lamp was then powered off following the procedures in Sect. 1.5.5.

5.3.2 SXR Ambient Measurements

This experiment was designed to estimate the uncertainty between using ambient versus dark measurements in SXR calibrations, and to measure the importance of secondary reflections from the calibration apparatus, in this case, an alignment laser.

5.3.2.1 Equipment

The equipment used for the SXR ambient measurements were as follows:

- Satlantic Optronic lamp F-539 (L003);
- Satlantic white (18 in) plaque 05816 (T001);
- The SXR (X001) with custom mount and digital voltmeter (V003);
- Current source OL83A 96113058 (C002);
- Shunt resistor 008308-C36814 (Z002);
- Voltmeter 3146A09840 (V002); and
- Lamp mount, ring mount, plaque mount, V-block with mount, four carriers, alignment grid, black occulter ($9.0\times9.1\,\mathrm{cm}^2$) and mount, and alignment laser LHRR-055 (S/N 3598–1592–65).

5.3.2.2 Procedures

The SXR (X001) was placed on the +45° rail on calibration table 1 and secured in its custom carrier mount. The front of the carrier was placed at 76 cm on the rail and the aperture was set to $f1.4$. The Satlantic plaque (T001) was placed on the center rail in the proper carrier mount. A paper cover was placed over the active area of the plaque to protect it during all adjustments and to provide for proper focusing of the SXR. The SXR was aligned and focused with respect to the plaque using the alignment laser and the procedures given in Sect. 1.5.2.

Lamp F-539 (L003) was aligned and powered on following the procedures in Sect. 1.5.3. The aperture was adjusted, so there were no shadows or diffraction edges on the plaque, and any stray light was minimized by following the practices given in Sect. 1.5.4. The acquisition system for the SXR was kept outside the cloth baffling for calibration table 1. Figure 18 shows the experimental setup.

An aperture cap was placed on the SXR lens. SXR dark data were recorded, then the occulter was placed in front of the lamp, and the SXR aperture cap removed, so ambient data could be recorded. Once completed, the alignment laser was uncovered, and another ambient reading was recorded. The occulter was then removed and signal data were recorded with the laser covered and then uncovered. The lamp was then powered off following the procedures in Sect. 1.5.5.

5.3.3 Results

The percent contribution ratio (PCR) of ambient light on a radiance calibration (using the data corresponding to when the alignment laser was uncovered) is quantified using:

$$\chi^{\mathrm{amb}}_{S_{\mathrm{ID}}}(\lambda) \;=\; 100\,\frac{\bar{A}_{S_{\mathrm{ID}}}(\lambda) - \bar{D}_{S_{\mathrm{ID}}}(\lambda)}{\bar{V}_{S_{\mathrm{ID}}}(\lambda) - \bar{D}_{S_{\mathrm{ID}}}(\lambda)} \qquad (12)$$

where $\bar{A}_{S_{\mathrm{ID}}}(\lambda)$ is the average voltage measured during the ambient measurement, $\bar{V}_{S_{\mathrm{ID}}}(\lambda)$ is the average voltage measured while viewing the plaque, and $\bar{D}_{S_{\mathrm{ID}}}(\lambda)$ is the average dark voltage. The numerator is the net voltage associated with the indirect light reaching the DUT, the denominator is the calibration signal voltage, and the resulting $\chi^{\mathrm{amb}}_{S_{\mathrm{ID}}}(\lambda)$ values give the spectral contribution of indirect light (in percent) to the calibration process (Fig. 19). Note, however, that when the lamp is occulted to make the ambient measurement, reflections from the alignment laser are automatically blocked, so the ambient data does not include laser reflections.

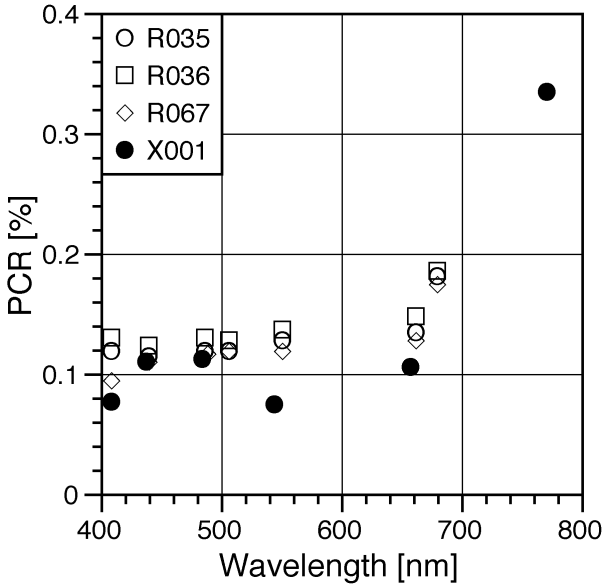

Fig. 19. The PCRs for the ambient measurements with respect to the radiance calibration signal level.

The Fig. 19 data show the largest influence in ambient light is in the red part of the spectrum, where the output of the FEL is maximal, but all contributions are below 0.4%. The spectral average of $\chi^{\mathrm{amb}}_{S_{\mathrm{ID}}}(\lambda)$ values for each sensor falls within a narrow range 0.12–0.14%, with an overall average across all sensors of 0.13% (0.11% in the blue–green and 0.17% in the red). The SXR data show the lowest values in comparison to the other sensors at a particular wavelength, which is a consequence of the narrower FOV and greater sensitivity of this instrument. The former is seen in the red part of the spectrum around 665 nm, and the latter in the blue around 412 nm (note the spread in the OCR-200 data).

The importance of secondary reflections from ancillary equipment on a radiance calibration (in this case, the alignment laser), is also quantified using the PCR statistical approach:

$$\chi^{\mathrm{cov}}_{S_{\mathrm{ID}}}(\lambda) \;=\; 100\,\frac{\bar{V}_{S_{\mathrm{ID}}}(\lambda) - \bar{V}^{\mathrm{cov}}_{S_{\mathrm{ID}}}(\lambda)}{\bar{V}_{S_{\mathrm{ID}}}(\lambda) - \bar{D}_{S_{\mathrm{ID}}}(\lambda)} \qquad (13)$$

where $\bar{V}^{\mathrm{cov}}_{S_{\mathrm{ID}}}(\lambda)$ is the average voltage measured while viewing the plaque with the laser covered. The numerator in (13) is the net voltage associated with reflections from the laser, the denominator is the calibration signal voltage, and the resulting $\chi^{\mathrm{cov}}_{S_{\mathrm{ID}}}(\lambda)$ values give the spectral contribution of laser reflections (in percent) to the calibration process (Fig. 20).

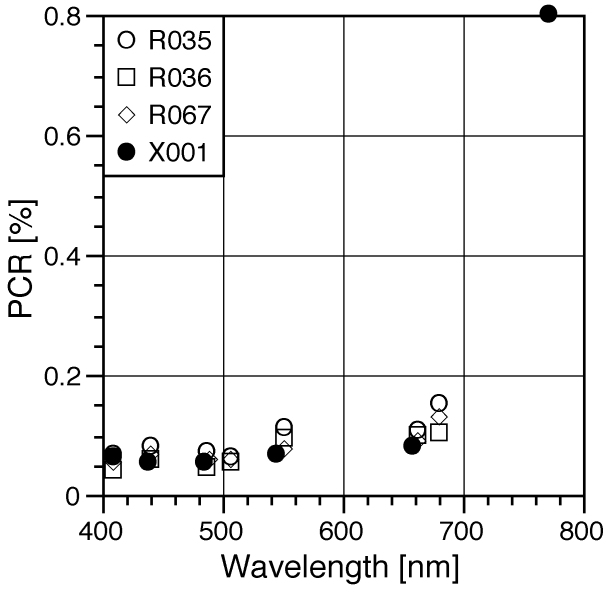

Fig. 20. The PCRs for laser reflections with respect to the radiance calibration signal level.

The Fig. 20 data show the largest influence in laser reflections on radiance calibrations is in the red part of the spectrum, again, where the output of the FEL is maximal. The spectral average of $\chi^{\mathrm{cov}}_{S_{\mathrm{ID}}}$ for the OCR-200 sensors falls within a narrow range, 0.07–0.09%, with an overall average across all OCR-200 sensors of 0.08%. The SXR data are very similar for all channels except the reddest wavelength,

775 nm (for which there is no corresponding channel in the OCR-200 sensors). If all the sensors are considered, the overall spectral uncertainty is 0.11% (0.06% in the blue–green and 0.19% in the red).

Chapter 6

Uncertainties in Irradiance Calibrations

Stanford B. Hooker
NASA/Goddard Space Flight Center
Greenbelt, Maryland

Giuseppe Zibordi
JRC/SAI/Marine Environment Unit
Ispra, Italy

Scott McLean
Jennifer Sherman
Satlantic, Inc.
Halifax, Canada

Abstract

Three types of experiments were conducted to estimate the uncertainties associated with irradiance calibrations using an FEL standard lamp: a) the repeatability uncertainty (based on one FEL standard lamp used during 11 trials with three different irradiance sensors) was less than 0.5% (0.2% on average, with usually larger uncertainties in the blue part of the spectrum and smaller uncertainties in the red); b) the additional uncertainty that can be removed from radiance calibrations if ambient rather than dark measurements are used was 0.05% (0.05% in the blue, 0.04% in the green, and 0.06% in the red); and c) the overall uncertainty from secondary reflections, originating from ancillary equipment used during the calibration process (in this case, an alignment laser) was 0.06% (0.03% in the blue–green wavelength domain and 0.12% in the red).

6.1 INTRODUCTION

Typically, the calibration coefficients for an irradiance sensor (identified by $S_{\rm ID}$) are computed using an FEL standard lamp ($L_{\rm ID}$) with a calibrated irradiance, $E^{\rm cal}_{L_{\rm ID}}(\lambda, 50)$. The general procedures require the lamp to be positioned a distance d on axis and normal to the faceplate of the irradiance sensor (Sect. 1.5.7). The irradiance sensor is capped, and dark (digital voltage) levels for the sensor are recorded from which average dark levels, $\bar{D}_{S_{\rm ID}}(\lambda)$, are calculated.

The lamp is powered on, and the voltage levels of the individual sensor channels are recorded, from which an average calibration voltage for each channel, $\bar{V}_{S_{\rm ID}}(\lambda)$, is obtained. The calibration coefficient is calculated using:

$$C^{\rm Irr}_{S_{\rm ID}}(\lambda) \;=\; \frac{E^{\rm cal}_{L_{\rm ID}}(\lambda, 50)}{\bar{V}_{S_{\rm ID}}(\lambda) - \bar{D}_{S_{\rm ID}}(\lambda)} \left[\frac{50\ {\rm cm}}{d}\right]^2, \qquad (14)$$

where d is given in centimeters.

Three types of experiments were conducted to explore the uncertainties associated with irradiance calibrations:

a) The same FEL standard lamp was used with three OCI-200 radiometers to estimate the repeatability uncertainty in irradiance calibrations (based on 11 trials for each sensor);

b) The importance of ambient versus dark measurements was explored with three OCI-200 sensors; and

c) The uncertainty associated with reflections from improperly baffled ancillary equipment used in the calibration process (in this case, an alignment laser) was measured with three OCI-200 sensors.

6.2 IRRADIANCE REPEATABILITY

This experiment was designed to estimate the uncertainties in irradiance calibrations (set up and executed following the usual procedures). Three OCI-200 sensors (I040, I050, and I097) were calibrated independently 11 times each. Although the trials were all executed with the same FEL standard lamp, the lamp was not powered on and off for each trial; it was left on to minimize the amount of time used with the lamp (standard FEL lamps are too expensive to include the warm-up time for each trial in the experiment).

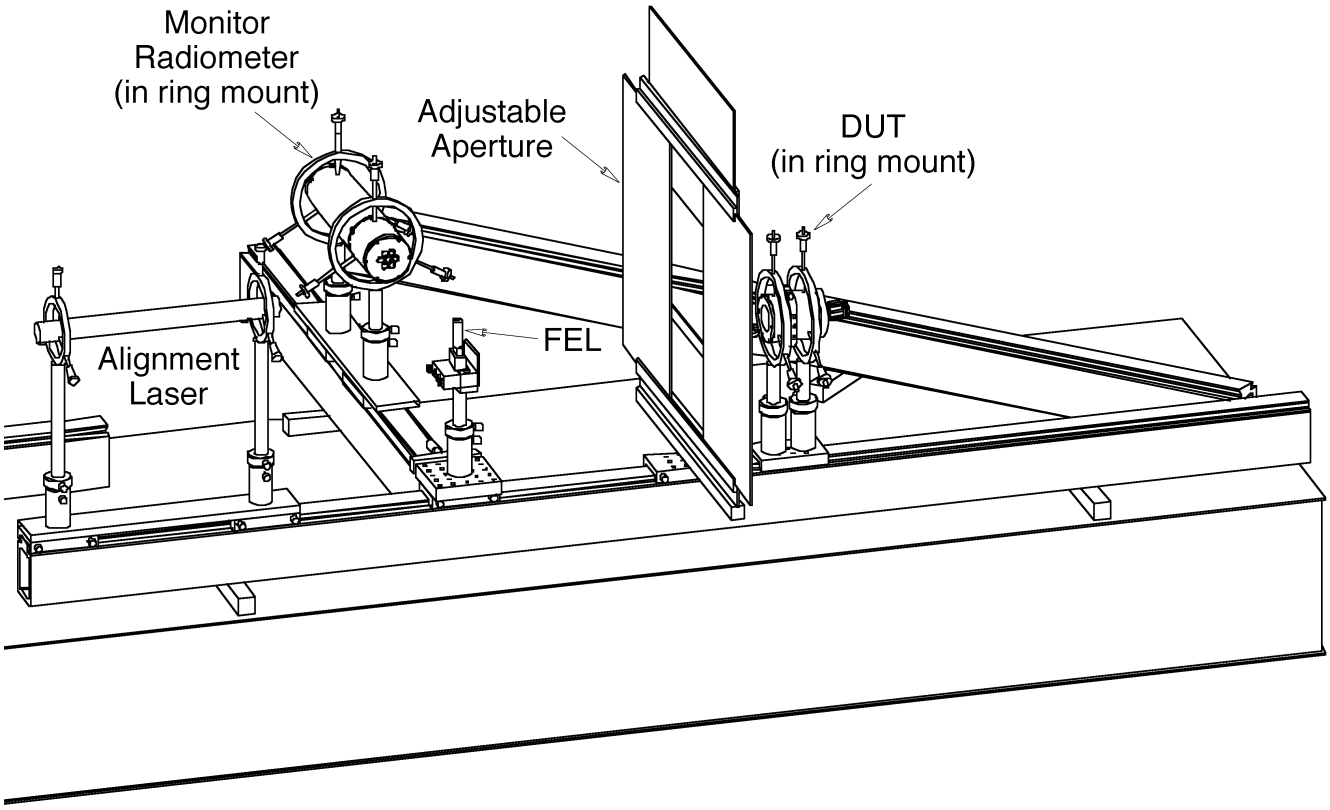

Fig. 21. The experimental setup for determining the uncertainties in irradiance calibrations with the DUT shown in ring carriers and mount.

6.2.1 Equipment

The equipment used for the irradiance repeatability trials was as follows:

- Satlantic Optronic lamp F-548 (L009);
- OCI-200 I040, I050, and I097 with DATA-100 (S/N 043);
- OCI-200 I121 with DATA-100 (S/N 047);
- Current source OL83A 99115110 (C001);
- Shunt resistor 008308-C36814 (Z002);
- Voltmeter US36037038 (V001); and
- Lamp mount, two ring mount sets, three carriers, alignment grid, and alignment laser (S/N 6391CK).

6.2.2 Procedures

The experiment took place on calibration table 2. Radiometer I121 was used as a monitoring sensor and was mounted on the rail facing the side view of the lamp using the rings and ring carrier (aligned following the procedures given in Sect. 1.5.6). Two ring carriers with a carrier mount were used to mount the DUT on the center rail, and the front of the carrier mount was set to 80.00 cm. The DUT was aligned with respect to the FEL lamp using the procedures in Sect. 1.5.7 (the front of the DUT had an offset of 3.90 cm).

Lamp F-548 (L009) was aligned and powered on following the procedures given in Sect. 1.5.3. The aperture was adjusted so there were no shadows or diffraction edges on the faceplate of the DUT, and any stray light was minimized using the practices in Sect. 1.5.4. Figure 21 shows the experimental setup.

The first step in collecting calibration data was placing aperture caps on the monitoring sensor and the DUT, after which, dark readings were taken for both. The aperture caps were removed and signal (light) data were recorded. The DUT was then removed from the rings, and the next DUT was aligned using the same methods as before. Both dark and light readings were then taken, and the DUT was once again removed from the rings. This cycle was repeated for each DUT, until all of the DUTs were measured 11 times, after which, the lamp was powered off following the procedures given in Sect. 1.5.5. The experiment did not use independent power cycling of the lamp. The cost of a calibrated FEL is too high to permit the extra time for independent power cycles, because each cycle would include a minimum 20 min warm-up time.

6.2.3 Results

The calibration coefficients for each sensor (at each wavelength) during each trial were calculated using (14).

The average and the standard deviation across all 11 trials were computed for each wavelength, and were used to calculate the NSD using (11). A plot of the NSD values in the irradiance calibration coefficients is given in Fig. 22. With the exception of the I040 sensor, there is a general decrease in the NSD values from the blue to the red domain, although, the I050 sensor is almost spectrally constant. The average NSD is always less than 0.5%, and the overall average NSD is 0.2%.

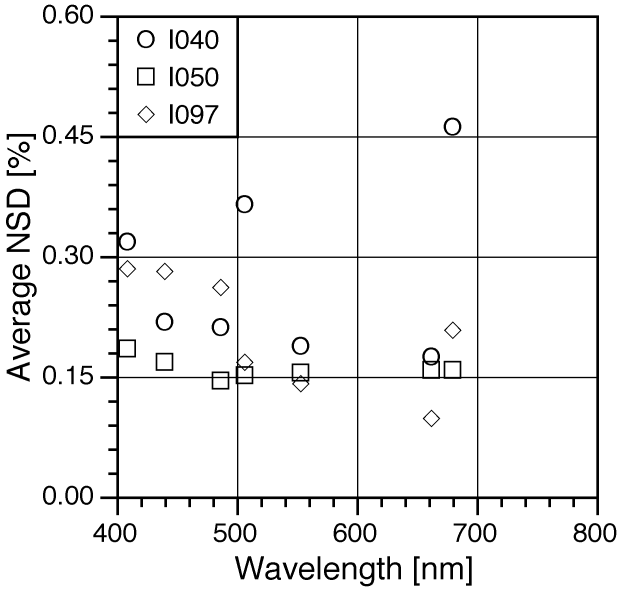

Fig. 22. The NSD values in the determination of the calibration coefficients for irradiance sensors.

It is important to remember each sensor in Fig. 22 was subjected to 11 trials, so the range of deviations are well resolved. This means the sensor-to-sensor variability is not an artifact of the sample size, but is instead, an indication of the differences in spectral changes of the individual sensors and detectors.

6.3 AMBIENT MEASUREMENTS

This experiment was designed to estimate the uncertainty between using ambient versus dark measurements in irradiance calibrations. Ambient and dark measurements were compared for the estimation of bias voltages using three OCI-200 sensors. The latter were also used to measure the importance of secondary reflections from the calibration apparatus, in this case, an alignment laser.

6.3.1 Equipment

The equipment used for the irradiance ambient measurements was as follows:

- Satlantic Optronic lamp F-548 (L009);
- OCI-200 I040, I050, and I097 with DATA-100 (S/N 043);
- OCI-200 I121 with DATA-100 (S/N 047);
- Current source OL83DS 99115110 (C003);
- Shunt resistor 1551570 (Z001);
- Voltmeter US36037038 (V001); and
- Lamp mount, ring mount, V-block and mount, four carriers, black occulter ($9.0\times9.1\,\mathrm{cm}^2$) and mount, alignment grid, and alignment laser (S/N 6391CK).

6.3.2 Procedures

The experiment took place on calibration table 2. Sensor I121 was used as a monitor sensor and was mounted on the horizontal rail facing the side view of the lamp using the rings and ring carrier; the sensor was aligned using the procedures given in Sect. 1.5.6.

The V-block was placed on the center rail and the front of the carrier was set to 101.50 cm. The DUT was aligned following the procedures in Sect. 1.5.7. A check was made that the front of the DUT was set at 107.10 cm on the rail.

Lamp F-548 (L009) was aligned and powered on following the procedures given in Sect. 1.5.3. The aperture was adjusted so there were no shadows or diffraction edges on the faceplate of the DUT, and any stray light was minimized by following the practices given in Sect. 1.5.4. Figure 23 shows the experimental setup.

The first step in collecting calibration data was placing aperture caps on the monitoring sensor and the DUT, after which, dark readings were taken for both. Once the darks were completed, the aperture caps were removed, and the occulter was placed in front of the lamp carrier at 138.00 cm. An ambient measurement was then recorded, after which, the occulter was removed and a light (signal) measurement was made. When this was completed, the black cloth was removed from the laser and another light measurement was made.

The next DUT was placed in the V-block mount and aligned with the correct orientation and the D-shaped collar firmly against the V-block mount. Dark, ambient, and two light measurements were made for each DUT and the monitoring sensor each time. This cycle was repeated for each DUT, until all of the DUTs were measured three times, after which, the lamp was powered off following the procedures given in Sect. 1.5.5. The order for the DUTs as they were cycled through the measurement sequences was as follows: a) I040, b) I050, and c) I097.

6.3.3 Results

The PCR of ambient light on an irradiance calibration (using data when the alignment laser was uncovered) is quantified using (12) to calculate $\chi^{\mathrm{amb}}_{S_{\mathrm{ID}}}(\lambda)$. The spectral contribution of indirect light (in percent) to the calibration process is presented in Fig. 24. Note, however, that when the lamp is occulted to make the ambient measurement, reflections from the alignment laser are automatically blocked, so the ambient data does not include laser reflections.

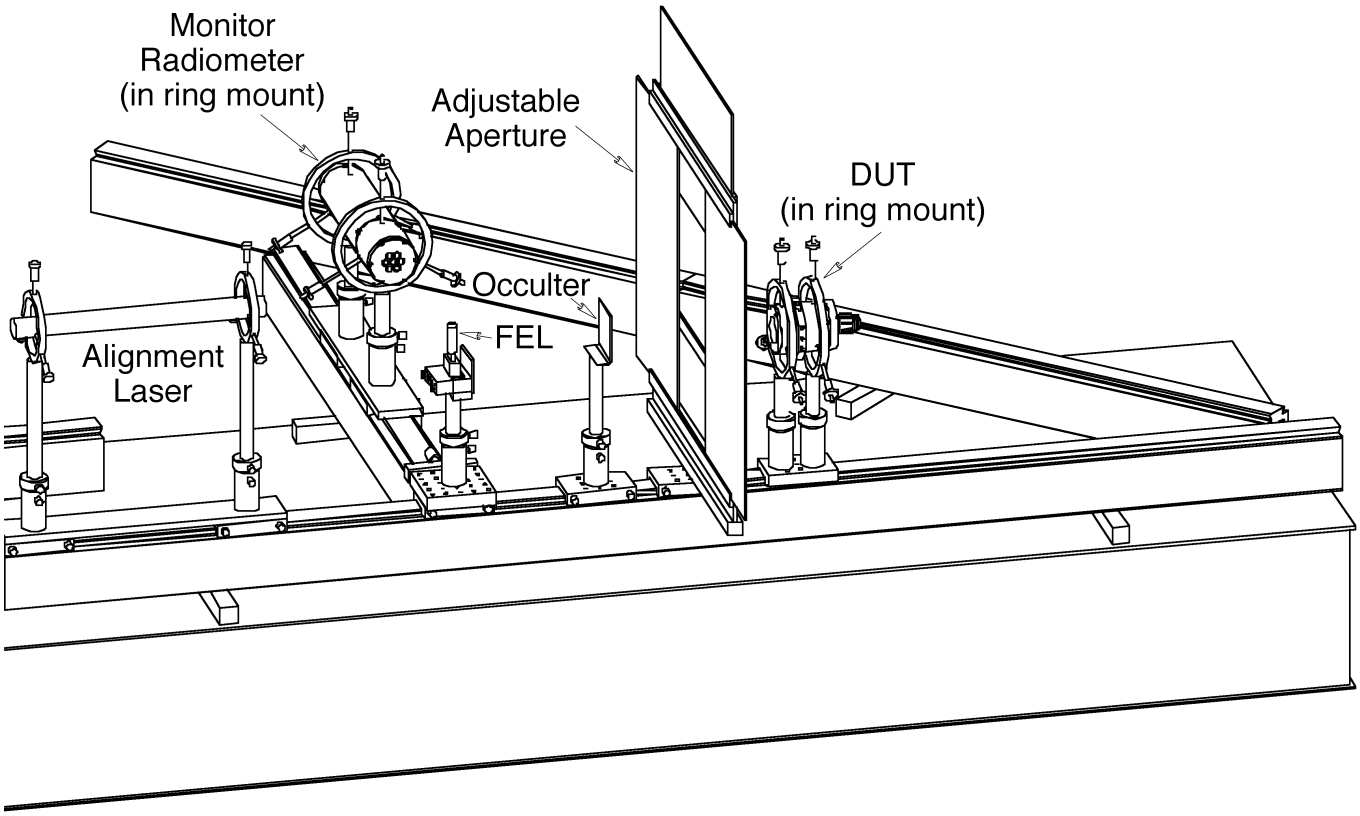

Fig. 23. The experimental setup for determining the uncertainty in ambient versus dark measurements in irradiance calibrations.

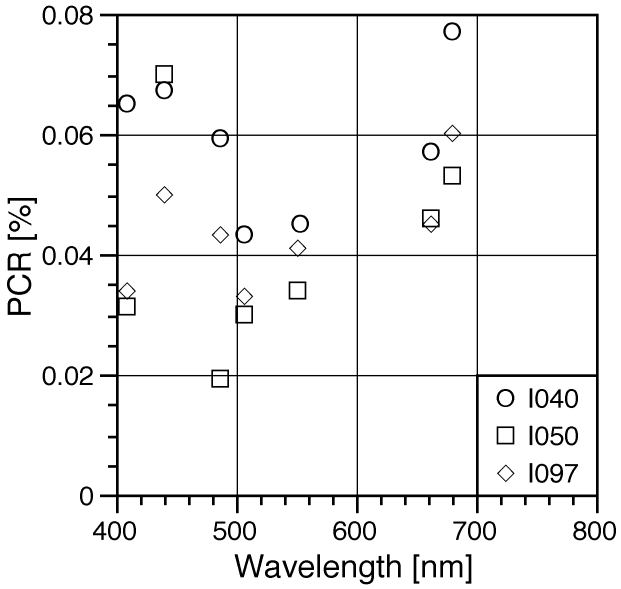

Fig. 24. The PCR values for the ambient measurements with respect to the irradiance calibration signal level.

The Fig. 24 data show the influence of ambient light is maximal in the blue and red parts of the spectrum, with the green wavelength domain showing the least amount of variation, but always less than 0.1%. The overall averages are 0.05% in the blue, 0.04% in the green, and 0.06% in the red. The spectral average of $\chi^{\rm amb}_{S_{\rm ID}}(\lambda)$ for each sensor falls within a narrow range 0.04–0.06%, with an overall average across all sensors of 0.05%.

The importance of secondary reflections from ancillary equipment on an irradiance calibration (in this case, the alignment laser), is also quantified using the PCR statistical approach (13):

$$\chi^{\rm cov}_{S_{\rm ID}}(\lambda) \;=\; 100\,\frac{\bar{V}^{\rm cov}_{S_{\rm ID}}(\lambda) - \bar{V}_{S_{\rm ID}}(\lambda)}{\bar{V}_{S_{\rm ID}}(\lambda) - \bar{D}_{S_{\rm ID}}(\lambda)} \qquad (15)$$

where $\bar{V}^{\rm cov}_{S_{\rm ID}}(\lambda)$ is the average voltage measured while viewing the lamp with the laser covered. The numerator in (15) is the net voltage associated with reflections from the laser, the denominator is the calibration signal voltage, and the resulting $\chi^{\rm cov}_{S_{\rm ID}}(\lambda)$ values give the spectral contribution of laser reflections (in percent) to the calibration.

PCR values (15) for the laser reflection experiment are plotted in Fig. 25; negative values correspond to a decrease in measured irradiance as a result of covering the laser (positive values correspond to an increase). The average PCR across all wavelengths and all measurements is −0.06%, which means covering the laser reduced the measured irradiance, on average, by less than a tenth of a percent. The Fig. 25 data show the spectral aspects between

the covered and uncovered measurements are not uniform. There is an increase in irradiance at 412 nm, and a decrease in all the other wavelenghts except 510 nm which exhibits almost a negligible PCR. The peak-to-peak variability as a function of wavelength is on the order of 0.5%.

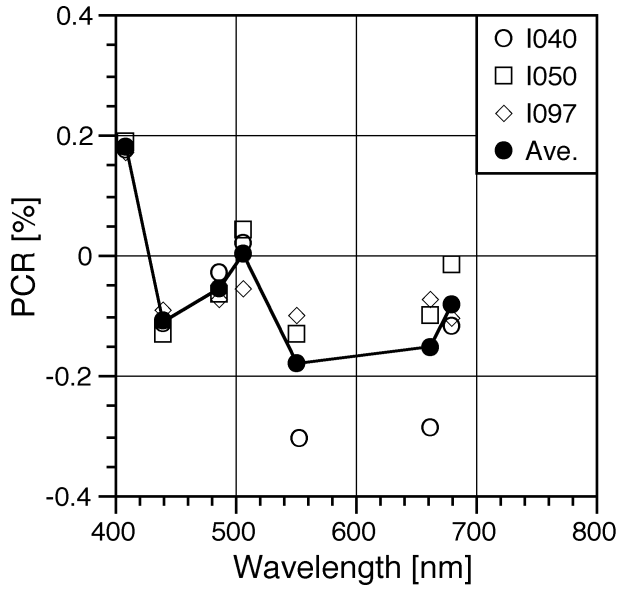

Fig. 25. The PCR values for laser reflections with respect to the irradiance calibration signal level. The average of the three sensors (open symbols) at each wavelength is given by the solid circles.

Chapter 7

Rotation and Polarization Uncertainties

Stanford B. Hooker
NASA/Goddard Space Flight Center
Greenbelt, Maryland

Scott McLean
Mark Small
Satlantic, Inc.
Halifax, Canada

Abstract

Separate experiments were conducted during SIRREX-7 to estimate the rotation and polarization uncertainties of radiometers during the calibration process. Rotational uncertainties for radiance sensors were usually less than 1%, with single and multiple aperture systems having average rotational uncertainties of 0.2–0.3% and 0.4–0.9%, respectively. Rotational uncertainties for a multiple aperture irradiance sensor was 0.7% on average, which was in close agreement with multiple aperture radiance sensors. The only significant spectral dependence was with an OCR-2000 (hyperspectral) sensor which had maximal effects in the bluest and reddest wavelengths and minimal effects in the green domain. The average polarization parameter, in percent, varied between 0.6–4.6%. The Satlantic instruments had an average polarization below 2.0%, but the OCR-200 sensors showed maximum polarization sensitivity in the blue part of the spectrum (1.4–2.4%), while the OCR-2000 instrument had maximum sensitivity in the red wavelength domain (2.1–2.6%).

7.1 INTRODUCTION

Two different experiments were designed to estimate the rotation and polarization effects on the calibration process. Although the former can be considered as a mechanical positioning problem, there are practical aspects of the problem which are more associated with the usual methods used during instrument calibration. For example, the angular positioning of the sensor during the calibration process is usually not maintained from one calibration to the next (in fact, many commercial radiometers are cylindrical and are not explicitly indexed), and the mounting hardware used is not always the best for reproducing an indexing scheme. The D-shaped collar was designed to overcome this limitation, and when used with a V-block is much easier to use for repositioning requirements than a ring carrier. In comparison, polarization is mostly an instrument design problem, with a design objective that is set by the optical protocols being used.

7.2 ROTATION EFFECTS

Two experiments were conducted to estimate the rotation sensitivity of radiance and irradiance sensors during the calibration process. Most Satlantic radiometers (e.g., the OCR-200 and OCR-1000 series of instruments) have separate apertures for each channel organized in one or more circular arrays around a central channel (Fig. 3), so changes in the orientation of the sensor in a V-block or ring mount will necessarily cause a change in what part of the plaque is viewed during the calibration process. The objective of the rotation experiments was to determine the level of uncertainty that can be associated with this part of the sensor positioning process.

Custom rotator mount adapters, which took advantage of the D-shaped collars, were built for the OCI-200 and OCR-200 series of radiometers. Separate custom adapters were also built for the SXR and the OCR-2000 instruments. The latter two also required a mechanical support (a V-block) to stabilize the large housings of these instruments during the rotation process. Although this helped maintain the stability of the large mass of these instruments during rotation, it did not ensure an axial symmetry for all trials, and some data were not used, because of unbalanced rotation.

7.2.1 Rotation of Radiance Sensors

Four types of radiance sensors were used for the rotation sensitivity experiments: R035, R064, P002, and X001.

An important difference in the radiometers was the SXR and OCR-2000 are single aperture instruments, whereas the OCR-200 sensors have multiple apertures arranged in a circular array with one channel positioned in the middle of the circle (as shown in Fig. 3 for an irradiance sensor).

The sensors also had different uses and FOVs: R035 (in-water, wide FOV sensor), R064 (in-air, narrow FOV sensor), P002 (in-water, wide FOV sensor), and X001 (laboratory, very narrow FOV sensor). The FOV of a multi-aperture sensor is important, because as the sensor is rotated, a narrow FOV sensor traces out a relatively small area across the plaque, whereas a large FOV sensor necessarily traces out a large area. The smaller the area, the greater the likelihood the sensor will detect illumination inhomogeneities in the plaque (Sect. 4.3) as it is rotated.

7.2.1.1 Equipment

The equipment used for the radiance rotation trials was as follows:

- Satlantic Optronic lamp F-548 (L009);
- Satlantic white (18 in) plaque 05816 (T001), and JRC white (18 in) plaque 22463 (T004);
- OCR-200 R035 and R064 with DATA-100 (S/N 043);
- Monitor sensor, OCI-200 I121 with DATA-100 (S/N 047);
- OCR-2000 P002;
- The SXR (X001) with custom rotator mount and digital voltmeter (V003);
- Current source OL83A 99115110 (C001);
- Shunt resistor 1151570 (Z001);
- Voltmeter 3146A09840 (V002);
- Oriel rotator model 13059 equipped with a custom D-shaped collar adapter;
- Oriel stepper control box model 20010 (S/N 542);
- Rotator D-shaped collar adapter; and
- Lamp mount, V-block and mount, plaque mount, seven carriers, alignment grid, and alignment laser 05-LHR-201-355.

7.2.1.2 Procedures

The DUT was placed on the 45° rail on calibration table 2 in the appropriate rotator mount. When the SXR was the DUT, a special mount was used to hold it to the rotator. All other radiometers were attached to the rotator using the D-shaped collar. The DUT was positioned on the rail such that the sensor was approximately 40 cm from the plaque along the rail axis, unless the DUT was the SXR, in which case the distance was set to 85 cm. A test was made to ensure the instrument could be rotated freely through 360° by driving the rotator through the full range of motion. Any wires were wound such that they would unwind during rotation and, thus, not hinder the circular movement or put tension on the DUT.

The plaque (T001 or T004) was placed on the center rail in the proper carrier mount. A paper cover was placed over the active area of the plaque to protect it during all adjustments and to provide for proper focusing of the SXR. The DUT was aligned with respect to the plaque using the alignment laser and the procedures given in Sect. 1.5.2. The alignment of the DUT was suboptimal, because it only had three degrees of freedom. It could be rotated around the post holding the rotator, it could slide along the rail, and it could be raised and lowered. A translator was added to the carrier to allow it to travel orthogonal to the rail. This was necessary when using the SXR and the hyperspectral instrument (OCR-2000 P002), because they needed to rest on a V-block to maintain stability (because of their larger size).

Lamp F-548 (L009) was aligned and powered on following the procedures in Sect. 1.5.3. The aperture was adjusted so there were no shadows or diffraction edges on the plaque, and any stray light was minimized by following the practices given in Sect. 1.5.4. Figure 26 shows the experimental setup.

The first step in collecting data began with placing aperture caps on the DUT and the monitor sensor (I121), and then collecting dark data. If the SXR was the DUT, background data were collected immediately after the dark data. The next step was to record data every 2° over 360°. During each test, the monitor sensor provided a measure of the stability of the lamp flux over the course of the rotation sequence.

7.2.2 Rotation of Irradiance Sensors

This experiment was designed to estimate the rotation sensitivity of irradiance sensors during the calibration process. The only type of irradiance sensor rotated was an OCI-200.

7.2.2.1 Equipment

The equipment used for the irradiance rotation trials was as follows:

- Satlantic Optronic lamp F-548 (L009);
- OCI-200 I040 with DATA-100 (S/N 043);
- Monitor sensor, OCI-200 I121 with DATA-100 (S/N 047);
- Current source OL83A 99115110 (C001);
- Shunt resistor 1151570 (Z001);
- Voltmeter 3146A09840 (V002);
- Oriel rotator model 13059 equipped with a custom D-shaped collar adapter;
- Oriel stepper control box model 20010 (S/N 542);

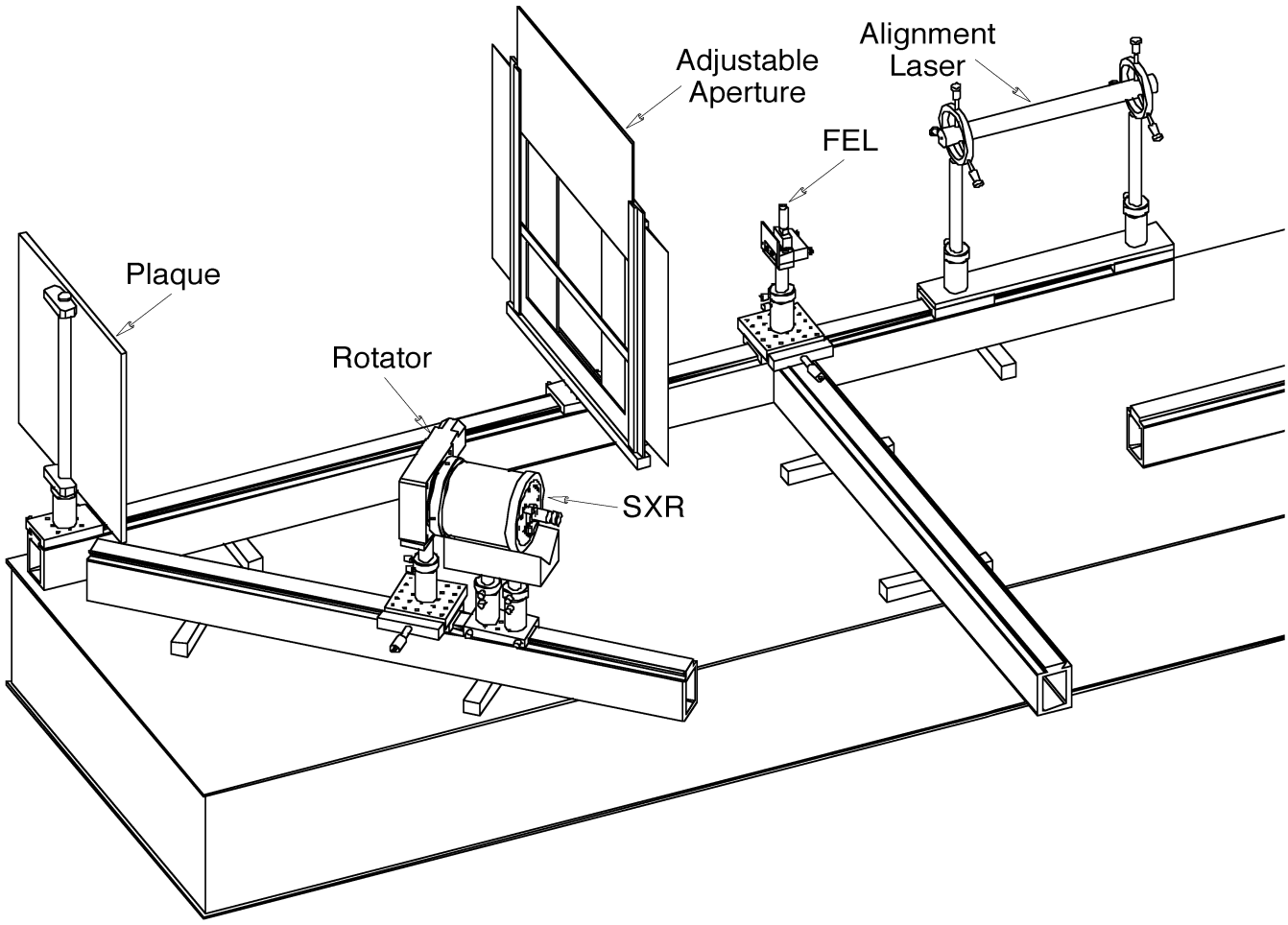

Fig. 26. The experimental setup for determining the sensitivity of radiance sensors to rotation, in this case, with the SXR as the DUT. Note that the SXR is supported by a V-block while it is being rotated at the front part of the instrument housing. The monitor sensor is not shown.

- Rotator D-shaped collar adapter; and
- Lamp mount, V-block and mount, plaque mount, seven carriers, alignment grid, and alignment laser 05-LHR-201-355.

7.2.2.2 Procedures

The DUT was placed on the 45° rail on calibration table 2 in the appropriate rotator mount. All of the radiometers attached to the rotator using the D-shaped collar. The DUT was positioned on the rail such that the sensor was approximately 50 cm from the plaque along the rail axis. A test was made to ensure the instrument could be rotated freely through 360° by driving the rotator through the full range of motion used in the experiment. Any wires were wound such that they did not hinder the circular movement or pull on the DUT.

The plaque (T001) was placed on the center rail in the proper carrier mount. A paper cover was placed over the active area of the plaque to protect it during all adjustments and to provide for proper focusing of the SXR. The DUT was aligned with respect to the plaque using the alignment laser and the procedures given in Sect. 1.5.2. The alignment of the DUT was suboptimal, because it only had three degrees of freedom—it could be rotated around the post holding the rotator, it could slide along the rail, and it could be raised and lowered. A translator was added to the carrier to allow it to travel orthogonal to the rail. Figure 27 shows the experimental setup.

Lamp F-548 (L009) was aligned and powered on following the procedures in Sect. 1.5.3. The aperture was adjusted so there were no shadows or diffraction edges on the plaque, and any stray light was minimized by following the practices given in Sect. 1.5.4.

The first step in collecting data began with placing aperture caps on the DUT and the monitor sensor (I121), and then collecting dark data. If the SXR was the DUT, background data were collected immediately after the dark

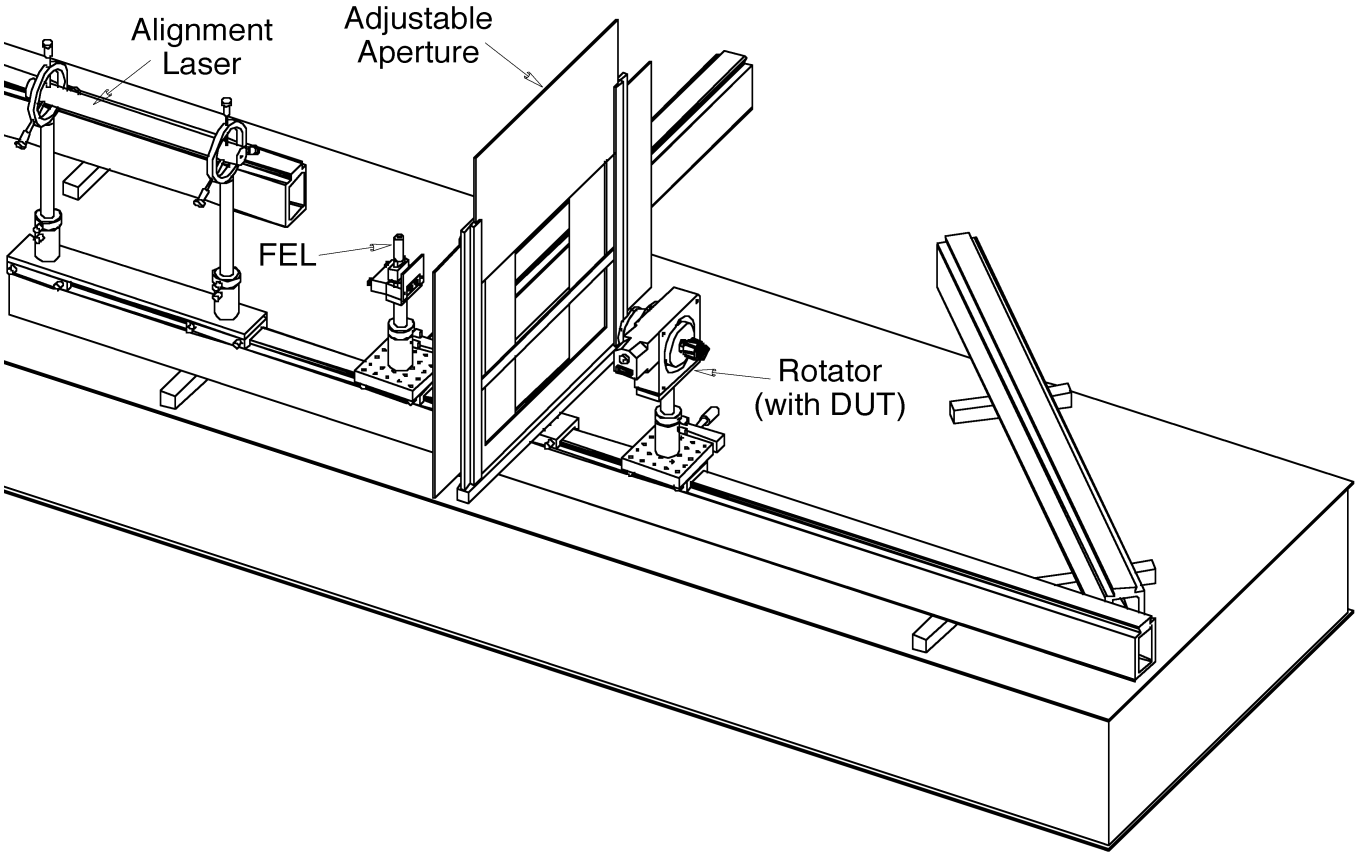

Fig. 27. The experimental setup for determining the rotation sensitivity of irradiance sensors. The DUT is an OCI-200 and is completely supported by the rotator. The monitor sensor is not shown.

data. The next step was to record data every 2° over 360°. During each test, the monitor sensor provided a measure of the stability of the lamp flux over the course of the rotation sequence.

7.2.3 Results

The uncertainty due to sensor rotation on the calibration process is quantified using the PCR statistic. The first step requires the ratio formed by comparing the calibrated response at a particular angle, θ, with respect to the average from a full 360° rotation of the sensor.

$$\chi^{\text{ratio}}_{S_{\text{ID}}}(\lambda,\theta) \;=\; \frac{100\left[\bar{V}_{S_{\text{ID}}}(\lambda,\theta)-\bar{D}_{S_{\text{ID}}}(\lambda)\right]}{\dfrac{1}{N_\theta}\displaystyle\sum_{\theta=0^\circ}^{360^\circ}\left[\bar{V}_{S_{\text{ID}}}(\lambda,\theta)-\bar{D}_{S_{\text{ID}}}(\lambda)\right]} \qquad (16)$$

where N_θ is the number of angular positions sampled (2° increments were used for the rotation experiments, so $N_\theta = 181$). An example of the PCR as a function of θ for the R064 (above-water) radiance sensor is presented in Fig. 28. The centermost channel, within the cluster of seven (Fig. 3), is number seven.

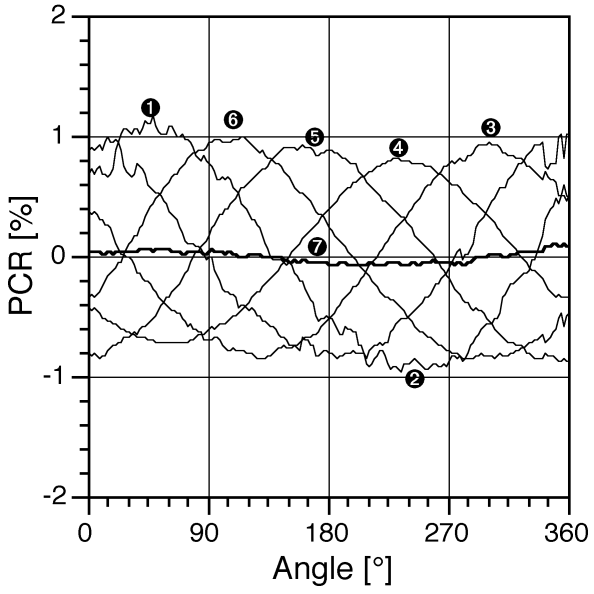

Fig. 28. The PCR values for R064 during rotation. The numbered bullets correspond to the channel numbers.

The summary statistic for the rotational effect on calibrations is formed from the maximum and minimum PCR values measured during the 360° rotation of the sensor, $\chi^{\max}_{S_{\rm ID}}(\lambda)$ and $\chi^{\min}_{S_{\rm ID}}(\lambda)$, respectively:

$$\chi^{\rm rot}_{S_{\rm ID}}(\lambda) \;=\; \frac{\chi^{\max}_{S_{\rm ID}}(\lambda) - \chi^{\min}_{S_{\rm ID}}(\lambda)}{2}. \qquad (17)$$

The $\chi^{\rm rot}_{S_{\rm ID}}(\lambda)$ values for the rotation uncertainty experiment are given in Table 10. The P002 and X001 sensors have single apertures; the R035, R064, and I040 sensors are seven-channel instruments with a centermost channel (Fig. 3) which is usually the highest wavelength (except for R064). For the seven-channel instruments, the minimum rotation effect is associated with the center channel; this is particularly notable for R064 (a narrow FOV radiance sensor) and I040 (an irradiance sensor). The smallest average effect occurs for the single-aperture instruments.

Table 10. The results from the rotational experiments executed during SIRREX-7. The FAFOV of the radiometers is given in degrees and the centermost channel for the seven-channel sensors in bold. Averages for multi-aperture sensors were calculated without including the center-most channel.

λ [nm]	*R035* 20°	*R064* 6°	*P002* 17°	*X001* 2.4°	*I040* 180°
412	0.3	1.1	0.4	0.2	0.6
443	0.3	0.9	0.2	0.2	0.7
490	0.3	0.9	0.1	0.3	0.7
510	0.5	0.9	0.2		0.7
555	0.5	0.9	0.2	0.2	0.7
665	0.4	**0.1**	0.3	0.3	0.7
683	**0.3**		0.3		**0.2**
775			0.5	0.3	
780		0.8	0.5		
Average	*0.4*	*0.9*	*0.3*	*0.2*	*0.7*

The single-aperture sensors have similar average rotational effects, which are the lowest for the five sensors, but they are clearly different from a spectral point of view. The SXR rotational effect is spectrally flat, whereas, the hyperspectral instrument has maximal effects in the bluest and reddest wavelengths and minimal effects in the green domain.

7.3 POLARIZATION EFFECTS

The polarization sensitivity of radiance sensors during the calibration process involved three types of sensors: two OCR-200s (R035 and R064), an OCR-2000 (P002), and the SXR (X001). The OCR-200 has multiple apertures (arranged in a circular array), while the OCR-2000 and SXR have single apertures. The latter was also distinguished by being the only instrument with mirrors in the optical pathway (one for each channel).

7.3.1 Equipment

The equipment used for the radiance polarization trials was as follows:

- Satlantic Optronic lamp F-548 (L009);
- Satlantic white (18 in) plaque 05816 (T001), and JRC white (18 in) plaque 22463 (T004);
- OCR-200 R035 with DATA-100 (S/N 043);
- Monitor sensor, OCI-200 I121 with DATA-100 (S/N 047);
- OCR-2000 P002;
- The SXR (X001) with custom rotator mount and digital voltmeter (V003);
- Current source OL83A 99115110 (C001);
- Shunt resistor 1151570 (Z001);
- Voltmeter 3146A09840 (V002);
- Oriel rotator model 13059 equipped with a custom D-shaped collar adapter;
- Oriel stepper control box model 20010 (S/N 542);
- Rotator D-shaped collar adapter;
- Polarizing sheet (Melles Griot model 03–FPG–013);
- Polarizer mount adapter (Melles Griot model 07–HPA–011);
- Polarizer rotating mount (Melles Griot model 07–HPR–007); and
- Lamp mount, V-block and mount, plaque mount, seven carriers, alignment grid, and alignment laser 05–LHR–201–355.

7.3.2 Procedures

The DUT was placed on the 45° rail on calibration table 2 in the appropriate rotator mount. When the SXR was the DUT, a special mount was used to hold it to the rotator. All other radiometers were attached to the rotator using the D-shaped collar. The DUT was positioned on the rail such that the sensor was approximately 40 cm from the plaque along the rail axis, unless the DUT was the SXR, in which case the distance was set to 85 cm. A test was made to ensure the instrument could be rotated freely through 360° by driving the rotator through the full range of motion used in the experiment. Any wires were wound such that they did not hinder the circular movement or pull on the DUT.

The plaque (T001 or T004) was placed on the center rail in the proper carrier mount. A paper cover was placed over the active area of the plaque to protect it during all adjustments and to provide for proper boresight focusing of the SXR. The DUT was aligned with respect to the plaque using the alignment laser and the procedures given in Sect. 1.5.2. The alignment of the DUT was suboptimal, because it only had three degrees of freedom. It could be rotated around the post holding the rotator, it could

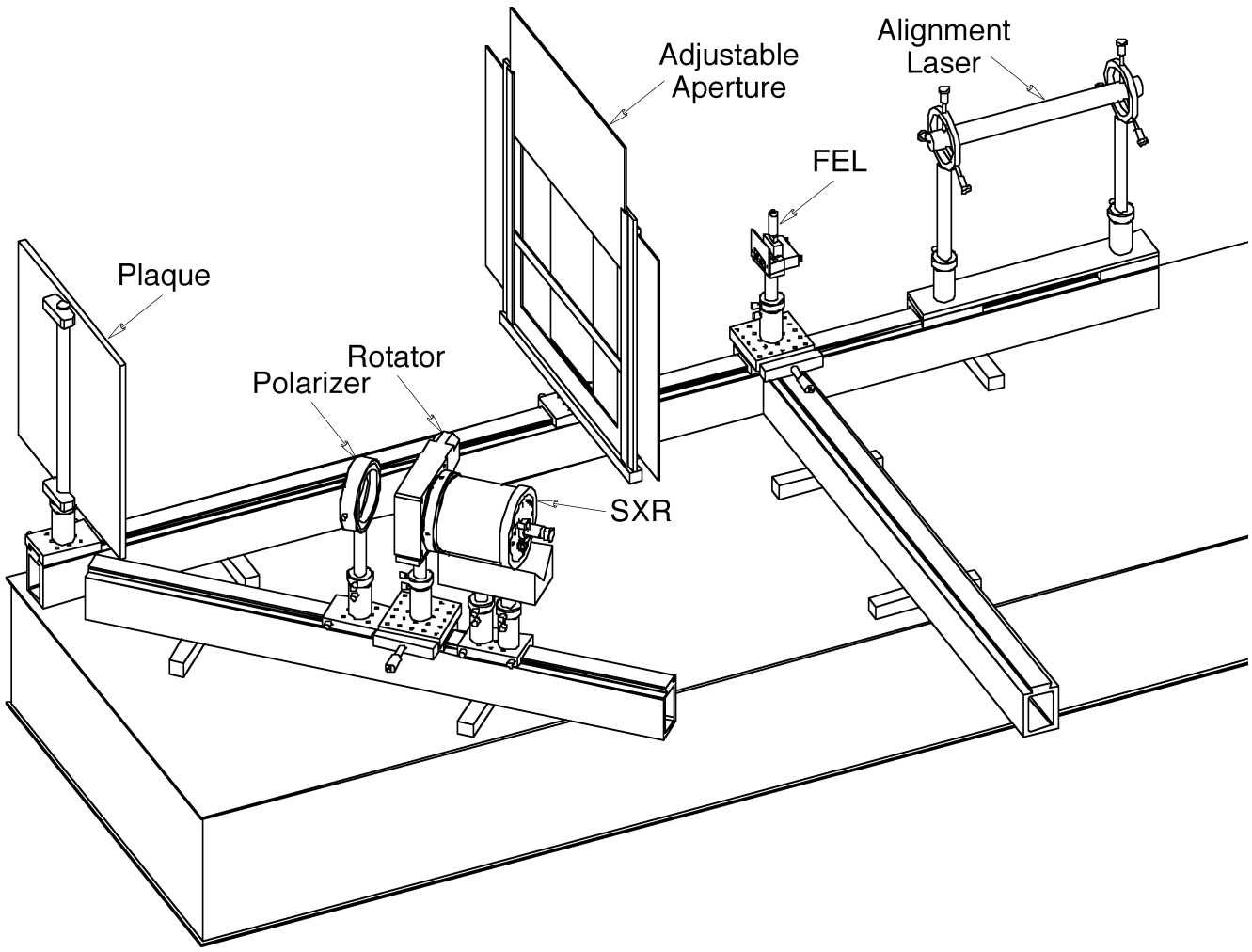

Fig. 29. The experimental setup for determining the polarization sensitivity of radiance sensors in radiance calibrations (in this case, with the SXR as the DUT). The adjustable aperture was opened or closed to ensure the plaque was completely illuminated, while making sure there were no shadows or diffraction edges on the plaque.

slide along the rail, and it could be raised and lowered. A translator was added to the carrier to allow it to travel orthogonal to the rail. This was necessary when using the SXR and the hyperspectral instrument (OCR-2000 P002) because they needed to rest on a V-block (due to their larger size).

Lamp F-548 (L009) was aligned and powered on following the procedures in Sect. 1.5.3. The aperture was adjusted so there were no shadows or diffraction edges on the plaque, and any stray light was minimized by following the practices given in Sect. 1.5.4. Figure 29 shows the experimental setup.

The first step in collecting data began with placing aperture caps on the DUT and the monitor sensor (I121), and then collecting dark data. If the SXR was the DUT, background data were collected immediately after the dark data. The next step was to record data every 2° over 360° without the polarizer. The polarizer was then placed immediately in front of the DUT and aligned following the procedures given in Sect. 1.5.2, after which, polarized data were recorded every 2° over a full 360° rotation of the sensor. During each measurement sequence, the monitor sensor provided a measure of the stability of the lamp flux over the course of the rotation sequence.

7.3.3 Results

The polarization parameter, P, for a particular radiance sensor (identified by the $S_{\rm ID}$ code) is defined in percent as

$$P_{S_{\rm ID}}(\lambda,\theta) \;=\; 100\,\frac{L^{\rm max}_{S_{\rm ID}}(\lambda,\theta) - L^{\rm min}_{S_{\rm ID}}(\lambda,\theta)}{L^{\rm max}_{S_{\rm ID}}(\lambda,\theta) + L^{\rm min}_{S_{\rm ID}}(\lambda,\theta)}, \qquad (18)$$

where $L^{\rm max}_{S_{\rm ID}}(\lambda,\theta)$ and $L^{\rm min}_{S_{\rm ID}}(\lambda,\theta)$ are the maximum and minimum radiances measured during the 360° rotation of the sensor, respectively.

The polarization parameters for four radiance sensors are presented in Table 11. Although all of the radiometers show a spectral dependence, they are not the same for each sensor type. The seven-channel sensors (R035 and R064) show maximal effects in the blue part of the spectrum which decrease towards the red domain, the hyperspectral instrument has minimal effects in the blue and maximal effects in the red, and the SXR exhibits only a mild spectral dependence with the largest effect in the bluest wavelength.

Table 11. The results from the polarization experiments executed during SIRREX-7. The center-most channels for the seven-channel sensors are shown in bold face.

λ [nm]	*R035*	*R064*	*P002*	*X001*
412	1.4	2.4	0.4	5.1
443	1.1	1.2	0.2	4.4
490	0.4	0.8	0.4	4.6
510	0.4	0.6	0.5	
555	0.5	0.9	0.7	4.5
665	0.5	**0.3**	1.5	4.3
683	**0.2**		2.0	
775			2.1	4.4
780		0.3	2.6	
Average	*0.6*	*0.9*	*1.2*	*4.6*

The smallest average polarization effect occurs for the seven-channel sensors, the hyperspectral instrument is a little larger, and the SXR is significantly larger. As was seen with the rotation experiments (Table 10), the centermost channel for the seven-channel sensors show the smallest effect, but as shown with the R064 sensor, part of this is associated with the spectral decrease from the blue towards the red domain.

The specification for polarization in the SeaWiFS Ocean Optics Protocols (Mueller and Austin 1995) is 2% or less. On average, all the Satlantic sensors are within this specification, although some individual wavelengths exceed this requirement. The SXR, in comparison, is always above 2%, with an average a little above 4.5%. In order to check whether or not the polarization values for the Satlantic above- and in-water OCR-200 sensors were typical, additional polarization experiments were conducted. The average polarization for the above-water sensor was 0.6%, and the average polarization for the in-water sensor was 0.9%. The average values are in close agreement to the SIRREX-7 values, but the values in the blue show the largest variability: the newest polarization values at 412 nm are 0.6% higher for the in-water sensor and 0.7% lower for the above-water sensor. This variability is also seen, in part, at 443 nm, so additional polarization experiments are probably needed to completely characterize this parameter.

Chapter 8

Absolute Calibration of the SQM and SQM-II

Stanford B. Hooker
NASA/Goddard Space Flight Center
Greenbelt, Maryland

Scott McLean
Gordana Lazin
Satlantic, Inc.
Halifax, Canada

Abstract

To better understand the capability of portable sources, a series of experiments were conducted to transfer an absolute calibration to the original SQM and four SQM-IIs, and to map the homogeneity of an SQM-II exit aperture. Approximately 25% of the central portion of the exit aperture was within 2% of the maximum signal, and about 40% was to within 5%. The decay in SQM flux over a 500 day time period, which included one shipping event, was estimated to be approximately 0.9% every 100 days. The decay for an SQM-II (S/N 004) over the same time period, but encompassing four shipping events, was approximately 2.2% every 100 days. The average and standard deviations in the coefficient of variation was used as a stability parameter for the SQM and SQM-II. Both sources showed a spectral dependence with the greatest stability in the red part of the spectrum, and the least stability in the blue. The standard deviation in the coefficient of variation was independent of wavelength for the SQM, but the SQM-II had a noticeable spectral dependence—the reddest wavelength (775 nm) had a standard deviation approximately half that of the blue wavelengths. Using the overall averages as generalized metrics for stability, the SQM was more stable than the SQM-II: the overall average was a factor of three smaller, and the overall standard deviation was an order of magnitude smaller.

8.1 INTRODUCTION

Most SeaWiFS validation campaigns have been on Atlantic Meridional Transect (AMT) cruises (Aiken et al. 2000), which occur twice a year and involve a transit of the Atlantic Ocean between Grimsby (UK) and Stanley (Falkland Islands) with a port call in Montevideo (Uruguay). In all of the AMT cruises the SQM was a part of, it was shipped long distances between the US, the UK, and the Falkland Islands or Uruguay (also once to South Africa) with no negative effects on performance both during the cruise time period and between cruises.

The SQM lamps were changed after its commissioning to produce a flux level more in keeping with the radiometers being deployed on AMT cruises, but the same lamp set was used during AMT-5 through AMT-7 (another lamp change was made after AMT-7 to fine tune the flux levels). During the design stage of the SQM, there was some controversy about running the lamps below their rated current (approximately 95% of rating), but there has been no observable degradation in the performance of the lamps as a result of this—indeed, they have survived long shipment routes using a variety of transportation vehicles (trucks, planes, etc.) on repeated occasions, as well as, the high vibration environment of a ship.

Figure 30 is a summary of SQM performance during the AMT-5 through AMT-7 time period (spanning 460 days). It shows the internal blue monitor signal, measured with the glass fiducial, as a function of time, but presented as the percent difference with respect to the mean value for the entire time period. A confirmation of the signal is given by the R035 radiometer for the 443 nm channel (which is very similar to the blue internal monitor), and it very nearly mirrors the internal monitor signal. The two detectors yield similar decay rates of approximately 0.007% per day, or approximately 0.25% for a 35-day cruise. This is an underestimate, however, because the degradation is due mostly to lamp usage, and this is most significant during use, and not during shipping and storage. This is best seen by looking at the individual cruises, and comparing them to the laboratory work after AMT-7.

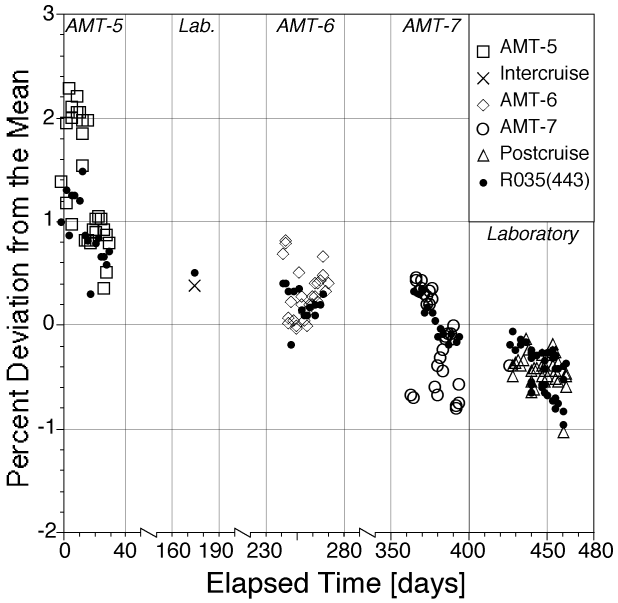

Fig. 30. The long-term stability of the original SQM (S000) as measured on a series of AMT cruises and laboratory exercises.

The stability and behavior of the SQM during AMT-5 was very similar to its performance on AMT-3 when it was first commissioned for field use (Hooker and Aiken 1998): the data indicate a stepwise change in the SQM flux level halfway through the cruise. All three detectors show the change, and if the three detector signals are averaged together, the emitted flux of the SQM decreased by approximately 0.87%. The change in flux was due to a partial short in one of the bulbs which resulted in a 1.2% decrease in the operating voltage of the lamp. The stability of the SQM during the periods before and after the change in light output, as estimated by one standard deviation (1σ) in the average of the three internal monitor signals, was to within 0.60% and 0.53%, respectively.

During AMT-6, the 1σ values of the red, blue, and white detectors while measuring the glass fiducial were 0.36, 0.46, 0.39%, respectively. The performance of the SQM during AMT-6 was the best out of all the cruises; no lamp anomalies were experienced and the standard deviation in the emitted flux was the lowest ever recorded in the field. The AMT-7 data show a stepwise change halfway through the cruise, as was seen during AMT-3 and AMT-5. Although the stability for the entire cruise was very good, to within $\pm 0.43\%$ as measured by the blue detector, the stability improves to $\pm 0.38\%$ and $\pm 0.28\%$ if the cruise is split into a first and second half, respectively.

Lamp performance after AMT-7 in the laboratory was very similar to that seen during AMT-6: the range of changes are all within 1% and the 1σ values of the red, blue, and white detectors while measuring the glass fiducial were 0.xx, 0.yy, 0.zz%, respectively. The SQM is clearly a robust instrument well suited to the task of calibration monitoring in the field, and is now an integral component for quantifying the stability of field radiometers during most SeaWiFS field campaigns. The long- and short-term stability of the SQM raises the possibility that this device can be used for absolute calibrations in the laboratory and in the field.

8.2 SQM-II APERTURE MAPPING

The original SQM had a design specification for uniformity in spectral radiance over the exit aperture of 5% or less; measurements of a prototype SQM had an aperture uniformity (over the active area viewed by an in-water OCR-200 sensor) of 4% (Johnson et al. 1998b). The design objective of the SQM-II was to meet or exceed this capability. The primary purpose of the SQM-II mapping experiment was to establish whether or not this objective was satisfied.

8.2.1 Equipment

The equipment used for mapping an SQM-II (S002) aperture was as follows:

- Satlantic SQM-II (S002) with the outer shadow collar removed (to expose the exit aperture);
- The xz-mapping radiometer (Y001) with its table, mount, filter holders, and filters; and
- Alignment laser 05–LHR–201–355.

8.2.2 Procedures

The shadow collar with D-shaped collar adapter plate was removed, so the entire exit aperture was visible. The xz-mapping table was mounted directly facing the SQM with the mapping detector 28 cm from the SQM-II diffuser. The alignment was done using the laser attached to the xz-mapper table, such that when the mapping radiometer was in the central position it would view the center of the SQM-II aperture.

The broadband filter on the mapping radiometer, with a 0.5° FOV, was mounted on the mapping detector. Dark data were collected for the SQM-II internal monitors and the xz-mapping radiometer. The SQM-II warm-up sequence was initiated using the low bank of lamps.

After the SQM-II had warmed up, the xz-mapping software was used to scan the SQM-II aperture in 5 mm increments, which took about 8 h. After the low bank illumination was mapped, the high bank illumination was mapped using the same procedures.

8.2.3 Results

The homogeneity of the SQM-II for high and low lamp levels is presented in Figs. 31a and 31b, respectively. Although both illumination levels show a symmetric decay in flux with respect to the centermost portion of the aperture, the low lamp level plot shows some small asymmetries.

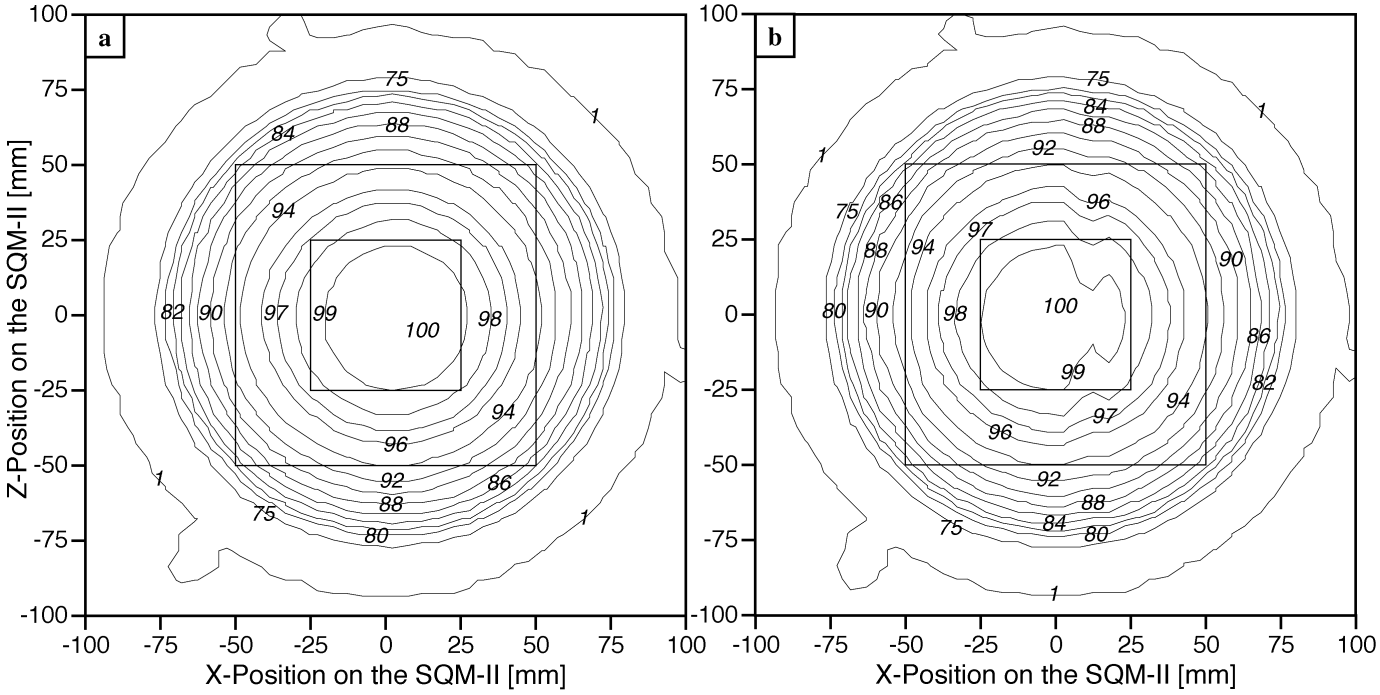

Fig. 31. The homogeneity of the SQM-II aperture (with shadow collar removed) for two different lamp illumination levels: **a)** high bank and **b)** low bank. The contours represent percentages of the maximum detected signal. The central portion of the exit aperture is delimited by the outermost central square, and the centermost central square represents 25% of the former. The latter encompasses the active viewing area of an in-water OCR-200 sensor.

The asymmetries appear along a particular x coordinate, so it is possible the asymmetries are due to positioning errors during the scanning of the exit aperture. The absence of any similar asymmetries in the high illumination level data suggests the asymmetries cannot be due to reflective inhomogeneities within the light chamber. A malfunctioning lamp would not produce an asymmetry confined to a single axis, so a scanning error is the most likely explanation.

Approximately 25% of the central portion of the exit aperture is within 2% of the maximum signal (the area viewed by an above- or in-water OCR-200 sensor), and about 40% is to within 5%. Although uniformity is an important requirement for a portable source, stability in the emitted flux level, both during a single session and between sessions, is also important. The latter is addressed in the next section, and the former can be inferred from Fig. 31. The circular contours in Fig. 31 are a direct indicator of the stability in the light field during the mapping session—if the flux levels were not stable, the contours would be distorted and would not be well-formed circles.

8.3 ABSOLUTE SQM CALIBRATION

The absolute calibration of the SQM and SQM-IIs was made using the SXR and several commercial radiometers, with the former being the primary sensor, because it has a NIST absolute calibration.

8.3.1 Equipment

The equipment used for the absolute SQM calibration measurements was as follows:

- NASA SQM (S000) with its external control hardware case, NASA SQM-II (S004), Satlantic SQM-IIs (S001 and S002), and JRC SQM-II (S003);
- The SXR (X001) with custom mount and digital voltmeter (V003);
- OCR-200 R035 with DATA-100 (S/N 043);
- Current sources OL83A 96113058 (C002) and 83DS 93200490 (C003);
- Shunt resistor 1551570 (Z001);
- Voltmeter 3146A09840 (V002); and
- Lamp mount, ring mount, plaque mount, four carriers, and alignment laser LHRR-055 (S/N 3598–1592–65).

8.3.2 Procedures

All radiometers were calibrated before the SQM measurements following the procedures given in Chapters 5 and 6.

The SQMs were warmed up while the radiometers were being calibrated. The start of each warm-up session was

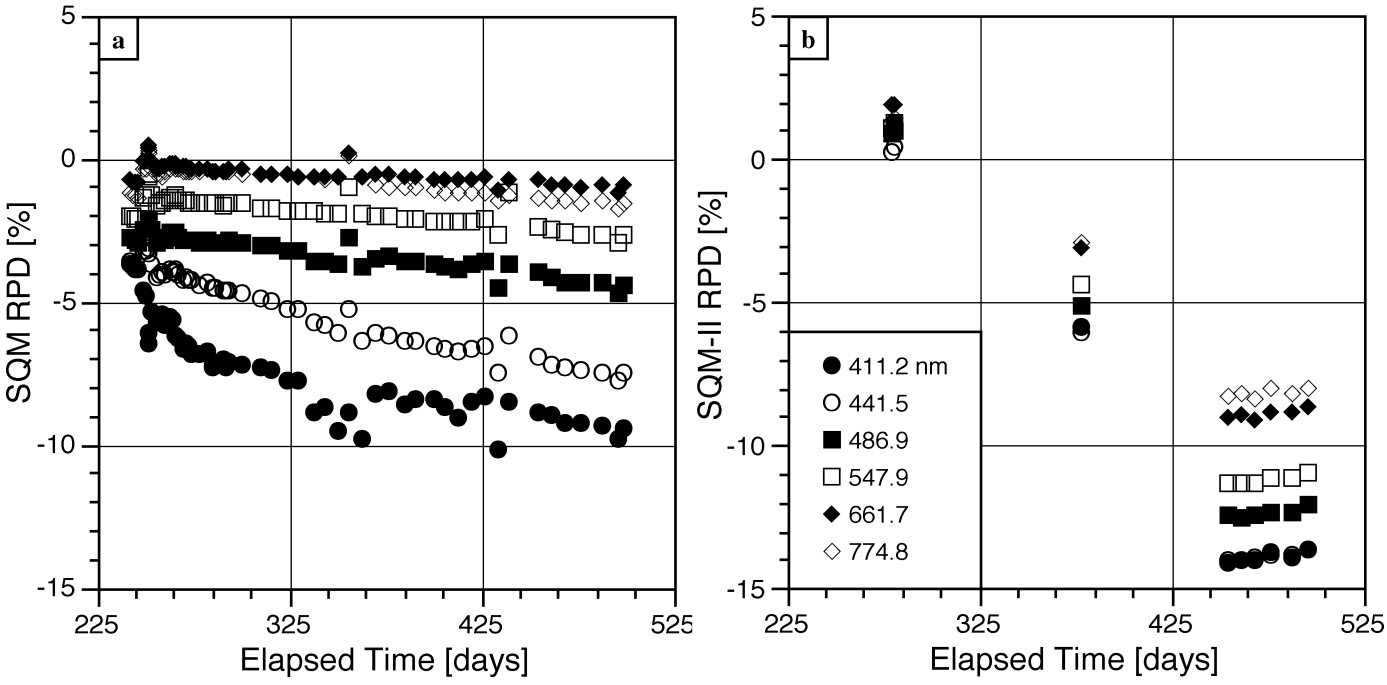

Fig. 32. The RPD values for the temporal evaluation of the absolute calibration of the **a)** SQM and **b)** SQM-II (S/N 004) performed during SIRREX-7. The elapsed time is with respect to the first SQM and SQM-II measurements executed during SIRREX-7.

staggered, so each SQM had a similar amount of time being on by the time it was used for a measurement. The radiometers were measured one at a time at each SQM. Dark radiometer data were collected first, and while these data were being taken, fiducial data were recorded at the SQM. Then the radiometer was mounted to the SQM using the D-shaped collar and signal data were recorded. The exception to the latter was the SXR. The SXR was placed 85 cm away from the SQM aperture with the aperture uncapped.

All radiometers were calibrated after the SQM measurements following the procedures given in Chapters 5 and 6. The entire process was repeated four times (three trials were planned, but a malfunctioning radiometer during the first trial resulted in the addition of another trial to be sure all radiometers were measured at least three times).

8.3.3 Results

The calibrated flux of the portable sources was measured using the SXR, both during SIRREX-7 and afterwards during special laboratory sessions at GSFC. From these data, two different types of diagnostic variables can be derived. The first involves using the average calibrated values from SIRREX-7 as a reference, and then calculating RPD values from the subsequent laboratory sessions by differencing the new values from the reference and dividing by the reference value (as was done in Sect. 3.2.3). The other diagnostic variable that can be considered is the coefficient of variation, $\zeta(\lambda)$, defined as the standard deviation in the measured light signal divided (or normalized) by the average of the signal. A time series of $\zeta(\lambda)$ can be constructed to investigate the temporal stability of the emitted flux, because higher standard deviations are associated with flux instability.

Figure 32 is a plot of the RPD values between the SQM and SQM-II (S/N 004) for a 250 day time period following SIRREX-7. The data show differing temporal resolution for two reasons: a) the SXR was not available for this type of work after SIRREX-7, because it was scheduled for another activity, and b) the SQM-II was used in several field campaigns after SIRREX-7, so it was available in between shipments for very brief periods. The two portable sources were, therefore, subjected to very different environments—the SQM was shipped back from SIRREX-7 and stayed in a laboratory, whereas the SQM-II was shipped back and then subsequently used in three different international cruises.

The SQM exhibits a small decrease in flux, about 2.4% on average, as a result of the shipment after SIRREX-7 (Fig. 32a). The largest changes are associated with the blue wavelengths, which steadily decrease as a function of time. By the end of the 250 day sequence, the decrease is 9.5% at 412 nm, but only 1.0% at 665 nm. These decay values are in keeping with the general stability of halogen lamps which show greater instability in the blue domain than in the red domain. Considering average performance over the time period this experiment encompasses,

the SQM decays by approximately 0.9% every 100 days (one shipping event).

In comparison, the SQM-II exhibits a small increase in flux, approximately 1.0% on average, as a result of being shipped back from SIRREX-7 and then from being used immediately in the field (Fig. 32b). As with the SQM, the largest changes are associated with the blue wavelengths, which steadily decrease as a function of time. Initally, the spread in the spectral values at any one measurement time is less than for the SQM, but by the end of the time series, the spread is similar. Considering the average performance over the experimental time period, the SQM-II decays by approximately 2.2% every 100 days (i.e., four shipping events).

The average and standard deviations in $\zeta(\lambda)$ for the SXR measurements of the SQM and SQM-II apertures during the absolute calibration trials, $\mu(\lambda)$ and $\sigma(\lambda)$, respectively, are presented in Table 12. Both sources show a spectral dependence with the greatest stability in the red part of the spectrum, and the least stability in the blue. The standard deviation in $\zeta(\lambda)$ is independent of wavelength for the SQM, but the SQM-II has a noticeable spectral dependence—the reddest wavelength (775 nm) has a standard deviation approximately half that of the blue wavelengths. Using the overall averages as metrics for stability (the last line in Table 12), the SQM is more stable than the SQM-II: the overall average is a factor of three smaller, and the overall standard deviation is an order of magnitude smaller.

Table 12. The average (μ) and standard deviations (σ) in the coefficient of variation (both in percent) for the SXR measurements of the SQM and SQM-II apertures during the absolute calibration trials.

SXR	*SQM*		*SQM-II*	
λ [nm]	$\mu(\lambda)$	$\sigma(\lambda)$	$\mu(\lambda)$	$\sigma(\lambda)$
411.2	0.07	0.005	0.16	0.043
441.5	0.04	0.004	0.15	0.042
486.9	0.03	0.004	0.13	0.035
547.9	0.03	0.004	0.12	0.036
661.7	0.03	0.003	0.10	0.036
774.8	0.03	0.005	0.09	0.022
Average	*0.04*	*0.004*	*0.13*	*0.036*

Chapter 9

SIRREX-7 Synthesis, Discussion, and Conclusions

Stanford B. Hooker
NASA/Goddard Space Flight Center
Greenbelt, Maryland

Giuseppe Zibordi
JRC/SAI/Marine Environment Unit
Ispra, Italy

Scott McLean
Satlantic, Inc.
Halifax, Canada

Abstract

A combined uncertainty budget for radiometric calibrations can be constructed from the SIRREX-7 data set. Although it is comprehensive, it does not address every source of uncertainty at the same level of detail and some must be considered as approximate. Nonetheless, the care taken in each experiment ensures the uncertainty estimates are representative of what can be expected if careful metrology and practices are used. Perhaps just as importantly, the consequences of discrepancies are also well estimated. To provide a range of possible outcomes in the calibration process, minimum, typical, and maximum uncertainties are computed from the various entries, which range from 1.1–3.4% and 1.5–6.7% for irradiance and radiance calibrations, respectively. The Satlantic facility falls somewhere between the minimum and typical values. If an additional (average) 1.0% is included to account for an unknown bias detected with the lamp and plaque uncertainty experiments (described in Sects. 3.2 and 4.2, and discussed in Sects. 9.2 and 9.5), the uncertainty for Satlantic irradiance calibrations is 1.8%, and the uncertainty for radiance calibrations is 2.3%.

9.1 INTRODUCTION

This chapter synthesizes the results from the various SIRREX-7 experiments and discusses the conclusions that can be drawn from them. The lessons learned are separated according to irradiance or radiance calibrations, and those applicable to both. Not all types of Satlantic sensor were included in SIRREX-7, in fact, the most common instrument was the model 200 series of radiance and irradiance sensors (Table 7). Most Satlantic instruments share design commonalities, however, so the results have some applicability to most instrument classes. An obvious exception is the difference between single- and multiple-aperture sensors: the latter have more complicated alignment effects, because they have multiple viewing axes.

A summary of the various experiments executed during SIRREX-7 is presented in Table 13. Although it was not possible to replicate all the experiments the same number of times, the primary experiments were executed as many times as economically feasible to ensure statistical reliability. Most of the experiments involved the use of all three principle components of radiometry, source, target, and detector, so most have results applicable to other objectives. The material presented here is organized primarily according to the order the experiments were presented in Chapters 3–8 (some information originally presented in different chapters was combined into one section).

9.2 LAMP UNCERTAINTIES

The results from the investigations into lamp uncertainties (Sect. 3.2.3) showed a deterministic bias when the irradiance of the lamps calculated from the SXR measurements of the NIST plaque were compared to the values supplied with the lamp (Fig. 5). Each component of the experiment has an uncertainty on the order of 1%, and given another (maximum) 1% from mechanical setup uncertainties, the range of uncertainty seen with the so-called *trusted* lamps is within the quadrature sum of these components, that is, the approximately 2% uncertainty in the blue part of the spectrum is very close to $\sqrt{4}$.

The spectral dependence in SXR uncertainties is approximately 0.5% (Johnson et al. 1998a), with maximal un-

Table 13. A summary of the experiments executed during SIRREX-7. The total number of trials, N_T, is the number of experimental replications times the number of devices tested for whatever part of the experiment was being varied (e.g., for plaque uncertainties, the targets were varied). The stability of of eacg source was checked by recording any power supply voltages and, in some cases, by measuring the emitted flux with a monitoring sensor (rightmost column). Note the SQMs have internal detectors for this purpose.

Section and Name	N_T	*Source(s)*	*Target(s)*	*Detector(s)*	*Monitor*
3.2 Lamp Uncertainties	30	L000–L009	T005	X001	R035
3.3 Calibration Comparison	2	L007, L010			
3.4 Lamp Repeatability	30	L000–L009	T001	X001	R035
4.2 Plaque Uncertainties	21	L003	T001–T007	X001	R035
4.3 Plaque Uniformity	3	L000, W005	T001	Y001	
4.4 Bidirectional Effects	7	L003	T001–T007	X001	
5.2 Radiance Repeatability	33	L008	T001	R035, R036, R067	I121
5.3 Ambient Measurements	12	L008, L003	T001	R035, R036, R067, X001	I121
6.2 Irradiance Repeatability	33	L009		I040, I050, I097	I121
6.3 Ambient Measurements	9	L009		I040, I050, I097	I121
7.2 Rotation Effects	5	L009	T001, T004	R035, P002, R064, X001, I040	I121
7.3 Polarization Effects	4	L009	T001, T004	R035, P002, R064, X001	I121
8.2 SQM-II Aperture Mapping	2	S002		Y001	
8.3 Absolute SQM Calibration	12	S000–S004		R035, X001	

certainties in the blue domain and minimal in the red (the average uncertainty is about 0.7%). Lamp uncertainties beyond those assigned to the lamp calibration (positioning, current stability, etc.) can have a spectral component, but the lamp repeatability experiments (Sect. 3.4) showed these were small (less than 0.2%), except for L005 which was unseasoned and not a *trusted* lamp (Fig. 8). Similar arguments can be made for the use of the NIST plaque, so the expected uncertainty curve for realizing the irradiance of a lamp using the NIST plaque and the (NIST) SXR is that the uncertainties would not show a strong spectral dependence. Figure 5 shows they clearly do, so there must be a bias above and beyond the SXR uncertainties.

Scattered light might explain the spectral dependence, because it is frequently hard to control in the lamp and plaque setup and can easily have a spectral component. The baffling in the Satlantic calibration facility is state of the art: the wall and ceiling paint, as well as the curtain partitions, were carefully selected and especially *black*. Although extensive experimentation to assess scattered light contributions was not executed, the ambient measurements (Sects. 5.3.3 and 6.3.3) indicated the scattered light contributions were small and spectrally independent for most of the visible spectrum (less than 0.2%); the only significant contributions were in the near-infrared (about 1.0%).

There are distance issues that are also relevant to the bias result. The SXR was sufficiently far from the plaque to ensure the entrance pupil was completely filled (which was verified by looking through the SXR boresight). The lamp-to-plaque distance was not varied for these experiments, but a partial inquiry into the importance of this was examined (Sect. 4.3). For the standard 1.3 m lamp-to-plaque distance and the narrow FOV of the SXR, this should have contributed less than 1% uncertainty (Fig. 13b).

In conclusion, the lamp uncertainty data identify a systematic bias that is on the order of the contributing uncertainties, but do not fully explain it, because the spectral properties are not the same. The spectral bias can be estimated using the average RPDs in Fig. 5 for the *trusted* lamps. The results of removing the bias from all the data are shown in Fig. 33.

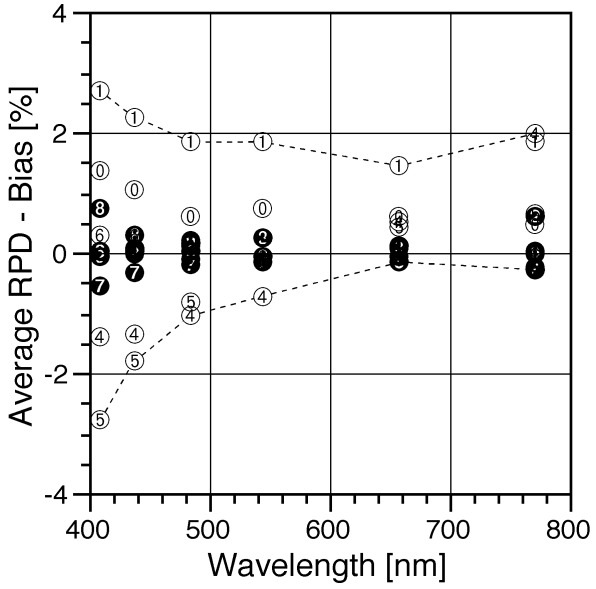

Fig. 33. The average RPDs between the experimental lamp irradiances versus those provided with the lamp, but with the bias (solid lines from Fig. 5) removed. The bullet symbols correspond to the lamp codes given in Table 5, i.e., 0 for L000, 1 for L001, etc. The darkened bullets correspond to the *trusted* lamps.

The net RPD values for the *trusted* lamps in Fig. 33 are well distributed around zero with the largest variance in the blue part of the spectrum which decreases to small values in the red domain. The other lamps still form the outer range of variance, which is maximal in the blue and minimal in the red.

9.3 CALIBRATION COMPARISON

The uncertainty of Optronic calibrations with respect to NIST is supposed to be within 1.0%. The results of the calibration comparison (Sect. 3.3) show an average intercomparison between the NIST and Optronic calibration of F-550 (L010) was 1.3%, which is not in agreement with this specification. The results also showed very little spectral dependence in the calibration (usually less than ±0.2% with respect to the average). This was an improvement over an earlier exercise with F-409 (L007) wherein a) Optronic procedures had to be improved to meet the specification, and b) a spectral dependence was clearly present (particularly in the shortest wavelengths). Unfortunately, it was also a degradation with respect to the earlier exercise which achieved agreement with NIST at the 0.8% level. If the two exercises are taken together, it seems likely that Optronic can meet the 1.0% spectification.

9.4 REPEATABILITY

Three types of repeatability experiments were executed during SIRREX-7: a) lamp use, b) radiance sensor calibration, and c) irradiance sensor calibration. The former is particularly important, because lamps are used for both types of calibrations at Satlantic.

Lamp repeatability (Sect. 3.4) was investigated by cycling 10 lamps through the radiance calibration process as measured with the SXR. The repeatability in radiance calibrations (Sect. 5.2) involved cycling three OCR-200 radiometers through the calibration process without changing anything associated with the lamp or plaque. The irradiance repeatability experiments (Sect. 6.2) were executed by cycling three OCI-200 sensors through the calibration process without altering anything with the FEL lamp.

The lamp repeatability experiments allow for the quantification of several important and combined uncertainties: a) power supply stability, b) lamp positioning, and c) lamp stability. The results (Fig. 8) show only the latter contributes at a significant level. For all the lamps tested, the uncertainty associated with these factors was less than 0.2% with the exception of (L005) which exhibited uncertainties as large as 0.5% in the blue domain. This lamp was not seasoned (i.e., not burned for 50 h before being used as a calibration standard), and unseasoned lamps usually exhibit larger flux variations at shorter wavelengths.

The results of the radiance and irradiance sensor repeatability experiments are a direct indicator of uncertainties associated with a) power supply stability, b) lamp stability, and c) radiometer alignment. The combined uncertainties for these elements during radiance calibrations was less than 0.2% (Fig. 16), and the average across all wavelengths was less than 0.1%. The results for the irradiance trials (Fig. 22) had an overall uncertainty of approximately 0.2% (with some large excursions in the individual sensors as high as almost 0.5%).

For Satlantic calibrations, all three repeatability experiments indicated a similar combined uncertainty as long as the lamp being used was properly seasoned: approximately 0.2% on average, with a maximum uncertainty of 0.5%.

9.5 PLAQUE UNCERTAINTIES

The lamp uncertainty data (Sect. 3.2) identified a systematic bias (Fig. 5) that was on the order of the contributing uncertainties, but did not fully explain it. The spectral bias was estimated using the average RPDs in Fig. 5 for the *trusted* lamps. The plaque uncertainty data (Sect. 4.2), independently realized (Fig. 10), show the same amplitude and form for the bias. The NIST plaque (T005) was used in both experiments, so the data corresponding to when the same lamp was used with this plaque can be used to further investigate the bias (Fig. 34).

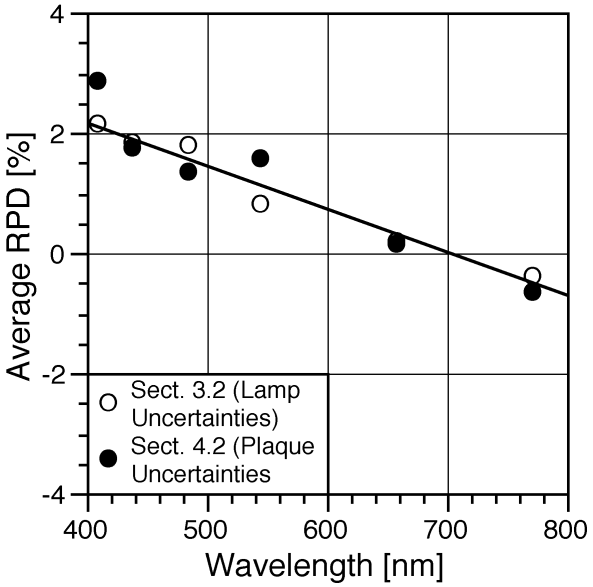

Fig. 34. The average RPD values for the T005 plaque illuminated with L003 (F-539) during the lamp (open circles) and plaque (closed circles) uncertainty experiments. The solid line is a least-squares fit to the data which has a coefficient of determination of $R^2 = 0.966$.

The Fig. 34 data show excellent agreement (the average difference between the two data sets is less than 0.4%), so whatever bias was present in the experimental procedures, it was well quantified by the T005 plaque uncertainty trials. The average RPD values between the experimental reflectances and those provided with the plaques (Fig. 10), but with the values from T005 used as a reference and

removed from the data, is presented in Fig. 35. The difference between the other plaques and T005 provides an unbiased estimate of the percent agreement of the calibration of these plaques with respect to NIST. Ignoring the old (T003), gray (T007), and damaged (T004) plaques, which were already discussed (Sect. 4.2.3), the remaining (white) plaques show good agreement with respect to T005, but there is a strong spectral dependence: approximately 1.1% in the blue, 0.8% in the green, 0.5% in the red, and 0.2% in the near infrared. The overall average difference is about 0.7%, which along with the individual spectral differences, is well within the 1.5% uncertainty specified by Labsphere.

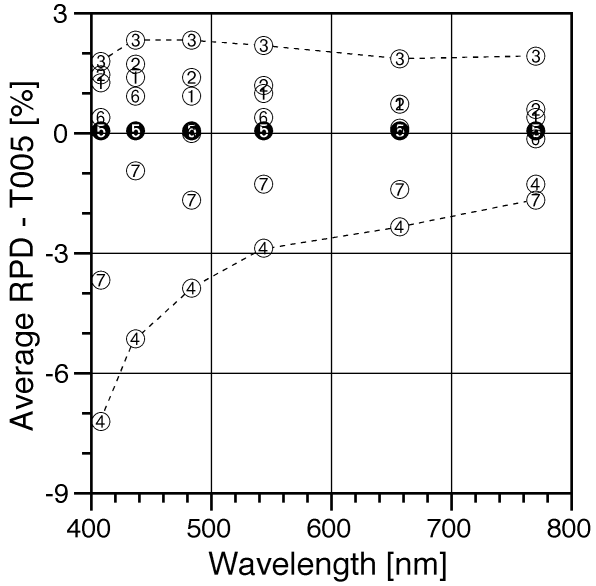

Fig. 35. The average RPDs between the experimental reflectances and those provided with the plaques (Fig. 10), but with the values from T005 used as a reference and removed. The bullet symbols correspond to the target codes given in Table 6, i.e., 1 for T001, 2 for T002, etc. The darkened bullets correspond to T005. The dashed lines delimit the overall performance of the plaques.

9.6 PLAQUE UNIFORMITY

The plaque uniformity experiments (Sect. 4.3) were designed to provide maps of the emitted flux from an FEL standard lamp at varying distances from the lamp, but obviously reflected off a Spectralon plaque. Nonetheless, they are applicable to both radiance and irradiance calibration problems if the sensor is only calibrated in a single session (i.e., each channel is not centered separately in a series of calibrations, so each channel is always looking at the same portion of the emitted light field). The reason both sensor types can be considered is the plaque approximates a lambertian surface, so the resulting map of the surface is a two-dimensional picture of the emitted flux at the calibration plane (i.e., the plaque or the irradiance sensor) and at a particular illumination distance.

The plaque uniformity maps in Fig. 13 show that sensor orientation during calibration for multi-aperture radiometers is an important parameter. For the typical illumination distance of 1.3 m (Fig. 13b), a randomly oriented channel within a multi-aperture sensor would view and, thus, integrate, different portions of the light patterns at the calibration plane. This problem is a function of the distance between the lamp and the calibration plane, as well as the FOV of the sensor. For the former, sensor orientation becomes increasingly important as the distance between the lamp and calibration plane decreases. Similarly, as the FOV of the sensor decreases, changes in orientation will result in larger discrepancies in the detected signal, because the asymmetries in the light patterns will become more apparent.

The large gradients in the 0.5 m plot (Fig. 13a) versus the more gradual gradients in the 1.3 m plot (Fig. 13b), suggest that radiance calibrations should be done with a lamp-to-plaque distance of 1.0 m or more (taking into account saturation and FOV issues if necessary). It is important to remember, however, that for irradiance calibrations, the calibration takes place at a mechanical point defined in the calibration process (usually 0.5 m). The shape of the gradients and the asymmetry in the z-axis also indicates the lamp is best modeled as a linear array of point sources and not as a solitary point source.

9.7 BIDIRECTIONAL EFFECTS

The importance of bidirectional effects during plaque calibrations of radiance sensors (Sect. 4.4) was not comprehensively explored, but the results (Fig. 14) point to some important aspects of how multi-aperture radiometers are frequently calibrated. Although most calibrations take place using the same rail (at Satlantic, the same rail is always used and the sensor is always oriented the same way by ensuring the serial number is in the same orientation), there are occasions when different rails are used. Changing rails will necessarily result in a new orientation of the radiometer with respect to the plaque if a compensating change is not implemented in the sensor orientation scheme, particularly for a multi-aperture sensor. This change can occur either by accident or design, so some understanding of the importance of this effect is needed.

The plaque is illuminated by a lamp, and the plaque uniformity results (Sect. 4.3) showed asymmetries in the light distribution on the plaque, so a primary contributor to any difference in using the $+45°$ or $-45°$ rail is expected to be the result of illumination inhomogeneities. The Fig. 14 data show the plaque that was not translated to compensate for the multi-aperture sensors, T005, exhibited small positive and negative spectral differences between the two rails, approximately 0.3% (using absolute differences). In this case, the SXR viewed very similar spots on the plaque, and there is no appreciable evidence for a bidirectional effect—the small uncertainty is within the operational uncertainties already quantified.

The white Spectralon plaques that had not been damaged or resurfaced, but had been translated, showed a difference of approximately 0.8%. This level of uncertainty is on the order of the expected difference for viewing a plaque with an x-axis offset of approximately 110 mm from two different sides (Fig. 13b) combined with the usual operational uncertainties. The two plaques that had been either damaged or resurfaced exhibited a slightly larger difference of 1.2%, approximately 0.5% of this uncertainty is probably due to bidirectional differences. In this case, the cause is most likely differences in damage and scratching between the two sides of the plaque.

The gray plaque had a unique behavior with respect to the white plaques, as well as the largest average difference in the bidirectional experiment, about 2.1%. There were no known defects or damage for this plaque, so given the rationale and results developed with the other plaques, it appears that approximately 1.0% can be attributed to bidirectional effects. Gray plaques are doped and are not as lambertian as white plaques, so a quantifiable bidirectional effect is expected.

9.8 AMBIENT MEASUREMENTS

The normal Satlantic calibration procedure is to use dark measurements to remove voltage biases from detector signal levels. The calibration equation is based on direct illumination and direct viewing, so indirect or *stray* light sources represent a corruption of the process. Ambient and dark measurements were compared for the estimation of bias voltages using three OCR-200 sensors and the SXR (Sect. 5.3), as well as three OCI-200 sensors (Sect. 6.3). The OCR-200 and OCI-200 trials were also used to measure the importance of secondary reflections from the calibration apparatus, in this case, an alignment laser that was positioned along the lalmp illumination axis.

Stray light contributions to the calibration process were smaller for irradiance sensors (always less than 0.1%) than for radiance sensors (a little more than 0.1% on average). If proper baffling is installed, as was the objective at the Satlantic facility (Fig. 2), stray light contributions can be kept to a negligible level (remembering here the limitations of the experiments conducted and that an unknown bias was seen in the lamp and plaque uncertainty trials). Stray light was mostly spectrally independent except for elevated uncertainties in the near-infrared part of the spectrum (almost as high as 0.4%).

The consequences of ignoring secondary reflections on the calibration process, which can also be considered within the requirements of proper baffling the calibration work space, were more variable. For the SXR, which has a narrow FOV, the extra uncertainty was less than 0.1% except in the near-infrared where it was almost 1.0%. For irradiance sensors, secondary reflections were largest in the blue part of the spectrum (almost 0.2%), although, the range in variations was similar.

9.9 ROTATION & POLARIZATION

Two experiments were conducted to estimate the rotation sensitivity of radiance and irradiance sensors during the calibration process. Rotational uncertainties for radiance sensors were usually less than 1%, with single and multiple aperture systems having average rotational uncertainties of 0.2–0.3% and 0.4–0.9%, respectively. The largest rotational uncertainties were for a narrow FOV in-air OCR-200 sensor. The rotational uncertainty for a multi-aperture irradiance sensor was 0.7% on average, which was in close agreement with the multiple aperture radiance sensor.

The most significant aspect of the rotational results is the sensitivity of a narrow FOV multi-aperture sensor to rotational effects. The projected FOV for a narrow FOV sensor traces out a relatively small area across the plaque, whereas a large FOV sensor necessarily traces out a large area. The smaller the area, the greater the likelihood that the sensor will detect lamp illumination inhomogeneities in the plaque (Sect. 4.3) as it is rotated.

The polarization results showed the Satlantic radiometers have an average polarization parameter below the 2% design objective (Mueller and Austin 1995), but some wavelengths exceed this. For the OCR-200 sensors, polarization values above 2% were seen in the bluest wavelengths, but for the OCR-2000 sensor, excessive values were seen in the reddest wavelengths. The SXR was the only sensor with mirrors, and the average polarization parameter was a little above 4.5%, with almost no spectral dependence (except at the bluest wavelength).

9.10 PORTABLE SOURCES

The experiments concerned with mapping the homogeneity of the SQM-II exit aperture (Sect. 8.2) showed approximately 25% of the central portion was within 2% of the maximum signal (the area viewed by an above- or in-water OCR-200 sensor), and about 40% was to within 5% (Fig. 31). These results are within the design specifications of the SQM-II and the documented capabilities of the original SQM (Johnson et al. 1998b).

Although the use of portable sources to monitor the stability of radiometers in the field was the primary objective in producing the SQM, a more powerful application of this technology would be its use as an absolute calibration source. The results of Sect. 8.3.3 (Fig. 32) show the emitted flux for both the SQM and SQM-II is very stable (Table 17), although the SQM was more stable, and the degradation over time is gradual (when it is in the laboratory)—shipping events might cause episodic shifts. The average decays per 100 days for the SQM and SQM-II were on the order of 0.9% and 2.2%, respectively. These values are from the SXR external monitoring of the devices. In neither case have the internal monitoring data been used as a possible correction source.

9.11 SUMMARY

A combined uncertainty budget for radiometric calibrations can be constructed from the SIRREX-7 data set. Although it is comprehensive, it does not address every source of uncertainty at the same level of detail, e.g., the effects of not centering each channel of a multi-aperture radiometer during calibration was not comprehensively considered, and some must be considered as approximate. Nonetheless, sufficient care was taken at all levels of the experimental process to ensure the uncertainty estimates are at representative of what can be expected if careful metrology and practices are adhered to. Perhaps just as importantly, the consequences of discrepancies are also well estimated. A summary of the uncertainty sources applicable to the SIRREX-7 activities are presented in Table 14.

Table 14. The estimated uncertainties in irradiance (E) and radiance (L) calibrations as determined from the SIRREX-7 experiments. The uncertainties are ranked as primary, secondary, or tertiary sources based on the difficulty of reducing the size of the uncertainty—tertiary sources are easier to reduce than secondary sources, etc.

Source of Uncertainty		*E*	*L*
NIST Lamp Standard	1	1.0	1.0
Secondary Lamp Standard	2	+1.0	+1.0
Excessive Lamp Age	3	+1.0	+1.0
Excessive Lamp Wear	3	+2.0	+2.0
Positioning Discrepancies	2	+1.5	+1.5
Unseasoned Lamp	3	+0.5	+0.5
Low Operating Current†	3	+1.0	+1.0
Mechanical Setup	1	0.5	0.5
Rotational Discrepancies	2	+0.5	+0.5
Alignment Discrepancies	2	+0.5	+0.5
Inadequate Baffling	2	+0.5	+0.5
NIST Plaque Standard	1		1.0
Secondary Plaque Standard	2		+1.0
Excessive Plaque Age	3		+2.0
Excessive Plaque Wear	3		+4.0
Non-White (Doped) Plaque	3		+2.0
1 *Minimum Quadrature Sum*		*1.1*	*1.5*
1 2 *Typical Quadrature Sum*		*2.3*	*2.7*
1 2 3 *Maximum Quadrature Sum*		*3.4*	*6.3*

† Based on one lamp with a Hoffman calibration.

The uncertainty sources listed in Table 14 are generalized entries. Although some match the experiments that were directly executed during SIRREX-7, others are combined or estimated from a variety of trials or experiences, and others are simply specified by NIST. In all cases, reasonable averages (or upper limits) are presented rather than worst case possibilities. In all likelihood, dedicated efforts can be undertaken to reduce some of the entries at a particular site, but others represent state-of-the-art achievements which some facilities will have a hard time reproducing.

To provide a range of possible outcomes in the calibration process, minimum, typical, and maximum quadrature sums (the square root of the sum of the squares) are computed from the various entries. The Satlantic facility falls somewhere between the minimum and typical quadrature sums—all of the primary sources, and some of the secondary sources, are applicable to calculating a final uncertainty budget for the Satlantic facility. If an additional (average) 1.0% is included to account for the unknown bias seen with the lamp and plaque uncertainty experiments (Sects. 3.2 and 4.2, respectively) above and beyond the SXR uncertainty, the uncertainty for Satlantic irradiance calibrations is 1.8%, and the uncertainty for radiance calibrations is 2.3%.

There are some other lessons learned during SIRREX-7 that do not fit neatly into the presentation of the uncertainty experiments, so they are recounted here:

1. V-blocks are more efficient and reliable than ring mounts, in terms of being able to rapidly set up or reproduce the alignment of a radiometer.
2. D-shaped collars (Fig. 3), or some other scheme that allows for reproducible mounting and angular orientation of the radiometer, is a needed part of the calibration process (particularly for multi-aperture sensors).
3. The baffling in the Satlantic calibration facility is very well designed, but it was still possible to have quantifiable effects from improperly baffled ancillary equipment.

Although the effect for the latter was small over the visible part of the spectrum, it was a clear demonstration of how attention to detail is a recurring requirement when working at the 1% uncertainty level.

Acknowledgments

SIRREX-7 could not have been executed at the high level that was achieved without the competent contributions of the technical staff at Satlantic, Inc. Many individuals, not immediately associated with the day-to-day execution of the experiments, responded willingly and cheerfully whenever their expertise or assistance was required.

Appendices

Appendix A

SIRREX-7 Science Team

The SIRREX-7 science team members are presented alphabetically.

James Brown
MPO/RSMAS/U. of Miami
4600 Rickenbacker Causeway
Miami, Florida 33149
Voice: 305–361–4770
Fax: 301–361–4622
Net: jim.brown@miami.edu

Cyril Dempsey
Satlantic, Inc.
Richmond Terminal, Pier 9
3481 North Marginal Road
Halifax, Nova Scotia B3K 5X8
CANADA
Voice: +1–902–492–4780
Fax: +1–902–492–4781
Net: cyril@satlantic.com

Stanford Hooker
NASA/GSFC/Code 970.2
Bldg. 28, Room W126
Greenbelt, Maryland 20771
Voice: 301–286–9503
Fax: 301–286–0268
Net: stan@ardbeg.gsfc.nasa.gov

Gordana Lazin
Satlantic, Inc.
Richmond Terminal, Pier 9
3481 North Marginal Road
Halifax, Nova Scotia B3K 5X8
CANADA
Voice: +1–902–492–4780
Fax: +1–902–492–4781
Net: gordana@satlantic.com

Scott McLean
Satlantic, Inc.
Richmond Terminal, Pier 9
3481 North Marginal Road
Halifax, Nova Scotia B3K 5X8
CANADA
Voice: +1–902–492–4780
Fax: +1–902–492–4781
Net: scott@satlantic.com

Jennifer Sherman
Satlantic, Inc.
Richmond Terminal, Pier 9
3481 North Marginal Road
Halifax, Nova Scotia B3K 5X8
CANADA
Voice: +1–902–492–4780
Fax: +1–902–492–4781
Net: jennifer@satlantic.com

Mark Small
Satlantic, Inc.
Richmond Terminal, Pier 9
3481 North Marginal Road
Halifax, Nova Scotia B3K 5X8
CANADA
Voice: +1–902–492–4780
Fax: +1–902–492–4781
Net: mark@satlantic.com

Giuseppe Zibordi
JRC/SAI/ME T.P. 272
I–21020 Ispra (VA)
ITALY
Voice: +39–0–332–785–902
Fax: +39–0–332–789–034
Net: giuseppe.zibordi@jrc.it

Glossary

A/D	Analog-to-Digital
AC	Alternating Current
AMT	Atlantic Meridional Transect
AMT-3	The Third AMT (cruise)
ASCII	American Standard Code for Information Interchange
BRDF	Bidirectional Reflectance Distribution Function
CERT	Calibration Evaluation and Radiometric Testing
CHORS	Center for Hydro-Optics and Remote Sensing
DATA-100	(Satlantic) Data (acquisition) Series 100 (unit)
DC	Direct Current
DUT	Device Under Test
DVM	Digital Voltmeter
FEL	Not an acronym, but a lamp designator.
FFT	Fast Fourier Transform
FAFOV	Full Angle Field of View
FOV	Field of View
FWHM	Full-Width at Half-Maximum
GMT	Greenwich Mean Time
GSFC	Goddard Space Flight Center
HEPA	High Efficiency Particle Arrestor
JRC	Joint Research Centre
MOBY	Marine Optical Buoy
NASA	National Aeronautics and Space Administration
NEC	Formerly, the Nippon Electric Corporation.
NIST	National Institute of Standards and Technology
NSD	Normalized Standard Deviation

OCI-200	Ocean Color Irradiance Series 200 (sensor)
OCR-200	Ocean Color Radiance Series 200 (sensor)
OCR-250	Ocean Color Radiance Series 250 (sensor)
OCR-1000	Ocean Color Radiance Series 1000 (sensor)
OCR-2000	Ocean Color Radiance Series 2000 (sensor)
OCTS	Ocean Color and Temperature Sensor (Japan)
PC	Personal Computer
PCR	Percent Contribution Ratio
PTFE	Polytetrafluoroethylene
RPD	Relative Percent Difference
RSMAS	Rosenstiel School for Marine and Atmospheric Science
S/N	Serial Number
SatView	The Satlantic data acquisition and visualization software package.
SDY	Sequential Day of the Year
SeaARCS	SeaWiFS Advanced Radiometer Control System
SeaLaMP	SeaWiFS Lamp Monitoring and Performance
SeaWiFS	Sea-viewing Wide Field-of-view Sensor
SIMBIOS	Sensor Intercomparison and Merger for Biological and Interdisciplinary Ocean Studies
SIRREX	SeaWiFS Intercalibration Round-Robin Experiment
SIRREX-1	The First SIRREX (July 1992)
SIRREX-2	The Second SIRREX (June 1993)
SIRREX-3	The Third SIRREX (September 1994)
SIRREX-4	The Fourth SIRREX (May 1995)
SIRREX-5	The Fifth SIRREX (July 1996)
SIRREX-6	The Sixth SIRREX (August–December 1997)
SIRREX-7	The Seventh SIRREX (March 1999)
SQM	SeaWiFS Quality Monitor
SQM-II	The Second Generation SQM
SXR	SeaWiFS Transfer Radiometer
T/N	Temporary (identification) Number
UPS	Uninterruptable Power Supply

Symbols

$\bar{A}_{S_{\rm ID}}(\lambda)$	The average voltage measured during the ambient measurement for sensor $S_{\rm ID}$.
$C^{\rm Irr}_{S_{\rm ID}}(\lambda)$	The spectral calibration coefficient for irradiance sensor $S_{\rm ID}$.
$C^{\rm Rad}_{S_{\rm ID}}(\lambda)$	The spectral calibration coefficient for radiance sensor $S_{\rm ID}$.
$\bar{C}^{\rm cal}_{S_{\rm ID}}(\lambda)$	The average of the spectral calibration coefficients for sensor $S_{\rm ID}$.
$\hat{C}^{\rm cal}_{S_{\rm ID}}(\lambda)$	The standard deviation in the spectral calibration coefficients for sensor $S_{\rm ID}$.
d	The distance from the lamp to the plaque (usually measured in centimeters).
$\bar{D}_{S_{\rm ID}}(\lambda)$	The average dark voltage level measured for sensor $S_{\rm ID}$.
$E(\lambda)$	Spectral irradiance.
$E_d(\lambda)$	Spectral downward irradiance.
$E^{50}_{L_{\rm ID}}(\lambda)$	The spectral irradiance of lamp $L^{50}_{\rm ID}$ (at 50 cm).
$E^{\rm cal}_{L3}(\lambda)$	The calibrated lamp irradiance supplied with lamp L003.
$E^{\rm cal}_{L_{\rm ID}}(\lambda)$	The calibrated spectral irradiance supplied with lamp $L_{\rm ID}$.
$E^{N}_{L_{\rm ID}}(\lambda)$	The calibrated spectral irradiance supplied by NIST for lamp $L_{\rm ID}$.
$E^{O}_{L_{\rm ID}}(\lambda)$	The calibrated spectral irradiance supplied by Optronic for lamp $L_{\rm ID}$.
$E_u(\lambda)$	Spectral upwelling irradiance.
i	A sequential index.
ID	The identification code for a lamp, plaque, sensor, etc.
$L_{\rm ID}$	The lamp identification code.
$L(\lambda)$	Spectral radiance.
$L^{\max}_{S_{\rm ID}}(\lambda,\theta)$	The maximum radiance measured during a 360° rotation of sensor $S_{\rm ID}$.
$L^{\min}_{S_{\rm ID}}(\lambda,\theta)$	The minimum radiance measured during a 360° rotation of sensor $S_{\rm ID}$.
$L^{-X1}_{T_{\rm ID}}(\lambda)$	The SXR ($X1$) spectral radiance measurements of plaque $T_{\rm ID}$ on the −45° rail.
$L^{+X1}_{T_{\rm ID}}(\lambda)$	The SXR ($X1$) spectral radiance measurements of plaque $T_{\rm ID}$ on the +45° rail.
$L^{X1}_{T_{\rm ID}}(\lambda)$	The SXR ($X1$) spectral radiance measurements of plaque $T_{\rm ID}$.
$L_u(\lambda)$	Spectral upwelling radiance.
$L_W(\lambda)$	The spectral water-leaving radiance.
N	The number of replicate trials for a particular sensor.
N_T	The total number of trials.
N_θ	The number of angular positions.
$P_{S_{\rm ID}}(\lambda,\theta)$	The polarization parameter for sensor $S_{\rm ID}$.
$R_{T7}(\lambda)$	The spectral reflectance to plaque T007.
$R^{\rm cal}_{T_{\rm ID}}(\lambda)$	The calibrated reflectance supplied with plaque $T_{\rm ID}$.
$R^{\rm X1}_{T_{\rm ID}}(\lambda)$	The reflectance of plaque $T_{\rm ID}$ calculated from SXR ($X1$) measurements.
$S_{\rm ID}$	The sensor identifcation number.
t_i	The trial number.
$T7$	The (abbreviated) target identification number for plaque T007.
$T_{\rm ID}$	The target identification number.
$\bar{V}_{S_{\rm ID}}(\lambda)$	The average spectral calibration voltage for sensor $S_{\rm ID}$.
$\bar{V}^{\rm cov}_{S_{\rm ID}}(\lambda)$	The average voltage measured while viewing the lamp with the laser covered.
x	The abscissa (or horizontal coordinate) coordinate perpendicular to the illumination axis.
y	The ordinate coordinate (along the illumination axis).
z	The vertical coordinate.
α_1	Carrier alignment parameter for calibration table 1 during 22.5° plaque rotation.
α_2	Carrier alignment parameter for calibration table 2 during 22.5° plaque rotation.
β_1	Carrier alignment parameter for calibration table 1 for on-axis plaque illumination.
β_2	Carrier alignment parameter for calibration table 2 for on-axis plaque illumination.
$\delta(\lambda)$	The spectral RPD.
$\delta_{L_{\rm ID}}(\lambda,t_i)$	The RPD between two different calibrations of lamp $L_{\rm ID}$.
$\delta^{X1}_{T_{\rm ID}}(\lambda)$	The spectral RPD between the reflectances calculated from the SXR ($X1$) measurements and the reflectances supplied with plaque $T_{\rm ID}$.
$\delta^{\pm X1}_{T_{\rm ID}}(\lambda)$	The spectral RPD between the reflectances calculated from the SXR ($X1$) measurements of plaque $T_{\rm ID}$ on the +45° and −45° calibration rails.

$\bar{\delta}^{X1}_{T_{\rm ID}}(\lambda)$ The average RPD between the reflectances calculated from the SXR ($X1$) measurements and the reflectances supplied with plaque $T_{\rm ID}$.

θ The angular coordinate.

$\zeta(\lambda)$ The NSD (or coefficient of variation) defined as the standard deviation in the measured light signal divided (or normalized) by the average of the signal.

$\zeta^{X1}_{L_{\rm ID}}(\lambda)$ The spectral NSD for SXR measurements ($X1$) of lamp $L_{\rm ID}$.

$\bar{\zeta}^{X1}_{L_{\rm ID}}(\lambda)$ The average spectral NSD for SXR measurements ($X1$) of lamp $L_{\rm ID}$.

$\zeta_{S_{\rm ID}}(\lambda)$ The spectral NSD in the calibration coefficients for sensor $S_{\rm ID}$.

λ Wavelength.

$\mu(\lambda)$ The average NSD.

$\bar{\mu}^{X1}_{L_{\rm ID}}(\lambda)$ The spectral average in SXR ($X1$) measurements of lamp $L_{\rm ID}$.

σ The standard deviation.

$\sigma(\lambda)$ The standard deviation in NSD.

$\sigma^{X1}_{L_{\rm ID}}(\lambda)$ The spectral standard deviation in SXR ($X1$) measurements of lamp $L_{\rm ID}$.

$\chi^{\rm amb}_{S_{\rm ID}}(\lambda)$ The PCR of ambient light on a radiance calibration for sensor $S_{\rm ID}$.

$\chi^{\rm cov}_{S_{\rm ID}}(\lambda)$ The PCR of laser reflections on a radiance calibration for sensor $S_{\rm ID}$.

$\chi^{\rm max}_{S_{\rm ID}}(\lambda)$ The maximum value of $\chi^{\rm ratio}_{S_{\rm ID}}(\lambda,\theta)$.

$\chi^{\rm min}_{S_{\rm ID}}(\lambda)$ The minimum value of $\chi^{\rm ratio}_{S_{\rm ID}}(\lambda,\theta)$.

$\chi^{\rm ratio}_{S_{\rm ID}}(\lambda,\theta)$ The PCR of sensor response at a particular angle θ with respect to the average from a full 360° rotation of sensor $S_{\rm ID}$.

$\chi^{\rm rot}_{S_{\rm ID}}(\lambda)$ The PCR of sensor rotation for sensor $S_{\rm ID}$.

References

Aiken, J., N.W. Rees, S. Hooker, P. Holligan, A. Bale, D. Robins, G. Moore, R. Harris, and D. Pilgrim, 2000: The Atlantic Meridional Transect: overview and synthesis of data. *Prog. Oceanogr.,* **45,** 257–312.

Hooker, S.B., and W.E. Esaias, 1993: An overview of the SeaWiFS project. *Eos, Trans., Amer. Geophys. Union,* **74,** 241–246.

——, and J. Aiken, 1998: Calibration evaluation and radiometric testing of field radiometers with the SeaWiFS Quality Monitor (SQM). *J. Atmos. Oceanic Tech.,* **15,** 995–1,007.

——, and S. Maritorena, 2000: An evaluation of oceanographic radiometers and deployment methodologies. *J. Atmos. Oceanic Technol.,* **17,** 811–830.

——, and C.R. McClain, 2000: The calibration and validation of SeaWiFS data. *Prog. Oceanogr.,* **45,** 427–465.

Johnson, B.C., S.S. Bruce, E.A. Early, J.M. Houston, T.R. O'Brian, A. Thompson, S.B. Hooker, and J.L. Mueller, 1996. The Fourth SeaWiFS Intercalibration Round-Robin Experiment (SIRREX-4), May 1995. *NASA Tech. Memo. 104566, Vol. 37,* S.B. Hooker and E.R. Firestone, Eds., NASA Goddard Space Flight Center, Greenbelt, Maryland, 65 pp.

——, F. Sakuma, J.J. Butler, S.F. Biggar, J.W. Cooper, J. Ishida, and K. Suzuki, 1997: Radiometric measurement comparison using the Ocean Color Temperature Scanner (OCTS) visible and near infrared integrating sphere. *J. Res. NIST,* **102,** 627–646.

——, J.B. Fowler, and C.L. Cromer, 1998a: The SeaWiFS Transfer Radiometer (SXR). *NASA Tech. Memo. 1998–206892, Vol. 1,* S.B. Hooker and E.R. Firestone, editors, NASA Goddard Space Flight Center, Greenbelt, Maryland, 58 pp.

——, P-S. Shaw, S.B. Hooker, and D. Lynch, 1998b: Radiometric and engineering performance of the SeaWiFS Quality Monitor (SQM): A portable light source for field radiometers. *J. Atmos. Oceanic Tech.,* **15,** 1,008–1,022.

——, H.W. Yoon, S.S. Bruce, P-S. Shaw, A. Thompson, S.B. Hooker, R.E. Eplee, Jr., R.A. Barnes, S. Maritorena, and J.L. Mueller, 1999: The Fifth SeaWiFS Intercalibration Round-Robin Experiment (SIRREX-5), July 1996. *NASA Tech. Memo. 1999–206892, Vol. 7,* S.B. Hooker and E.R. Firestone, Eds., NASA Goddard Space Flight Center, 75 pp.

McClain, C.R., W.E. Esaias, W. Barnes, B. Guenther, D. Endres, S.B. Hooker, G. Mitchell, and R. Barnes, 1992a: Calibration and Validation Plan for SeaWiFS. *NASA Tech. Memo. 104566, Vol. 3,* S.B. Hooker and E.R. Firestone, Eds., NASA Goddard Space Flight Center, Greenbelt, Maryland, 41 pp.

Mueller, J.L., 1993: The First SeaWiFS Intercalibration Round-Robin Experiment, SIRREX-1, July 1992. *NASA Tech. Memo. 104566, Vol. 14,* S.B. Hooker and E.R. Firestone, Eds., NASA Goddard Space Flight Center, Greenbelt, Maryland, 60 pp.

——, and R.W. Austin, 1992: Ocean Optics Protocols for SeaWiFS Validation. *NASA Tech. Memo. 104566, Vol. 5,* S.B. Hooker and E.R. Firestone, Eds., NASA Goddard Space Flight Center, Greenbelt, Maryland, 43 pp.

——, B.C. Johnson, C.L. Cromer, J.W. Cooper, J.T. McLean, S.B. Hooker, and T.L. Westphal, 1994: The Second SeaWiFS Intercalibration Round-Robin Experiment, SIRREX-2, June 1993. *NASA Tech. Memo. 104566, Vol. 16,* S.B. Hooker and E.R. Firestone, Eds., NASA Goddard Space Flight Center, Greenbelt, Maryland, 121 pp.

——, and R.W. Austin, 1995: Ocean Optics Protocols for SeaWiFS Validation, Revision 1. *NASA Tech. Memo. 104566, Vol. 25,* S.B. Hooker, E.R. Firestone, and J.G. Acker, Eds., NASA Goddard Space Flight Center, Greenbelt, Maryland, 66 pp.

——, B.C. Johnson, C.L. Cromer, S.B. Hooker, J.T. McLean, and S.F. Biggar, 1996: The Third SeaWiFS Intercalibration Round-Robin Experiment (SIRREX-3), 19–30 September 1994. *NASA Tech. Memo. 104566, Vol. 34,* S.B. Hooker, E.R. Firestone, and J.G. Acker, Eds., NASA Goddard Space Flight Center, Greenbelt, Maryland, 78 pp.

Riley, T., and S. Bailey, 1998: The Sixth SeaWiFS/SIMBIOS Intercalibration Round-Robin Experiment (SIRREX-6) August–December 1997. *NASA Tech. Memo. 1998–206878,* NASA Goddard Space Flight Center, Greenbelt, Maryland, 26 pp.

Walker, J.H., R.D. Saunders, J.K. Jackson, and D.A. McSparron, 1987: Spectral Irradiance Calibrations. *NBS Special Publication 250–20*, U.S. Dept. of Commerce, National Bureau of Standards, Washington, DC, 37 pp. plus appendices.

The SeaWiFS Postlaunch Technical Report Series

Vol. 1

Johnson, B.C., J.B. Fowler, and C.L. Cromer, 1998: The SeaWiFS Transfer Radiometer (SXR). *NASA Tech. Memo. 1998–206892, Vol. 1,* S.B. Hooker and E.R. Firestone, Eds., NASA Goddard Space Flight Center, Greenbelt, Maryland, 58 pp.

Vol. 2

Aiken, J., D.G. Cummings, S.W. Gibb, N.W. Rees, R. Woodd-Walker, E.M.S. Woodward, J. Woolfenden, S.B. Hooker, J-F. Berthon, C.D. Dempsey, D.J. Suggett, P. Wood, C. Donlon, N. González-Benítez, I. Huskin, M. Quevedo, R. Barciela-Fernandez, C. de Vargas, and C. McKee, 1998: AMT-5 Cruise Report. *NASA Tech. Memo. 1998–206892, Vol. 2,* S.B. Hooker and E.R. Firestone, Eds., NASA Goddard Space Flight Center, Greenbelt, Maryland, 113 pp.

Vol. 3

Hooker, S.B., G. Zibordi, G. Lazin, and S. McLean, 1999: The SeaBOARR-98 Field Campaign. *NASA Tech. Memo. 1999–206892, Vol. 3,* S.B. Hooker and E.R. Firestone, Eds., NASA Goddard Space Flight Center, Greenbelt, Maryland, 40 pp.

Vol. 4

Johnson, B.C., E.A. Early, R.E. Eplee, Jr., R.A. Barnes, and R.T. Caffrey, 1999: The 1997 Prelaunch Radiometric Calibration of SeaWiFS. *NASA Tech. Memo. 1999–206892, Vol. 4,* S.B. Hooker and E.R. Firestone, Eds., NASA Goddard Space Flight Center, Greenbelt, Maryland, 51 pp.

Vol. 5

Barnes, R.A., R.E. Eplee, Jr., S.F. Biggar, K.J. Thome, E.F. Zalewski, P.N. Slater, and A.W. Holmes 1999: The SeaWiFS Solar Radiation-Based Calibration and the Transfer-to-Orbit Experiment. *NASA Tech. Memo. 1999–206892, Vol. 5,* S.B. Hooker and E.R. Firestone, Eds., NASA Goddard Space Flight Center, 28 pp.

Vol. 6

Firestone, E.R., and S.B. Hooker, 2000: SeaWiFS Postlaunch Technical Report Series Cumulative Index: Volumes 1–5. *NASA Tech. Memo. 2000–206892, Vol. 6,* S.B. Hooker and E.R. Firestone, Eds., NASA Goddard Space Flight Center, Greenbelt, Maryland, 14 pp.

Vol. 7

Johnson, B.C., H.W. Yoon, S.S. Bruce, P-S. Shaw, A. Thompson, S.B. Hooker, R.E. Eplee, Jr., R.A. Barnes, S. Maritorena, and J.L. Mueller, 1999: The Fifth SeaWiFS Intercalibration Round-Robin Experiment (SIRREX-5), July 1996. *NASA Tech. Memo. 1999–206892, Vol. 7,* S.B. Hooker and E.R. Firestone, Eds., NASA Goddard Space Flight Center, 75 pp.

Vol. 8

Hooker, S.B., and G. Lazin, 2000: The SeaBOARR-99 Field Campaign. *NASA Tech. Memo. 2000–206892, Vol. 8,* S.B. Hooker and E.R. Firestone, Eds., NASA Goddard Space Flight Center, 46 pp.

Vol. 9

McClain, C.R., E.J. Ainsworth, R.A. Barnes, R.E. Eplee, Jr., F.S. Patt, W.D. Robinson, M. Wang, and S.W. Bailey, 2000: SeaWiFS Postlaunch Calibration and Validation Analyses, Part 1. *NASA Tech. Memo. 2000–206892, Vol. 9,* S.B. Hooker and E.R. Firestone, Eds., NASA Goddard Space Flight Center, 82 pp.

Vol. 10

McClain, C.R., R.A. Barnes, R.E. Eplee, Jr., B.A. Franz, N.C. Hsu, F.S. Patt, C.M. Pietras, W.D. Robinson, B.D. Schieber, G.M. Schmidt, M. Wang, S.W. Bailey, and P.J. Werdell, 2000: SeaWiFS Postlaunch Calibration and Validation Analyses, Part 2. *NASA Tech. Memo. 2000–206892, Vol. 10,* S.B. Hooker and E.R. Firestone, Eds., NASA Goddard Space Flight Center, 57 pp.

Vol. 11

O'Reilly, J.E., S. Maritorena, M.C. O'Brien, D.A. Siegel, D. Toole, D. Menzies, R.C. Smith, J.L. Mueller, B.G. Mitchell, M. Kahru, F.P. Chavez, G.F. Cota, S.B. Hooker, C.R. McClain, K.L. Carder, F. Müller-Karger, L. Harding, A. Magnuson, D. Phinney, G.F. Moore, J. Aiken, K.R. Arrigo, R. Letelier, and M. Culver 2000: SeaWiFS Postlaunch Calibration and Validation Analyses, Part 3. *NASA Tech. Memo. 2000–206892, Vol. 11,* S.B. Hooker and E.R. Firestone, Eds., NASA Goddard Space Flight Center, 49 pp.

Vol. 12

Firestone, E.R., and S.B. Hooker, 2000: SeaWiFS Postlaunch Technical Report Series Cumulative Index: Volumes 1–11. *NASA Tech. Memo. 2000–206892, Vol. 12,* S.B. Hooker and E.R. Firestone, Eds., NASA Goddard Space Flight Center, Greenbelt, Maryland, 24 pp.

Vol. 13

Hooker, S.B., G. Zibordi, J-F. Berthon, S.W. Bailey, and C.M. Pietras, 2000: The SeaWiFS Photometer Revision for Incident Surface Measurement (SeaPRISM) Field Commissioning. *NASA Tech. Memo. 2000–206892, Vol. 13,* S.B. Hooker and E.R. Firestone, Eds., NASA Goddard Space Flight Center, Greenbelt, Maryland, 24 pp.

Vol. 14

Hooker, S.B., H. Claustre, J. Ras, L. Van Heukelem, J-F. Berthon, C. Targa, D. van der Linde, R. Barlow, and H. Sessions, 2000: The First SeaWiFS HPLC Analysis Round-Robin Experiment (SeaHARRE-1). *NASA Tech. Memo. 2000–206892, Vol. 14,* S.B. Hooker and E.R. Firestone, Eds., NASA Goddard Space Flight Center, Greenbelt, Maryland, 42 pp.

Vol. 15

Hooker, S.B., G. Zibordi, J-F. Berthon, D. D'Alimonte, S. Maritorena, S. McLean, and J. Sildam, 2001: Results of the Second SeaWiFS Data Analysis Round Robin, March 2000 (DARR-00). *NASA Tech. Memo. 2001–206892, Vol. 15,* S.B. Hooker and E.R. Firestone, Eds., NASA Goddard Space Flight Center, Greenbelt, Maryland, 71 pp.

Vol. 16

Patt, F.S., 2002: Navigation Algorithms for the SeaWiFS Mission. *NASA Tech. Memo. 2002–206892, Vol. 16,* S.B. Hooker and E.R. Firestone, Eds., NASA Goddard Space Flight Center, Greenbelt, Maryland, 17 pp.

Vol. 17

Hooker, S.B., S. McLean, J. Sherman, M. Small, G. Lazin, G. Zibordi, and J.W. Brown, 2002: The Seventh SeaWiFS Intercalibration Round-Robin Experiment (SIRREX-7), March 1999. *NASA Tech. Memo. 2002–206892, Vol. 17,* S.B. Hooker and E.R. Firestone, Eds., NASA Goddard Space Flight Center, Greenbelt, Maryland, 69 pp.